

Ultrafast Switching and Control of Nanoparticles' Magnetization

Dissertation

zur Erlangung des akademischen Grades
Doctor rerum naturalium (Dr. rer. nat.)

vorgelegt der
Naturwissenschaftlichen Fakultät II
der Martin-Luther-Universität Halle-Wittenberg

von Herrn **Alexander Sukhov**
geboren am 14.04.1981 in Uljanowsk (Russland)

angefertigt am Max-Planck-Institut
für Mikrostrukturphysik und
an der Martin-Luther-Universität Halle-Wittenberg
in Halle an der Saale

Gutachter:

1. Prof. Dr. J. Berakdar
2. Prof. Dr. S. Trimper
3. Prof. Dr. V. K. Dugaev

Halle an der Saale, den 24. Februar 2009

verteidigt am 1. Juli 2009

Contents

Abbreviations and Notations	vii
1 Introduction	1
1.1 Motivation and Aims of the Thesis	1
1.2 Energy Contributions to the magnetic Nanoparticle	2
2 Systems studied	5
2.1 Uniaxial Anisotropy	6
2.2 Cubic Anisotropy	7
2.3 Comparison of the Anisotropy Types	8
3 Overview of Models and Methods	9
3.1 Static Treatment	9
3.1.1 Stoner-Wohlfarth Model	9
3.1.2 Néel-Brown Model	12
3.1.3 Statistical Solution	13
3.2 Dynamic Treatment	15
3.2.1 Stochastic Landau-Lifshitz-Gilbert Equation	15
3.2.2 Equations similar to the Landau-Lifshitz-Gilbert	17
3.2.3 Monte Carlo Method	18
3.2.4 Fokker-Planck Equation	20
3.2.5 Discussion of the dynamical Methods	21
3.3 Comparison of the static and the dynamic Approaches	23
4 Relaxation in ferromagnetic Systems	25
4.1 Review of Experiments for the Measurement of the Damping Parameter	25
4.2 Mechanisms and Models of the Magnetization Damping	26
5 Numerical Procedure	29
5.1 Stochastic Calculus for the Langevine Type Equations	29
5.2 Numerical Integration Scheme	30
6 Dynamical Properties of the Magnetization in the Presence of continuous Fields	33
6.1 Static magnetic Fields	33
6.1.1 Analytical Study at Zero Temperature	33
6.1.2 Numerical Study for Nanoparticles with a uniaxial Anisotropy at Nonzero Temperatures	34
6.1.3 Numerical Study for Nanoparticles with a cubic Anisotropy at Non-zero Temperatures	37

6.2	Continuous Time-Dependent magnetic Fields	40
6.2.1	New Strategy for Switching	40
6.2.2	Numerical Study for Nanoparticles with a uniaxial Anisotropy at Nonzero Temperatures	42
6.2.3	Numerical Study for Nanoparticles with a cubic Anisotropy at Non- zero Temperatures	44
6.3	Discussion and Interpretation of the Results obtained	45
7	Dynamical Properties of the Magnetization in the Presence of pulsed Fields	49
7.1	Analytical Model	49
7.1.1	Theory	49
7.1.2	Principle of controlled Switching	56
7.2	Numerical Illustrations	57
7.2.1	Rectangular shaped magnetic Pulses	57
7.2.2	Gaussian shaped magnetic Pulses	63
7.3	Discussion	64
8	Concluding Remarks and future Perspectives	67
8.1	Summary	67
8.2	Perspectives for future Studies	68
8.2.1	Spin-Torque Effect	68
	Bibliography	73
	Eidesstattliche Erklärung	85
	Acknowledgements	87
	Curriculum Vitae	89
	List of Publications	91
	Conference Contributions and invited Talks	93

List of Figures

1.1	A two-level magnetic system	2
2.1	Energy representation for a uniaxial anisotropy	6
2.2	Energy representation for a cubic anisotropy	7
2.3	Anisotropy profiles for fixed angles	8
3.1	Alignment of the magnetic moment and the applied field in the Stoner-Wohlfarth model	10
3.2	The Stoner-Wohlfarth astroid	11
3.3	Projection of the magnetic moment on the applied field as a function of the external magnetic field and temperature	13
3.4	Temperature dependence of the net magnetic moment for a ferromagnet	15
3.5	Illustration of torques acting on the magnetic moment introduced by the Landau-Lifshitz-Gilbert equation	16
3.6	Minimal switching field as a function of the diameter of a nanoparticle	22
4.1	Schematic representation of damping channels	26
6.1	Magnetization reversal of a nanoparticle with a uniaxial anisotropy and for a static field	35
6.2	Trajectories of the magnetic moment in the $E(\theta, \phi)$ space for a static field and a uniaxial anisotropy	35
6.3	Critical field amplitudes as a function of damping for a static field applied to a nanoparticle with a uniaxial anisotropy	36
6.4	Reversal times versus damping parameter for a static field and a uniaxial anisotropy	37
6.5	Magnetization reversal of a nanoparticle with a cubic anisotropy in the presence of a static field	38
6.6	Trajectories of the magnetic moment in the $E(\theta, \phi)$ space for a cubic anisotropy in the presence of a static field	39
6.7	Critical field amplitudes as a function of damping for a static field applied to a nanoparticle with a cubic anisotropy	39
6.8	Reversal times versus damping parameter for a static field and a cubic anisotropy	40
6.9	Magnetization reversal of a nanoparticle with a uniaxial anisotropy and for a time-dependent field	41
6.10	Trajectories of the magnetic moment in the $E(\theta, \phi)$ space in the presence of an oscillating field	42
6.11	Critical field amplitudes as a function of damping for a time-dependent field applied to a nanoparticle with a uniaxial anisotropy	44

6.12	Reversal times versus damping parameter for a time-dependent field and a uniaxial anisotropy	44
6.13	Magnetization reversal of a nanoparticle with a cubic anisotropy and for a time-dependent field	45
6.14	Trajectories of the magnetic moment in the $E(\theta, \phi)$ space in the presence of an oscillating field and for a cubic anisotropy	46
6.15	Critical field amplitudes as a function of damping for a time-dependent field applied to a nanoparticle with a cubic anisotropy	47
6.16	Reversal times versus damping parameter for a time-dependent field and a cubic anisotropy	47
7.1	Illustration of torques exerted by a magnetic pulse for two diverse angle shifts	52
7.2	Change of θ directly after the pulse versus $\delta\phi$ for different damping . . .	53
7.3	Change of θ directly after the pulse versus $\delta\phi$ for various field amplitudes	53
7.4	Dependence of critical field amplitudes b_{ocr} on angle $\theta(t_i^-)$ for $\delta\phi_i = 3\pi/2$ and $\delta\phi_i = 0$ for a fixed time lag	55
7.5	Dependence of critical field amplitudes b_{ocr} on angle $\theta(t_i^-)$ for $\delta\phi_i = 3\pi/2$ and $\delta\phi_i = 0$ for various time lags	55
7.6	Evolution of θ within the proposed scheme	57
7.7	Evolution of θ for two angle shifts $\delta\phi_i = 3\pi/2$ and $\delta\phi_i = 0$ (low values of damping)	57
7.8	Evolution of θ for two angle shifts $\delta\phi_i = 3\pi/2$ and $\delta\phi_i = 0$ (high values of damping)	58
7.9	$\theta(t)$ for different pulse durations for rectangular-shaped magnetic pulses .	59
7.10	Evolution of angle θ for different strategies of pulse application and for $\delta\phi_{i,1} = 3\pi/2$	60
7.11	Evolution of angle θ for different strategies of the pulse application and for $\delta\phi_{i,1} = 0$	60
7.12	Evolution of angle θ for a Co-nanoparticle for $\delta\phi_i = 3\pi/2$ and different field strengths	61
7.13	Temperature-dependent evolution of angle θ for $\delta\phi_i = 3\pi/2$ and $\delta\phi_i = 0$ for pulses being applied only when $\theta < \pi/2$	62
7.14	Temperature-dependent evolution of angle θ for $\delta\phi_i = 3\pi/2$ and $\delta\phi_i = 0$ for pulses being applied even when $\theta > \pi/2$	63
7.15	Freezing with respect to both θ and ϕ	64
7.16	Thermal-assisted controlled switching	65
7.17	Trajectories of the magnetic moment for a nanoparticle with a cubic anisotropy	66
7.18	Evolution of θ for different pulse durations for Gaussian-shaped pulses . .	66
8.1	Experimental setup for current-induced switching and $dV/dI(I)$ measurements	69
8.2	Schematic view of the system where a current-driven reversal occurs . . .	71
8.3	Demonstration of the torque directions exerted onto the magnetization by a spin-torque	72

Abbreviations and Notations

AC	Alternate Current (field)
AFM	Antiferromagnet
BB	Bloch-Blöembergen (equation)
BF	Brillouin Function
CPP	Current Perpendicular Plane
DBP	Detailed Balance Principle
DC	Direct Current (field)
FM	Ferromagnet
FMR	Ferromagnetic Resonance
FP	Fokker-Planck (equation)
HM	Heun Method
LCT	Local Control Theory
LD	Langevin Dynamics
LF	Langevin Function
LL	Landau-Lifshitz (equation)
LLB	Landau-Lifshitz-Bloch (equation)
LLG	Landau-Lifshitz-Gilbert (equation)
MAE	Magnetocrystalline Anisotropy Energy
MC	Monte Carlo
ME	Master Equation
MM	Milstein Method
PF	Partition Function
SW	Stoner-Wohlfarth (model)
SWA	Stoner-Wohlfarth Astroid

α	Gilbert damping parameter
β	Reciprocal temperature energy
γ	Gyromagnetic ratio
$\zeta_i(t)$	Cartesian component of the white noise term
θ	Polar angle of the magnetic moment in spherical coordinates
λ	Landau damping parameter
μ_0	Vacuum permeability
$\boldsymbol{\mu}$	Magnetic moment
μ_B	The Bohr magneton
$\boldsymbol{\mu}_S$	Saturation of the magnetic moment
ϕ	Azimuthal angle of magnetic moment in spherical coordinates
ω	Frequency of an AC field
ω_A	Frequency associated with the B_A field
b_{cr}	Critical reduced field
A	Exchange stiffness constant
B_A	Anisotropy field
B_C	Coercive field
D	Anisotropy energy strength
F	Free energy of the nanoparticle
\mathbf{H}^{eff}	Effective field calculated through the total energy
\mathcal{H}	Total energy of the nanoparticle
$\tilde{\mathcal{H}}$	Total energy of the nanoparticle in reduced units
K	Anisotropy energy density
S	Reduced magnetic moment
V	Nanoparticle's volume
Z	Partition function

1 Introduction

1.1 Motivation and Aims of the Thesis

Magnetic phenomena have always fascinated people and magnetism has been known for about thousands of years. However, the early usage of magnetism was limited to determining the location of north pole. A remarkable step ahead was made by J. C. Maxwell [1] who introduced in his famous work the concept of a field and explained magnetic and electric phenomena, and their interactions, within a unified picture. Maxwell's findings inspired further research in the area of electromagnetism and since that time both experimental and theoretical studies went hand in hand in uncovering a variety of new phenomena.

Later, the effects of resonant absorption of electromagnetic energy, e.g. Ferromagnetic Resonance (FMR), in (ferro-) magnetic samples were predicted (Arkad'ev [2]), and experimentally observed (Griffiths [3] and Zavoiskii [4]). The experiments of Stern and Gerlach [5] paved the way to establish the concept of the electron *spin*. The *exchange interaction* effect was discovered by Heisenberg [6] and Dirac [7] and finally the effect of *magnetic anisotropy* (e.g. the work of Meiklejohn and Bean [8] or basically [9]) they all build the fundamentals of solid state magnetism.

Together with the broadening of theoretical and experimental studies a necessity to access smaller dimensions of a magnetic solid emerged. Thus, the role of engineering and technical science arose as never before. As a result, new imaging techniques appeared: Scanning Electron Microscopy (SEM, 1935), Transmission Electron Microscopy (TEM, 1935), Atomic (Magnetic) Force Microscope (A(M)FM), Scanning Tunneling Microscopy (STM, 1981), and Spin-Polarized STM (SPSTM) to name but a few. At the same time methods for creating micro- and nano- structured objects down to one dimension were developed, such as Molecular Beam Epitaxy (MBE), Pulsed Laser Deposition (PLD) and chemically self-assembly methods. Together with experimental techniques, additionally designed for the micro- and nano- structures, e.g. Superconducting QUantum Interference Device (SQUID), Magneto Optical Kerr- Effect (MOKE) techniques, microwave spectroscopy (FMR, ESR, PSR) techniques and X-ray Magnetic Circular Dichroism (XMCD) techniques. These all furnish a new insight into the world of small (magnetic) structures.

Nowadays, interest in nanostructured magnetism is twofold. On the one hand, although there exists a huge number of magnetic phenomena, effects, theories and models describing them, magnetism as a whole is not fully understood, i.e. a unifying theory is still missing. Additionally, important discoveries made during the last decades (e.g. Giant- and Tunnel-Magneto Resistance, GMR and TMR, respectively) may lead to new findings. On the other hand, industrial applications ranging from magnetic sensors and medical equipment to high density storage devices is the driving force for new development and research.

In the present work we focus on magnetic nanoparticles as utilized in the information storage. The ultimate goal in information technology [10–13] is to store a bit of information on a single magnetic nanoparticle with two stable orientations of magnetization. One stable state is referred to as the "spin up" orientation or "logical one", whereas the other

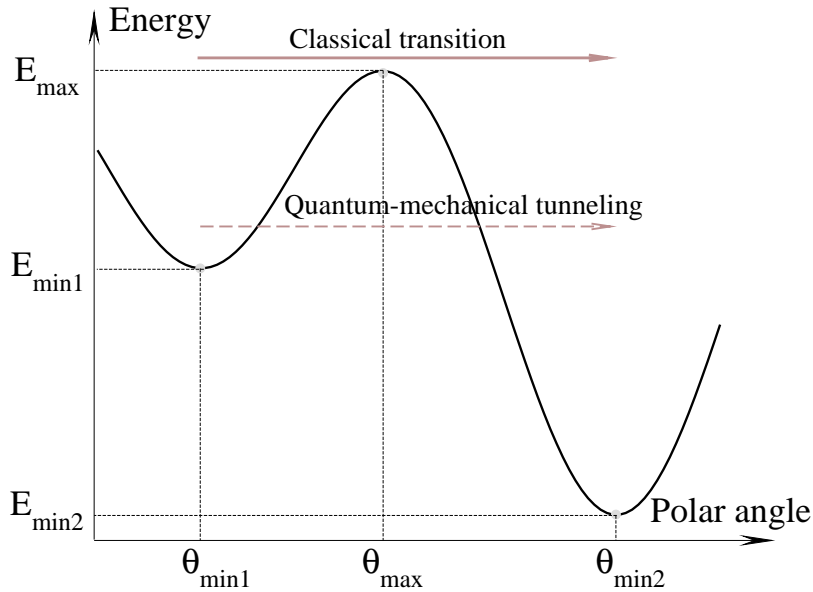


Figure 1.1: General representation of a two-level magnetic system. States, marked by $\theta_{\min1}$ and $\theta_{\min2}$ represent the energy minima of the magnetic moment. They are separated by a maximum θ_{\max} over which a classical transition or through which a quantum tunneling can occur.

state is noted as a "spin down" one or "logical zero" (energetically corresponding to the two minima in Fig. 1.1). The process of information writing amounts to changing the one state to the other. Reading of information can be achieved by detecting the orientation of the particle's magnetization. In this respect, the major questions for technological applications are:

- How to increase the density of information storage;
- How to access and control single storage units within the shortest time;
- How to save energy when reading or writing the information.

In the thesis it is aimed to address the second and the third questions from a fundamental point of view, whereas the first issue is rather technological and will be partly addressed in Chapter 2.

1.2 Energy Contributions to the magnetic Nanoparticle

In order to fulfil the simple picture of the two-level system shown in Fig. 1.1 one should list all possible effects that can influence the system. These effects might be expressed as

contributions to the total energy \mathcal{H} of the magnetic nanoparticle in the Heisenberg model

$$\begin{aligned} \mathcal{H} = & -J \sum_{\langle ij \rangle} \mathbf{s}_i \cdot \mathbf{s}_j - D f_A(\mathbf{S}) - \frac{\mu_0 \mu_1^2}{4\pi a^3} \sum_{i < j} \frac{3(\mathbf{s}_i \cdot \mathbf{e}_{ij})(\mathbf{e}_{ij} \cdot \mathbf{s}_j) - \mathbf{s}_i \cdot \mathbf{s}_j}{r_{ij}^3} \\ & - \mu_1 \mathbf{B} \sum_i \mathbf{s}_i. \end{aligned} \quad (1.1)$$

The first term stands for the exchange interaction with isotropic exchange constant J between the neighbor magnetic moments $\mathbf{s}_{i,j}$ within the nanoparticle. The second term describes the magnetocrystalline anisotropy contribution expressed by the function $f_A(\mathbf{S})$ which could be any anisotropy type that possesses two local minima. D denotes the anisotropy energy strength. The third term accounts for the dipole-dipole interaction between the magnetic moments within the nanoparticle with a lattice constant a and a magnetic moment per atom μ_1 . The magnetic moment is usually expressed in units of the Bohr magneton $\mu_B = 9.27 \cdot 10^{-24}$ J/T; $\mu_0 = 4\pi \cdot 10^{-7}$ Vs/(Am) is the vacuum permeability. \mathbf{e}_{ij} denote the unit vectors which point from the magnetic moment \mathbf{s}_i towards the \mathbf{s}_j , i.e. $\mathbf{e}_{ij} = (\mathbf{r}_j - \mathbf{r}_i)/|\mathbf{r}_j - \mathbf{r}_i|$ and $r_{ij} = |\mathbf{r}_j - \mathbf{r}_i|/a$. Finally, the last term expresses the Zeeman interaction with the external applied magnetic field \mathbf{B} .

Domain walls in nanoparticles. Magnetism is a collective phenomenon. This implies that the short ranged exchange interaction energy and the long ranged dipole-dipole energy compete. These considerations bring us to the first possible effect which may arise in magnetic nanoparticles - building of domain walls. Indeed, starting from a certain size of the nanoparticle a reduction of its dimension will not lead to a spatial variation of the spin orientations since this entails too much exchange energy. A critical diameter of the nanoparticle is usually compared with the domain wall thickness and reads [14]

$$d_c = 2\sqrt{\frac{A}{K}}, \quad (1.2)$$

where A is called the exchange stiffness and K is the anisotropy energy strength. Above the critical diameter d_c domain walls start to build leading to incoherent rotation of the spin orientations [15]. Rough estimates for the averaged values of $A = 10^{-11}$ J/m and $K = 10^6$ J/m³ for ferromagnetic nanoparticles [14] give the critical diameter around 60 nm. Therefore, we restrict ourselves to the range below the d_c .

Quantum-mechanical tunneling. The model which will be presented in the next chapters is valid for diameters below d_c . However, it fails for infinitely small magnetic systems, such as molecular magnets where quantum-tunneling effects show up (Fig. 1.1). This effect can be estimated within the Landau-Zener model [16, 17] using the following formula for the tunneling probability P [18]

$$P_{m,m'} = 1 - \exp \left[- \frac{\pi \Delta_{m,m'}^2}{2\hbar g \mu_B |m - m'| \mu_0 dB_z/dt} \right], \quad (1.3)$$

where m and m' are the quantum numbers associated with the energy gap $\Delta_{m,m'}$, dB_z/dt is the constant field sweeping rate, $g \approx 2$, and $\hbar = 1.05 \cdot 10^{-34}$ Js is the Planck constant. Quantum tunneling effect is negligible for the nanoparticles considered here.

Temperature effects. Once the system is coupled to a thermal bath thermal fluctuations may cause a reduction of the net magnetization when approaching the *Curie*-temperature

T_C , where the net magnetization can even vanish. Therefore, the model presented in Chapter 3 is valid well below T_C .

In contrast to that effect, which is of a purely static nature, another effect can arise when the time scale of the measurement τ_{meas} is longer than the mean time (*escape time*) τ

$$\tau = \tau_0 \exp \left[\frac{KV}{k_B T} \right] \quad (1.4)$$

needed for the nanoparticle with the volume V to escape from one minimum to the other (Fig. 1.1) due to thermal activation. This dynamical effect which will also be addressed in Chapter 3 is known as *superparamagnetism* and should be taken into account when considering the dynamical properties of the system.

The thesis is organized as follows. Chapter 2 describes the properties of the systems used for the calculations. Chapter 3 presents a detailed overview of static and dynamic models employed for the description of the system stability or dynamics. Different mechanisms of damping used in the Landau-Lifshitz-Gilbert (LLG) equation are listed and explained in Chapter 4. The next chapter is devoted to the numerical solution of the stochastic LLG equation. Chapter 6 includes results obtained for DC- and AC- continuous fields. Here the critical fields of a single-domain nanoparticle and the corresponding reversal times are calculated for both a uniaxial and a cubic anisotropy and at finite temperatures. Chapter 7 lists the main results acquired for the magnetization switching and control in the presence of magnetic pulses in the spirit of the local control theory (LCT) [19–21]. Finally, the last chapter concludes the thesis and provides an outlook for further calculations.

2 Systems studied

A steady demand to increase the storage density has led to new technologies in fabrication of information storage materials. The focus slowly shifted from cobalt-based ferromagnetic thin films that are commercially used at present for recording to ferromagnetic alloys fabricated via self-organization methods [22, 23]. Note, that when scaling down the volume of the nanoparticle V (equation (1.4)) in order to achieve the same stability ratio $KV/(k_B T)$, the anisotropy density constant K should at least be higher than in conventional cobalt-based materials. Surprisingly, in the ferromagnetic alloys addressed below this is exactly the case granting thus the usage of them as potential storage media even at room temperatures.

In the following we will concentrate on iron-platinum alloys $\text{Fe}_x\text{Pt}_{1-x}$, where x denotes the relative volume iron concentration expressed in per cents. The $\text{Fe}_x\text{Pt}_{1-x}$ alloys are chemically synthesized by the decomposition of iron pentacarbonyl, $\text{Fe}(\text{CO})_5$, and the reduction of platinum acetylacetonate, $\text{Pt}(\text{acac})_2$, in a solvent at high temperature [24]. Via combination of Fe- and Pt-containing species from the reduction of Pt salt an FePt nucleus is yielded. As a result each FePt-nanoparticle is surrounded by a thick organic coating layer. The size of the nanoparticles can easily be tuned in the range from several to ten nanometers via the molar ratio of Fe and Pt precursors. The distance as well as the form of such close-packed arrays can also be controlled. The process of formation of nanoparticles arrays is called nanoparticles self-assembly. The organic shell can be removed by a soft *in situ* hydrogen plasma treatment [25]. However, the nanoparticles obtained at this stage possess a disordered fcc structure and a low anisotropy constant. After a thermal annealing the particles change their inner structure to the fct with a maximal anisotropy constant value. Since the anisotropy value depends also on the concentration of iron, it reaches its maximum at around $x = 50\%$ [26]. This is called the maximal anisotropy constant of the $L1_0$ fct ordered phase for $\text{Fe}_x\text{Pt}_{1-x}$ with x centered around 50%, $K = 10^7 \text{ J/m}^3$ [24].

The dependence on temperature and on the magnetic moment of the anisotropy constant for $\text{Fe}_x\text{Pt}_{1-x}$ alloys is known in the literature and addressed on the basis of first principles method in [27, 28] and experimentally [29, 30].

For the model presented in this work the knowledge of the anisotropy type, i.e. $f_A(\mathbf{S})$ (equation (1.1)), is required. Anisotropy, which is a property of a ferromagnetic material to keep the magnetization in a certain direction or plane at thermal equilibrium, can be caused either by the crystal structure - magnetocrystalline anisotropy (MA), or by the form of the specimen - form anisotropy [9, 31]. Below the main factors of the MA are pointed out.

The exchange interaction given by the first term of equation (1.1) can not be responsible for the MA since it is space invariant. The spin-orbit coupling (SOC) is the main reason which causes the MA. Calculations of the magnetocrystalline anisotropy energy (MAE) and the type of it are usually based on the SOC and are widely addressed [32–34].

A clear picture emerges from a phenomenological model proposed by van Vleck [35]. He considered a pair interaction between the neighbor magnetic moments. The environment for each moment is included in the anisotropy energy reflecting the symmetry of the

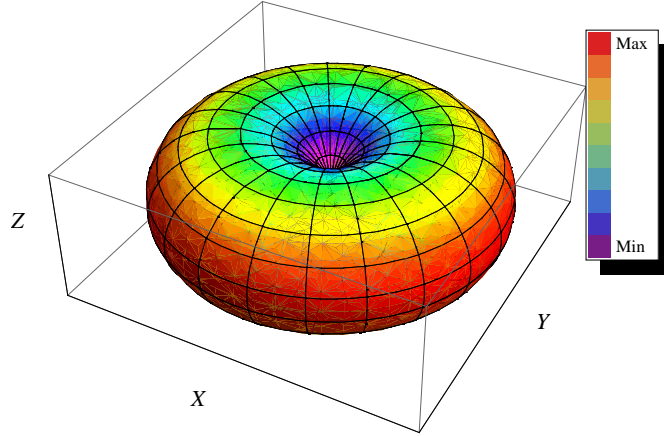


Figure 2.1: A schematic representation of the magnetocrystalline anisotropy of a uniaxial type aligned along the Z -direction, $K_2 > 0$

Fe ₅₀ Pt ₅₀					
Mean diameter	Magnetic moment	Anisotropy energy density	Anisotropy energy	Precessional period	Curie temperature
d, [nm]	μ_S , [μ_B]	K_2 , [J/m ³]	D, [J]	T^{prec} , [s]	T_C , [K]
6.3	22000	$5.9 \cdot 10^6$	$7.7 \cdot 10^{-19}$	$4.6 \cdot 10^{-12}$	710

Table 2.1: Parameters used for a Fe₅₀Pt₅₀-nanoparticle [36, 37]

crystal. An expansion of the anisotropy energy \mathcal{H}_a for the direction cosines $\alpha_i = \boldsymbol{\mu} \cdot \mathbf{e}_i$ is also proposed, where $\boldsymbol{\mu}$ denotes the magnetic moment of the nanoparticle. These considerations are consistent with the experimental data originally obtained as hysteresis loops in different directions of the crystal [9].

2.1 Uniaxial Anisotropy

For a uniaxial anisotropy no odd exponents of α_i in the \mathcal{H}_a expansion are allowed due to the rotational symmetry. Hence, one can write down for the expansion in case when the Z axis and the easy axis coincide [31]

$$\mathcal{H}_{ua} = -K_0 - K_2\alpha_z^2 - K_4\alpha_z^4 - \dots = -K_0 - K_2 \cos^2 \theta - K_4 \cos^4 \theta - \dots, \quad (2.1)$$

whereas all terms after K_2 will be truncated and K_0 can be omitted.

This anisotropy type is schematically shown in Fig. 2.1: For positive K_2 the magnetic moment $\boldsymbol{\mu}$ of the nanoparticle has two stable orientations 0 and π and they are separated by a maximum at $\pi/2$, which all are encoded by the color in Fig. 2.1.

Ab initio calculations reveal for the Fe₅₀Pt₅₀-nanoparticles a uniaxial anisotropy type

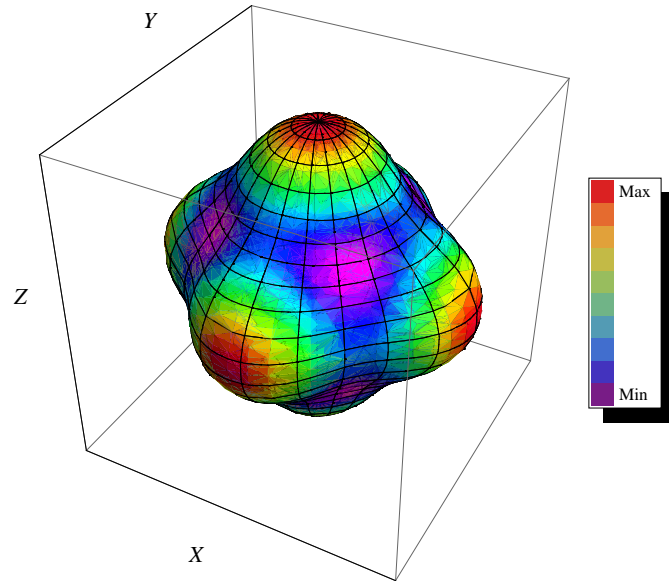


Figure 2.2: A schematic representation of the magnetocrystalline anisotropy of a cubic type, $K_4 > 0$

Fe ₇₀ Pt ₃₀					
Mean diameter	Magnetic moment	Anisotropy energy density	Anisotropy energy	Precessional period	Curie temperature
d, [nm]	μ_S , [μ_B]	K_4 , [J/m ³]	D, [J]	T^{prec} , [s]	T_C , [K]
2.3	2000	$8.0 \cdot 10^5$	$5.1 \cdot 10^{-21}$	$6.5 \cdot 10^{-11}$	420

Table 2.2: Parameters used for a Fe₇₀Pt₃₀-nanoparticle [29]

[36]; Various parameters are listed in Table 2.1.

2.2 Cubic Anisotropy

For a cubic anisotropy all odd terms in α_i and also terms dependent on α_i^2 vanish due to equivalence of the main axes X , Y , Z in a cubic crystal with respect to the change of sign. For the remaining terms the anisotropy energy reads [31]

$$\mathcal{H}_{ca} = -K_4(\alpha_x^2\alpha_y^2 + \alpha_y^2\alpha_z^2 + \alpha_x^2\alpha_z^2) - K_6(\alpha_x^4\alpha_y^4\alpha_z^4) - \dots \quad (2.2)$$

Truncation after the first term in equation (2.2) yields for the energy expressed via azimuthal (ϕ) and polar (θ) angles

$$\mathcal{H}_{ca} = -K_4(\cos^2 \phi \sin^2 \phi \sin^4 \theta + \sin^2 \theta \cos^2 \theta). \quad (2.3)$$

In Fig. 2.2 the energy landscape for a cubic anisotropy is demonstrated. In contrast to the uniaxial anisotropy type the cubic anisotropy possesses eight stable orientation of the

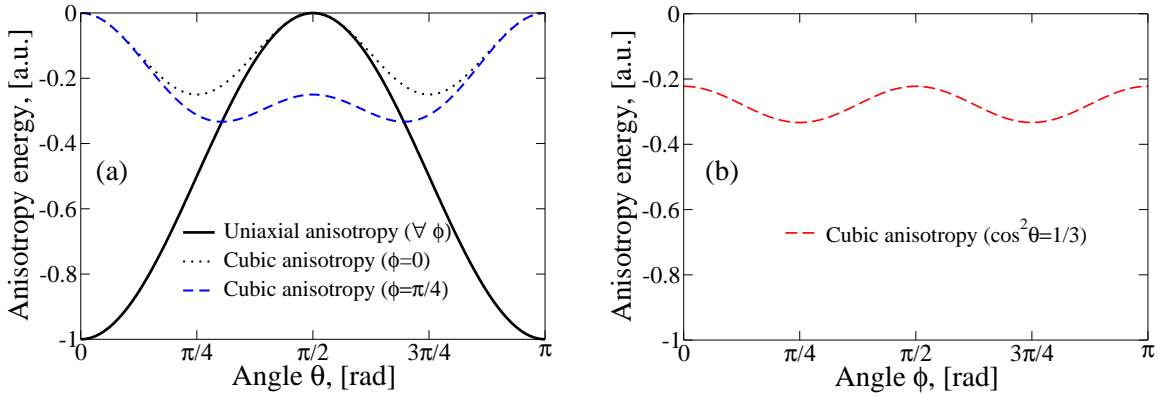


Figure 2.3: Anisotropy energy dependence on the polar angle θ (a) and on the azimuthal angle ϕ (b). The solid black line corresponds to the uniaxial anisotropy which can be imagined as a cut of the energy depending on θ and ϕ for a fixed ϕ (a). The cubic anisotropy is shown for both ϕ - and θ -cuts (other curves in both (a) and (b)).

magnetization in thermal equilibrium encoded with the violet in the figure. These are along $\langle 111 \rangle$ -directions if K_4 is positive.

For the cubic anisotropy $\text{Fe}_{70}\text{Pt}_{30}$ -nanoparticles are chosen [29]. Further parameters are recorded in Table 2.2.

2.3 Comparison of the Anisotropy Types

For applications a uniaxial anisotropy is the most popular, since it clearly indicates a parallel and an antiparallel state. It is well understood and relatively simple in the analytical treatment. When studying a cubic anisotropy a new concept of the switching process is demanded. Indeed, switching can be defined either as a one between the parallel and antiparallel states, thus, similar to the uniaxial anisotropy, or as a transition from a stable orientation to any other neighbor orientation. The last issue opens a perspective for saving more than one bit of information on the systems with a cubic anisotropy. Additionally, the question of the magnetization trajectory arises since not all paths are energetically equivalent (Fig. 2.2). This particular question will be addressed in Chapter 6.

Fig. 2.3 schematically shows a quantitative comparison of uniaxial and cubic anisotropies. The anisotropy constants K_2 and K_4 are chosen to be equal to one in arbitrary units. The uniaxial anisotropy creates a higher barrier (solid black curve) than that for the cubic anisotropy. The other curves are cross sections of the energy profile in Fig. 2.2 for fixed angles ϕ (a) and θ (b) passing through the corresponding minima.

3 Overview of Models and Methods

Before discussing our own results a brief overview of basic models and methods is given in this chapter. These might be classified into two groups: Static and dynamic.

Static in this context means that the system goes adiabatically (quasi statically) through all possible states. Additionally, one is interested here in the equilibrium final state. This treatment was the first and accounts for the Stoner-Wohlfarth model (SW) [38, 39], where, from energy minimization the hysteresis and magnetization states of a single domain ferromagnetic nanoparticle (Stoner particle) under the influence of an external magnetic field are derived. The Néel-Brown model [40–43] addresses properties of a Stoner particle coupled additionally to a thermal bath. Statistical methods [9, 44, 45] have been put forward. The main analytical tool is a partition function which includes all imaginable states of the system and allows the calculation of free energy, averaged magnetization or magnetic susceptibility, to name but a few.

Dynamically the properties of the system are handled such that all states are known for every moment in the time propagation. Knowing these nonequilibrium states the corresponding averaged quantities can be calculated using the stochastic Landau-Lifshitz-Gilbert (LLG) equation for the magnetization motion [46–48]. The Monte Carlo (MC) method [15, 49, 50] was used and the correspondence to the LLG Fokker-Planck (FP) equation [51, 52] is pointed out.

3.1 Static Treatment

3.1.1 Stoner-Wohlfarth Model

In the framework of the SW model [38, 39] a spherical magnetic nanoparticle with the volume V and magnetic moment at saturation μ_S is assumed to be in a single-domain state and with a uniaxial magnetocrystalline anisotropy of density K . Thermal fluctuations of the magnetic moment are ignored in this model. The particle is placed in an external magnetic field \mathbf{B} such that the easy axis and the Z axis of the coordinate system coincide. In the following the field applied will be expressed in the units of the coercive field $B_C = 2KV/\mu_S$, i.e. $\mathbf{b} = \mathbf{B}/B_C$, the anisotropy and total energies can thus be denoted in the units of the maximum uniaxial anisotropy energy $\mu_S B_C$. To simplify matters one restricts the treatment to a certain plane where the applied field and the magnetization lie (see Fig. 3.1). Thus, the total energy ϵ might be written down as

$$\epsilon = -\frac{1}{2} \cos^2 \theta - b \cos(\theta_b - \theta), \quad (3.1)$$

where θ and θ_b are the angles between the magnetization and the easy axis direction and between the applied field and the easy axis direction, respectively (Fig. 3.1).

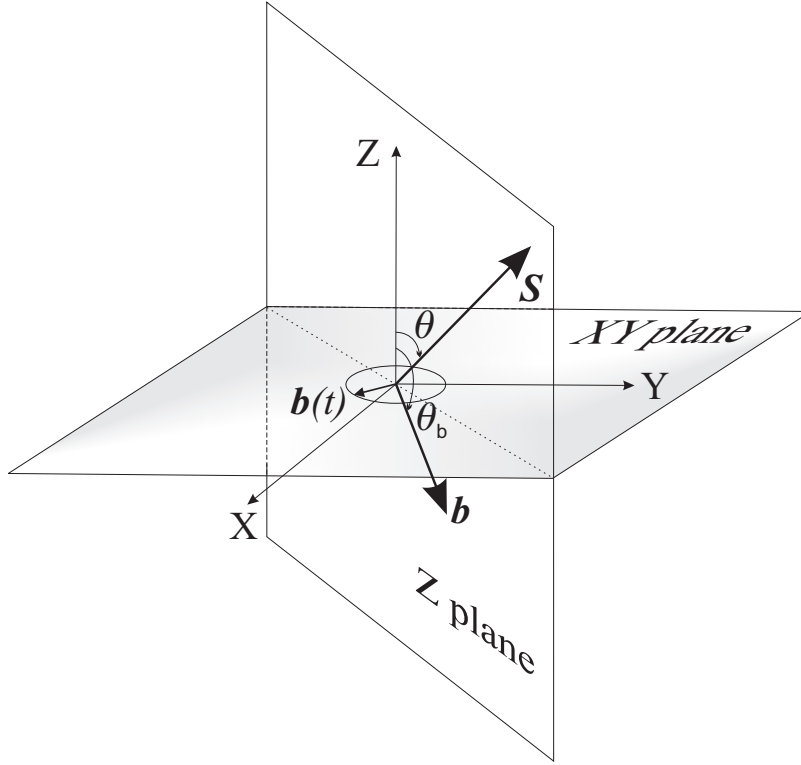


Figure 3.1: Alignment of the magnetic moment S and the static magnetic field b . A derivation for the SW astroid is based on the assumption that S changes in the same plane as b , denoted as the Z -plane.

Equilibrium states can be found from the condition $\partial\epsilon/\partial\theta = 0$ and the stability of the system is expressed by $\partial^2\epsilon/\partial\theta^2 = 0$. From the first condition we find

$$\frac{\partial\epsilon}{\partial\theta} = \cos\theta \sin\theta - b_{\perp} \cos\theta + b_{\parallel} \sin\theta = 0, \quad (3.2)$$

with the new notations $b_{\perp} = b \sin\theta_b$ and $b_{\parallel} = b \cos\theta_b$. Dividing the last equation by $\sin\theta \cos\theta$ we arrive at

$$\frac{b_{\perp}}{\sin\theta} - \frac{b_{\parallel}}{\cos\theta} = 1. \quad (3.3)$$

The stability condition yields

$$\frac{\partial^2\epsilon}{\partial\theta^2} = -\sin^2\theta + \cos^2\theta + b_{\perp} \sin\theta + b_{\parallel} \cos\theta = 0. \quad (3.4)$$

Equation (3.4) divided by $\sin^2\theta$ and under the assumption of equation (3.3) gives after simplification, $b_{\parallel} = -\cos^3\theta$. Inserting the last expression into equation (3.3) we find $b_{\perp} = \sin^3\theta$. The last two equations

$$\begin{cases} b_{\parallel} = -\cos^3\theta, \\ b_{\perp} = \sin^3\theta, \end{cases} \quad (3.5)$$

establish the so called Stoner-Wohlfarth astroid, a curve with four cusps and known mathematically as a hypocycloid [53]. In polar representation the dependence of b on θ_b is often used

$$b = \left[\cos^{\frac{2}{3}}\theta_b + \sin^{\frac{2}{3}}\theta_b \right]^{-\frac{3}{2}}. \quad (3.6)$$

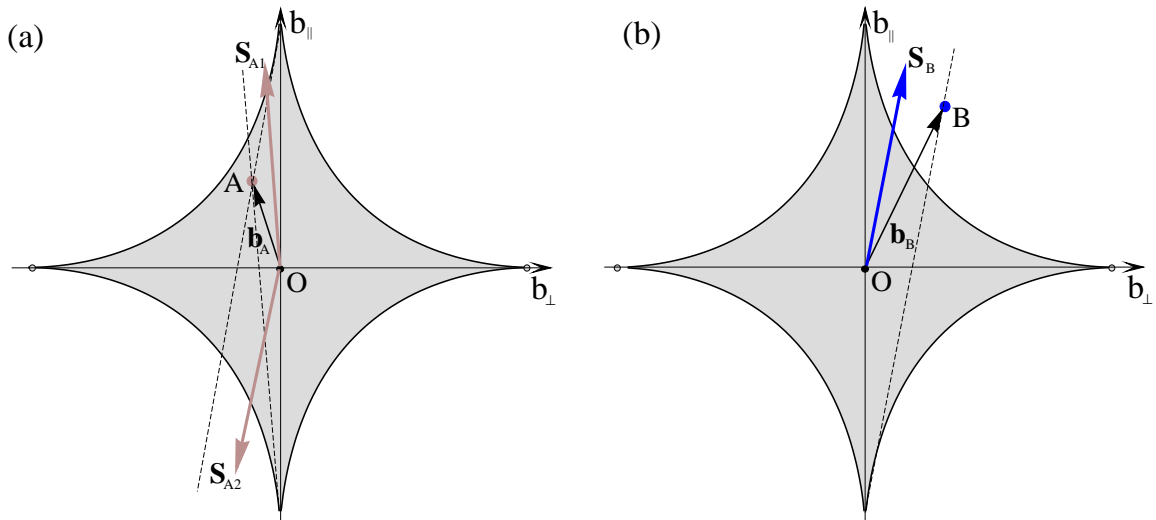


Figure 3.2: The Stoner-Wohlfarth astroid. The easy axis is aligned along the Y axis in the figure (b_{\parallel}) and the hard axis is denoted with b_{\perp} . The astroid separates stable states of the magnetic moment \mathbf{S}_{A1} and \mathbf{S}_{A2} , where no switching occurs (a), from those where the reversal takes place and only one stable orientation of the magnetic moment \mathbf{S}_B is realized (b).

The Stoner-Wohlfarth astroid is schematically illustrated in Fig. 3.2 and represents a distribution of switching fields in equilibrium. The astroid separates the stable states (filled area), where no switching of the magnetization from the parallel to the antiparallel orientations occurs, from those where a magnetization reversal is realized (unfilled area). At the same time the astroid shows a dependence of switching fields on the relative orientation of the applied field with respect to the easy axis. The smallest switching field achievable in this respect at zero temperature is under the angle of $3\pi/4$.

By using the Slonczewski graphical method [54] one can also find the orientation of the magnetization in equilibrium. First, one connects points O and A (Fig. 3.2 (a)) which means the direction of the applied field (\mathbf{b}_A). Then, one connects the point A and the tangents to the astroid close to the easy axis (b_{\parallel} -axis). Lines that are parallel to the tangents and going through the point O give the magnetization orientations \mathbf{S}_{A1} and \mathbf{S}_{A2} in equilibrium. The existence of two such fields implies that the field applied does not exceed the switching field. When repeating the same procedure for the point B (Fig. 3.2 (b)) one obtains the only orientation of the magnetization in equilibrium. Since point B is out of the astroid there exists only one stable orientation \mathbf{S}_B in the part where the field is applied.

It was recently shown that the so called dynamical SW astroid exists [55], which differs from the static one. Applying an external magnetic field, perpendicularly to the easy axis the solution of the Landau-Lifshitz-Gilbert equation provides a lowering of fields close to the b_{\perp} axis.

A graphical solution for any anisotropy type and for two- and three-dimensional SW astroids has been found [56, 57]. It might be useful for experimentally determining the switching fields when the anisotropy type is unknown.

The influence of temperature on the astroid has been studied experimentally [58] and theoretically [59].

3.1.2 Néel-Brown Model

In [40] Néel suggested a way to describe the mean time at which the magnetization of a ferromagnetic nanoparticle in a single domain state overcomes the potential barrier $\Delta E = |E_{\min 2} - E_{\min 1}|$ (Fig. 1.1) with the Arrhenius law

$$\tau = \tau_0 e^{\frac{\Delta E}{k_B T}}. \quad (3.7)$$

Originally, this was done for the probability of escaping a state which is a reciprocal function of the escape time.

On the basis of equation (3.7) the effect of *superparamagnetism* can be elucidated. Suppose, one measures with a certain time τ_{meas} for temperatures well below the Curie-temperature. When $\tau_{\text{meas}} > \tau$, one would measure a zero net magnetization. Hence, one obtains superparamagnetic behavior. For $\tau_{\text{meas}} < \tau$ the probability of thermal switching is non-zero, however, without a magnetic field applied the switching does not take place. These considerations illustrate that superparamagnetism is a dynamical effect.

In the absence of any applied field and when the system has a uniaxial symmetry the energy barrier is $\Delta E = KV$. If the temperature is too low to cause the switching or the time scale of measurement is too short a magnetic field could assist the switching. We assume an external field is applied under the angle $\theta_b = \pi$ (Fig. 3.1). The energy of the particle in reduced units transforms thus from equation (3.1) to

$$\epsilon = -\frac{1}{2} \cos^2 \theta + b \cos \theta. \quad (3.8)$$

The derivative, $\partial\epsilon/\partial\theta$ gives

$$\frac{\partial\epsilon}{\partial\theta} = \sin \theta (\cos \theta - b) = 0. \quad (3.9)$$

This equation reveals that the system possesses two minima, namely $\theta_{\min 1} = 0$ and $\theta_{\min 2} = \pi$ (with $\epsilon(\theta_{\min 1}) = -1/2 + b$, $\epsilon(\theta_{\min 2}) = -1/2 - b$), and a maximum $\cos(\theta_{\max}) = b$ ($\epsilon(\theta_{\max}) = b^2/2$). The height of the potential barrier ($\Delta E = \Delta\epsilon\mu_S B_C$) caused by the uniaxial anisotropy and changed by the magnetic field when $b < 1$ is

$$\Delta\epsilon = \epsilon(\theta_{\max}) - \epsilon(\theta_{\min 1}) = \frac{b^2}{2} + 1 - b = \frac{1}{2}(1 - b)^2. \quad (3.10)$$

Assuming equations (3.7) and (3.9) we finally come to

$$\tau = \tau_0 e^{\frac{KV}{k_B T}(1-b)^2}. \quad (3.11)$$

At the beginning Néel supposed τ_0 to be a constant. Further studies [60–62] showed that τ_0 is a complicated function of the applied field, anisotropy type, temperature and dynamical damping. Brown [43], using the stochastic Landau-Lifshitz-Gilbert equation, where in addition to the deterministic effective field he included an additive white noise, constructed the corresponding Fokker-Planck equation (section 3.2.4). From it he derived escape rates for the limit $\Delta E \gg k_B T$

$$\tau_0 = \frac{1 + \alpha^2}{\alpha} \frac{1}{\gamma B_C} \sqrt{\frac{k_B T}{KV(1-b)^2}} \frac{\pi}{1 - b^2}, \quad (3.12)$$

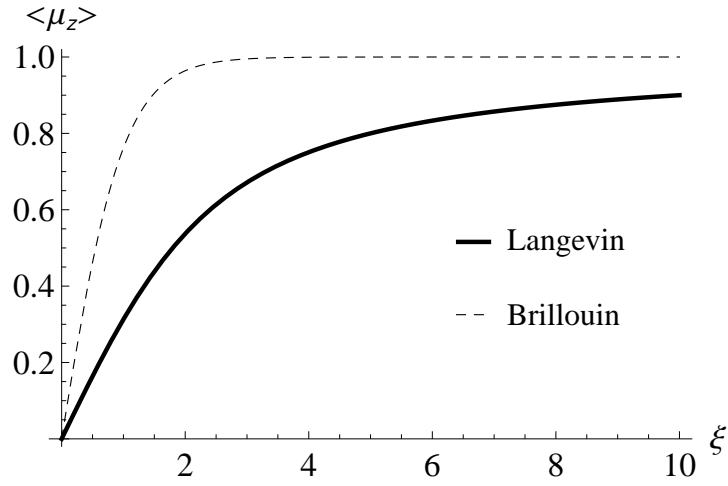


Figure 3.3: Projection of the magnetic moment onto the field direction as a function of the external magnetic field and temperature $\xi = \mu_S B / (k_B T)$, calculated for the isotropic case (Langevin-function) and the case of infinite anisotropy (Brillouin-function).

where α is a dimensionless magnetization damping in a Gilbert form (Section 3.2.1 and Chapter 4). Expressions (3.10) and (3.11) form the main results of the Néel-Brown model which addresses the stability of the magnetization of a small ferromagnetic nanoparticle with a uniaxial anisotropy under the influence of an external magnetic field along with thermal fluctuations.

3.1.3 Statistical Solution

The equilibrium properties of a small ferromagnetic nanoparticle can be addressed with statistical methods [44]. Consider a canonical ensemble (where exchange of heat between the system and the environment occurs) with a total energy E . From statistical mechanics the canonical partition function is [44]

$$Z = \sum_i e^{-\beta E_i} = \text{Sp}(e^{-\beta E_i}), \quad (3.13)$$

where the summation runs over the eigenvalues and $\beta = 1/(k_B T)$. Let us assume we are dealing with a semiclassical system (the magnetic moment is large). Hence, the summation in (3.13) can be replaced by the integral over all states in spherical coordinates

$$Z = \frac{1}{V} \int_V e^{-\beta E} dV \rightarrow \int_\theta \int_\phi e^{-\beta E} \sin \theta d\theta d\phi. \quad (3.14)$$

The average magnetic moment $\langle \mu \rangle$ in an external magnetic field \mathbf{B} is the field derivative of the free energy F

$$\langle \mu \rangle = -\frac{\partial F}{\partial \mathbf{B}}, \quad (3.15)$$

with $F = -k_B T \ln Z$. Introducing a new variable $\xi = \mu_S \mathbf{B} / (k_B T)$ expression (3.15) then reads

$$\langle \mu \rangle = -\mu_S \frac{1}{Z} \frac{\partial Z}{\partial \xi}. \quad (3.16)$$

The free energy of a small ferromagnetic nanoparticle can be written

$$F = -KV \cos^2 \theta + \mu_S B \cos \theta. \quad (3.17)$$

Keeping in mind the expression for ξ being a projection onto the field direction and introducing $\zeta = \beta KV$ and $x = \cos \theta$ the partition function becomes

$$Z = 2\pi \int_{-1}^{+1} e^{-\zeta x^2 - \xi x} dx. \quad (3.18)$$

Note that the field is applied antiparallel to the initial state of the magnetic moment. The partition function can be calculated exactly via the error function

$$\text{Erf}(x) = (2/\sqrt{\pi}) \int_0^x e^{-t^2} dt \quad [63, 64]$$

$$Z = \frac{\sqrt{\pi}}{2\sqrt{\zeta}} e^{-\frac{\xi^2}{4\zeta}} \left[\text{Erf} \left(\sqrt{\zeta} + \frac{\xi}{2\sqrt{\zeta}} \right) + \text{Erf} \left(\sqrt{\zeta} - \frac{\xi}{2\sqrt{\zeta}} \right) \right]. \quad (3.19)$$

Using formula (3.16) we find

$$\langle \mu_z \rangle = -\mu_S \left(-\frac{\xi}{2\zeta} + \frac{2}{\sqrt{\pi\zeta}} \frac{e^{\xi + \frac{\xi^2}{4\zeta}} \sinh \xi}{\left[\text{Erf} \left(\sqrt{\zeta} + \frac{\xi}{2\sqrt{\zeta}} \right) + \text{Erf} \left(\sqrt{\zeta} - \frac{\xi}{2\sqrt{\zeta}} \right) \right]} \right). \quad (3.20)$$

From a fundamental point of view two particular cases are interesting: An isotropic case ($\zeta = 0$); and a case with an infinite anisotropy. Thus, when $\zeta = 0$ the partition function is

$$Z_{\zeta \rightarrow 0} = \frac{2\pi}{\xi} 2 \sinh \xi. \quad (3.21)$$

The averaged magnetic moment of a ferromagnetic nanoparticle is given by the Langevin function

$$\langle \mu_z \rangle_{\zeta \rightarrow 0} = -\mu_S \left(\frac{1}{\tanh \xi} - \frac{1}{\xi} \right). \quad (3.22)$$

The case with the infinite uniaxial anisotropy can be understood as if only two states in the system would have been allowed, namely with $+\mu$ and $-\mu$. The partition function is then $Z = e^\xi + e^{-\xi}$ and thus the averaged magnetic moment

$$\langle \mu_z \rangle_{\zeta \rightarrow \infty} = -\mu_S \tanh \xi. \quad (3.23)$$

This expression is known in the literature as a Brillouin 1/2 function.

Both functions are shown in Fig. 3.3 as a function of ξ . This might be interpreted as a function of either the external magnetic field or of the inverse temperature. This graph clearly demonstrates that the averaged magnetic moment of a small particle is always between the Langevin or Brillouin 1/2 functions. The Brillouin 1/2 function depicts a saturation at smaller fields since only two states are allowed, whereas the Langevin function allows for many states between the parallel and antiparallel states of the magnetic moment.

Fig. 3.3 clearly illustrates what happens from a statistical point of view with the magnetic moment when an external magnetic field is applied. However, when the field is zero the magnetic moment vanishes according to this figure which is not the case for a ferromagnet. Indeed, this physical picture is valid for an ideal paramagnet and for a ferromagnet

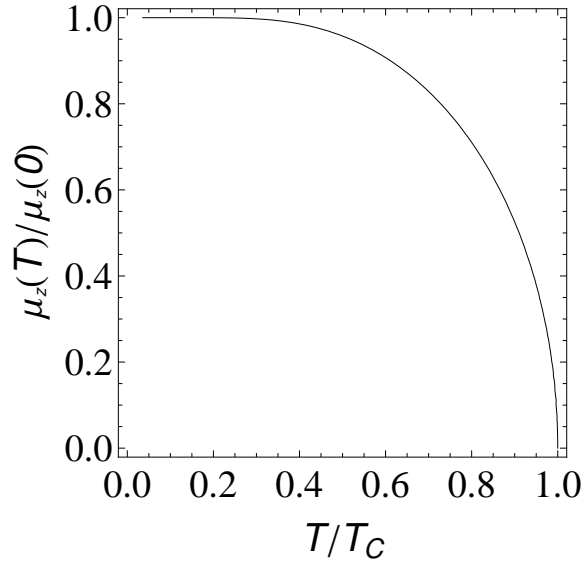


Figure 3.4: Temperature dependence of the net magnetic moment for a ferromagnet.

the external field should be replaced by a molecular field $B = \kappa \langle \mu_z \rangle$ [9]. Therefore, the net magnetic moment of a ferromagnet in the absence of an external field is

$$\langle \mu_z \rangle = \mu_S \tanh \left(\frac{\mu_S \kappa \langle \mu_z \rangle}{k_B T} \right). \quad (3.24)$$

This dependence is represented in Fig. 3.4: Approaching the Curie temperature the magnetic moment gradually diminishes. For instance, even at $T/T_C = 0.9$ the magnetic moment is 1/2 of its saturation value.

3.2 Dynamic Treatment

3.2.1 Stochastic Landau-Lifshitz-Gilbert Equation

Suppose $\mathbf{S} = \boldsymbol{\mu}/\mu_S$ is a unit vector of a magnetic moment with saturation μ_S . In an effective field \mathbf{H}^{eff} the magnetic moment precesses. Landau and Lifshitz [46] proposed an equation describing the dynamics of such a moment

$$\frac{d\mathbf{S}}{dt} = -\gamma [\mathbf{S} \times \mathbf{H}^{\text{eff}}] - \lambda\gamma [\mathbf{S} \times [\mathbf{S} \times \mathbf{H}^{\text{eff}}]], \quad (3.25)$$

where $\gamma = |e|g_e/(2m_e) = 1.76 \cdot 10^{11}(\text{Ts})^{-1}$ is the gyromagnetic ratio and λ is dimensionless. The effective field is defined as a gradient of the total energy \mathcal{H} (real units) with respect to \mathbf{S}

$$\mathbf{H}^{\text{eff}} = -\frac{1}{\mu_S} \frac{\partial \mathcal{H}}{\partial \mathbf{S}}. \quad (3.26)$$

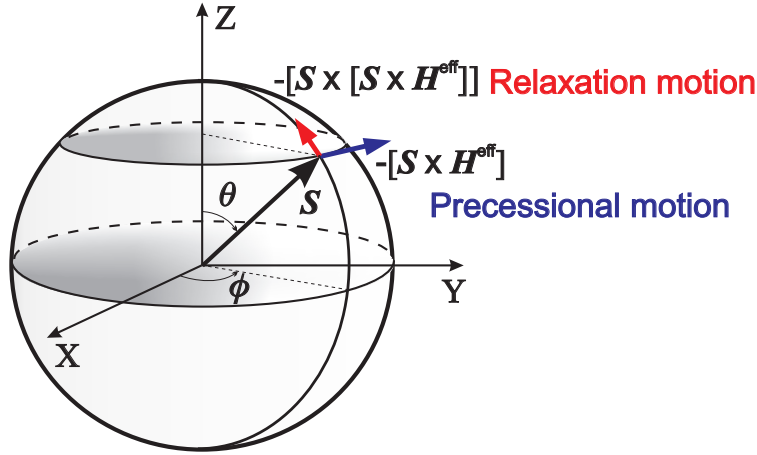


Figure 3.5: Schematic illustration of torques acting on the magnetization vector introduced by the Landau-Lifshitz-Gilbert equation of motion. The precessional term is shown with a blue vector, the relaxation term is marked by a red vector. The direction of the effective field \mathbf{H}^{eff} is along the Z axis.

Equation (3.25) is called the Landau-Lifshitz (LL) equation. Conventionally both terms are denoted as exchange terms. The absolute value of the magnetic moment is conserved. Fig. 3.5 depicts the meaning of both terms in the LL equation. The first term stands for a precessional motion of the magnetic moment around the effective field, whereas the second term describes a relaxation motion towards the effective field with a relaxation rate λ . Initially, Landau and Lifshitz did not focus on the origins of the relaxation, but simply qualitatively explained this process. However, somewhat later it was noticed that the LL equation leads to wrong physical results for high damping λ . Indeed, for $\lambda \gg 1$ the derivative $\dot{\mathbf{S}} \rightarrow -\infty$, although it should vanish. This problem was solved by Gilbert who phenomenologically introduced another equation of motion [47, 48, 65]

$$\frac{d\mathbf{S}}{dt} = -\gamma [\mathbf{S} \times \mathbf{H}^{\text{eff}}] + \alpha \left[\mathbf{S} \times \frac{d\mathbf{S}}{dt} \right], \quad (3.27)$$

where the dimensionless damping parameter α was introduced via the Rayleigh dissipation function [48]. Geometrically, the Gilbert equation yields the same physical picture for the precession and relaxation as the LL equation. Moreover, the Gilbert equation can be brought to the form of the LL equation, namely

$$\frac{d\mathbf{S}}{dt} = -\frac{\gamma}{1 + \alpha^2} [\mathbf{S} \times \mathbf{H}^{\text{eff}}] - \frac{\alpha\gamma}{1 + \alpha^2} [\mathbf{S} \times [\mathbf{S} \times \mathbf{H}^{\text{eff}}]]. \quad (3.28)$$

Usually in the literature [10, 66], this equation is referred to as the Landau-Lifshitz-Gilbert (LLG) equation.

Albeit the LLG equation was phenomenologically introduced, the precession motion can be explained from the quantum-mechanical point of view, namely when considering the Heisenberg equation of motion in the classical limit [67]. The microscopic origins of the damping process will be addressed in chapter 4.

A qualitative interpretation of damping without any microscopic details can be found in [68]. In equation (3.25) for $\lambda \rightarrow 0$ the effective field \mathbf{H}^{eff} is determined by the immediate magnetic configuration. This can only be the case for a very slow magnetization motion

which allows all relevant microscopic degrees of freedom to immediately readjust themselves to the changing magnetization. When this is not true, the effective field requires a certain time delay which is related to the dissipation. Thus,

$$\mathbf{H}^{\text{eff}}(t) \rightarrow -\frac{\partial \mathcal{H}(\mathbf{S}(t - \tau))}{\partial \mathbf{S}} \approx \mathbf{H}^{\text{eff}} - \tau \left(\frac{\partial \mathbf{S}}{\partial t} \cdot \frac{\partial}{\partial \mathbf{S}} \right) \mathbf{H}^{\text{eff}}. \quad (3.29)$$

Inserting the effective field in form of equation (3.29) into the (3.25) for $\lambda \rightarrow 0$ we end up with the equation similar to that of Gilbert.

The assumption that all states of the magnetic moment belong to the sphere (Fig. 3.5) allows for the usage of the LLG in spherical coordinates with two spacial coordinates ϕ and θ . Further the LLG will be employed in the following form [10]

$$\begin{cases} (1 + \alpha^2) \frac{d\phi}{dt} = \frac{1}{\sin \theta} \cdot \frac{\partial \tilde{\mathcal{H}}}{\partial \theta} - \frac{\alpha}{\sin^2 \theta} \cdot \frac{\partial \tilde{\mathcal{H}}}{\partial \phi}, \\ (1 + \alpha^2) \frac{d\theta}{dt} = -\frac{1}{\sin \theta} \cdot \frac{\partial \tilde{\mathcal{H}}}{\partial \phi} - \alpha \cdot \frac{\partial \tilde{\mathcal{H}}}{\partial \theta}, \end{cases} \quad (3.30)$$

where the total energy $\tilde{\mathcal{H}}$ is expressed in units of the uniaxial anisotropy field $\mu_S B_A$ with $B_A = 2D/\mu_S$. Time is expressed in units of the field-free precessional time $t \leftarrow t\gamma B_A$. The LLG equation in form (3.28) together with (3.26) is unable to address the properties of magnetization dynamics when the system is coupled to the thermal bath. W. F. Brown [43] proposed to extend the effective field with an additional white noise term ζ that takes into account thermal fluctuations

$$\mathbf{H}^{\text{eff}}(t) = -\frac{1}{\mu_S} \frac{\partial \mathcal{H}}{\partial \mathbf{S}} + \boldsymbol{\zeta}(t). \quad (3.31)$$

Similar to the Brownian motion of microscopic particles in a liquid, the characteristics of the additive noise are

$$\begin{aligned} \langle \zeta_i(t) \rangle &= 0, \\ \langle \zeta_i(t) \zeta_j(t + \Delta t) \rangle &= q \delta_{ij} \delta(\Delta t), \end{aligned} \quad (3.32)$$

with i and j being the Cartesian components of ζ and Δt the time interval. Such characteristics are typical for Gaussian-distributed *Markov processes* (no correlations in time) [45, 51]. The coefficient q could be found using the Fluctuation-Dissipation Theorem [44, 45]. Generally, processes other than Markov could be considered. In particular, the role of colored noise (an *Ornstein-Uhlenbeck* process [51]) might also be considered, however, we will focus on the properties of white noise (cf. equation (3.32)) in this work.

Thus, taking into account equations (3.28) or (3.30) and (3.31) together with (3.32) we mathematically deal with a nonlinear stochastic first order ordinary differential equation, leaving the aspects of numerical simulations for one of the further chapters.

3.2.2 Equations similar to the Landau-Lifshitz-Gilbert

Besides the LL (3.25) and the LLG (3.28) equations a general type of equation of the magnetization motion can be considered [69] due to expansion of the change of the magnetic moment into three orthogonal vectors

$$\frac{d\mathbf{S}}{dt} = A\mathbf{S} + B[\mathbf{S} \times \mathbf{H}^{\text{eff}}] + C[\mathbf{S} \times [\mathbf{S} \times \mathbf{H}^{\text{eff}}]] + \dots \quad (3.33)$$

This equation includes the effect of the modulus variation of \mathbf{S} . This becomes important when approaching the Curie-temperature of a ferromagnet (cf. Fig. 3.4). One of the equations taking into account the effect of modulus change of \mathbf{S} is the Landau-Lifshitz-Bloch equation [70]. It reads (in the notations of [70])

$$\frac{d\mathbf{S}}{dt} = -\gamma [\mathbf{S} \times \mathbf{H}^{\text{eff}}] - \Lambda_N \left(1 - \mathbf{S} \frac{\boldsymbol{\xi}}{\xi}\right) \mathbf{S} - \gamma\lambda \left(1 - \frac{1}{\xi}\right) [\mathbf{S} \times [\mathbf{S} \times \mathbf{H}^{\text{eff}}]], \quad (3.34)$$

where $\Lambda_N = 2\lambda\gamma k_B T / \mu_S$ is the Néel attempt frequency and $\boldsymbol{\xi} = \mu_S \mathbf{B} / (k_B T)$ is the reduced field.

Another class of ferromagnetic dynamical equations are variants of the Bloch equations [71]. These equations typically have two relaxation times: One for the component of the magnetic moment parallel to the effective field \mathbf{H}^{eff} and one for the perpendicular component, T_1 (longitudinal) and T_2 (transversal), respectively. The Bloch-Bloembergen equation can be written

$$\frac{d\mathbf{S}}{dt} = -\gamma [\mathbf{S} \times \mathbf{H}^{\text{eff}}] - \frac{\mathbf{S} \cdot \mathbf{H}^{\text{eff}} - H^{\text{eff}}}{T_1} \frac{\mathbf{H}^{\text{eff}}}{(H^{\text{eff}})^2} - \frac{(S_x \mathbf{e}_x + S_y \mathbf{e}_y)}{T_2}. \quad (3.35)$$

3.2.3 Monte Carlo Method

The Monte Carlo (MC) method can also be applied to handle the problem of magnetization stability. Here, we point out the essential issues of the method.

The MC method can be defined as a method that describes the states of a system on the basis of physical laws by use of random numbers [52]. In fact, every numerical method where random numbers play an important role might be called a MC method.

Random numbers reproduce stochastic processes coming about in almost all realistic physical systems and are caused by thermal fluctuations of any quantity in the system. MC methods can be successfully applied when one is not interested in details of fluctuations of any quantity but in equilibrium thermodynamics implying an average of a large number of the stochastic states. One usually defines a stochastic process used in the MC simulations as a Markov process [72], i.e. a process where all states in the future do not depend on the past.

Now it will be demonstrated what forms a basis for MC-methods. Imagine we have a system which is a canonical ensemble. Assume, for any state S_i there exists an energy of the state E_{S_i} . Suppose $P_{S_i}(t)$ is a probability to be in state S_i for the time t and $P_{S_j}(t)$ is a probability to stay in state S_j for t . Then, the Master equation (ME) [52] for changing the probability to be in state $P_{S_i}(t)$ is

$$\frac{dP_{S_i}(t)}{dt} = \sum_{S_j} \left(P_{S_j}(t) W(S_j, S_i) - P_{S_i}(t) W(S_i, S_j) \right). \quad (3.36)$$

Here the sum is calculated over all possible states S_j . $W(S_i, S_j)$ and $W(S_j, S_i)$ are the transition rates from S_i to S_j and S_j to S_i , respectively.

In thermodynamic equilibrium

$$\sum_{S_j} P_{S_j}(t) W(S_j, S_i) = \sum_{S_j} P_{S_i}(t) W(S_i, S_j), \quad (3.37)$$

is valid, where $P_{S_i, j} = P_{S_i, j}(t)$.

On the other hand it is obvious that for any state S_j

$$P_{S_j}(t)W(S_j, S_i) = P_{S_i}(t)W(S_i, S_j). \quad (3.38)$$

The latter condition is known as the Detailed Balance Principle (DBP) [52]. From the last equation one can find

$$\frac{W(S_i, S_j)}{W(S_j, S_i)} = \frac{P_{S_j}}{P_{S_i}}. \quad (3.39)$$

A canonical ensemble obeys the Boltzmann distribution, where the probability to be in the state S_i or S_j is

$$P_{S_i, j} = \frac{e^{-\frac{E_{S_i, j}}{k_B T}}}{Z}, \quad (3.40)$$

with Z the partition function $Z = \sum_{S_j} e^{-\frac{E_{S_j}}{k_B T}}$. The summation runs through all states.

Using equations (3.40) and (3.39) one can easily find

$$\frac{W(S_i, S_j)}{W(S_j, S_i)} = \frac{P_{S_j}}{P_{S_i}} = e^{\frac{E_{S_i} - E_{S_j}}{k_B T}}. \quad (3.41)$$

This relation is the key point for the MC method since it obeys the ME in equilibrium.

Usually, numerically one uses either the *Metropolis algorithm* [50] which defines the transition rate as

$$\begin{cases} W(S_i, S_j) = 1, & \text{if } E_{S_j} - E_{S_i} \leq 0 \\ W(S_i, S_j) = e^{-\frac{E_{S_i} - E_{S_j}}{k_B T}}, & \text{otherwise,} \end{cases} \quad (3.42)$$

or the *Glauber algorithm* [49]

$$W(S_i, S_j) = \frac{1}{1 + e^{-\frac{E_{S_i} - E_{S_j}}{k_B T}}}. \quad (3.43)$$

It is not difficult to show that both of these algorithms satisfy the relation (3.41) and hence the DBP as well.

Historically, first MC simulations for magnetic systems were applied to the Ising model [73], where only two states of magnetic moment were permitted, namely $+1$ and -1 . In such system, also called a system with an infinite anisotropy (expression (3.23)), the question of time step does not arise, since there exists only one possible next state. In the quasi-classical system studied here, there are many states between $+1$ and -1 . Thus, the question of time quantification may arise. In the literature one usually assumes a *single-spin flip algorithm*, which means that a trial step for a single spin is made. The whole procedure works as follows [15, 74]:

- First, one chooses randomly or regularly some spin S_i .
- Then, one makes a trial time step such that one ends up with the spin S_j . The method of making the trial step can be different [15].

- After this one calculates the change of energy $E_{S_i} - E_{S_j}$. To decide, whether this step is accepted a random number $r \in [0; 1]$ is generated. In the case if $r < W(S_i; S_j)$, the trial step is accepted and the procedure can be repeated with other spins. Note, that $W(S_i, S_j)$ is calculated with either Metropolis or Glauber algorithms. One step for a spin is called a Monte Carlo Step (MCS).

Thus, this procedure can be repeated many times by finally averaging over all states to calculate a static quantity of interest, e.g. the average magnetic moment.

3.2.4 Fokker-Planck Equation

The general Fokker-Planck (FP) equation [51, 75] for several variables describes the time evolution of the distribution function $P(\{x\}, t)$ of N macroscopic variables $\{x\} = x_1, \dots, x_N$

$$\frac{\partial P(\{x\}, t)}{\partial t} = \left[- \sum_{i=1}^N \frac{\partial}{\partial x_i} D_i^{(1)}(\{x\}) + \sum_{i=1}^N \frac{\partial^2}{\partial x_i \partial x_j} D_{ij}^{(2)}(\{x\}) \right] P(\{x\}, t), \quad (3.44)$$

where $D_i^{(1)}(\{x\})$ is a drift vector and $D_{ij}^{(2)}(\{x\})$ is a diffusion vector. By solving the FP equation one obtains distribution functions from which any averages of macroscopic variables can be found via integration.

This equation can be applied to the broad variety of nonequilibrium phenomena including Brownian motion of small particles, laser physics and others. We will construct a FP equation which corresponds to the stochastic LLG equation of motion. For this we consider the LLG in the form of equation (3.28) inserting there a relation for the effective field (3.31) with the properties (3.32). Separating between the deterministic and the stochastic parts in this equation we come to the Langevin type equation which generally might be expressed as

$$\frac{dS_i}{dt} = A_i(S_i, t) + \sum_k B_{ik}(\mathbf{S}, t) \zeta_k(t), \quad (3.45)$$

where S_i are the cartesian components of the reduced magnetic moment and $A_i(S_i, t)$, $B_{ik}(\mathbf{S}, t)$ are the deterministic and the stochastic parts of the LLG equation with the thermal noise components $\zeta_k(t)$. The corresponding FP equation is then [51]

$$\frac{\partial P}{\partial t} = - \sum_i \frac{\partial}{\partial S_i} \left[\left(A_i + q \sum_{jk} B_{jk} \frac{\partial B_{ik}}{\partial S_j} \right) P \right] + \sum_{ij} \frac{\partial^2}{\partial S_i \partial S_j} \left[\left(q \sum_k B_{ik} B_{jk} \right) P \right]. \quad (3.46)$$

Simplifying the second sum in equation (3.46) we find [76]

$$\frac{\partial P}{\partial t} = - \sum_i \frac{\partial}{\partial S_i} \left[A_i - q \sum_k B_{ik} \left(\sum_j \frac{\partial B_{jk}}{\partial S_j} \right) - q \sum_{jk} B_{ik} B_{jk} \frac{\partial}{\partial S_j} \right] P. \quad (3.47)$$

Comparing (3.45) with (3.28) one finds

$$A_i(S_i, t) = - \frac{\gamma}{1 + \alpha^2} ([\mathbf{S} \times \mathbf{H}_d^{\text{eff}}]_i + \alpha [\mathbf{S} \times [\mathbf{S} \times \mathbf{H}_d^{\text{eff}}]]_i), \quad (3.48)$$

with $\mathbf{H}_d^{\text{eff}} = -(1/\mu_S)(\partial \mathcal{H} / \partial \mathbf{S})$ being the deterministic part of the effective field. For B_{ik} we deduce

$$B_{ik}(\mathbf{S}, t) = \frac{\gamma}{1 + \alpha^2} \left[- \sum_j \epsilon_{ijk} S_j + \alpha (\delta_{ik} \mathbf{S}^2 - S_i S_k) \right], \quad (3.49)$$

with ϵ_{ijk} the totally antisymmetric unit tensor (Levi-Civita symbol) and δ_{ij} to be the Kronecker-delta symbol [53]. Similarly it can be shown that

$$\sum_j \frac{\partial B_{jk}}{\partial S_j} = -\frac{2\alpha\gamma}{1+\alpha^2} \quad (3.50)$$

and hence

$$\sum_k B_{ik} \left(\sum_j \frac{\partial B_{jk}}{\partial S_j} \right) = 0. \quad (3.51)$$

For the last term in equation (3.47) we find

$$-q \sum_{jk} B_{ik} B_{jk} \frac{\partial}{\partial S_j} = q \frac{\alpha^2 \gamma^2}{(1+\alpha^2)^2} \mathbf{S}^2 \left[\mathbf{S} \times \left[\mathbf{S} \times \frac{\partial}{\partial \mathbf{S}} \right] \right]_i. \quad (3.52)$$

The coefficient in (3.52) is defined via the Néel time

$$\frac{1}{\tau_N} = \frac{2q\gamma^2\alpha^2}{(1+\alpha^2)^2}, \quad (3.53)$$

where the Néel time is the characteristic time of diffusion in the absence of a potential [70]. Thus, the corresponding FP equation for the LLG is

$$\begin{aligned} \frac{\partial P}{\partial t} = & - \frac{\partial}{\partial \mathbf{S}} \left\{ -\frac{\gamma}{1+\alpha^2} \left([\mathbf{S} \times \mathbf{H}_d^{\text{eff}}] + \alpha [\mathbf{S} \times [\mathbf{S} \times \mathbf{H}_d^{\text{eff}}]] \right) \right. \\ & \left. + \frac{1}{2\tau_N} \left[\mathbf{S} \times \left[\mathbf{S} \times \frac{\partial}{\partial \mathbf{S}} \right] \right] P \right\}. \end{aligned} \quad (3.54)$$

If one assumes that the stationary solution of the FP equation has the Boltzmann distribution, i.e. $P_0(\mathbf{S}) \sim e^{-\beta\mathcal{H}(\mathbf{S})}$, then the Néel time can be obtained as [70]

$$\frac{1}{\tau_N} = \frac{2\alpha\gamma}{(1+\alpha^2)} \frac{1}{\beta\mu_S} \quad (3.55)$$

and finally the coefficient which enters the correlation function in (3.32) is

$$q = \frac{1+\alpha^2}{\alpha} \frac{k_B T}{\gamma\mu_S}. \quad (3.56)$$

Thus, constructing the corresponding FP equation one can find the characteristic time scale for the given stochastic process and the coefficient in the correlation function. In principle, the FP equation can also be solved analytically in very limited cases since it is a partial differential equation. For a more general situation numerical methods should be used.

3.2.5 Discussion of the dynamical Methods

All the dynamical methods listed above can be compared using the three following criteria: Analytical procedure, numerical integration and results obtained.

Analytical procedure. The LLG equation extended for finite temperatures can be exactly solved in very limited cases at zero temperature [77]. The methods to solve nonlinear dynamical equations are discussed in [78].

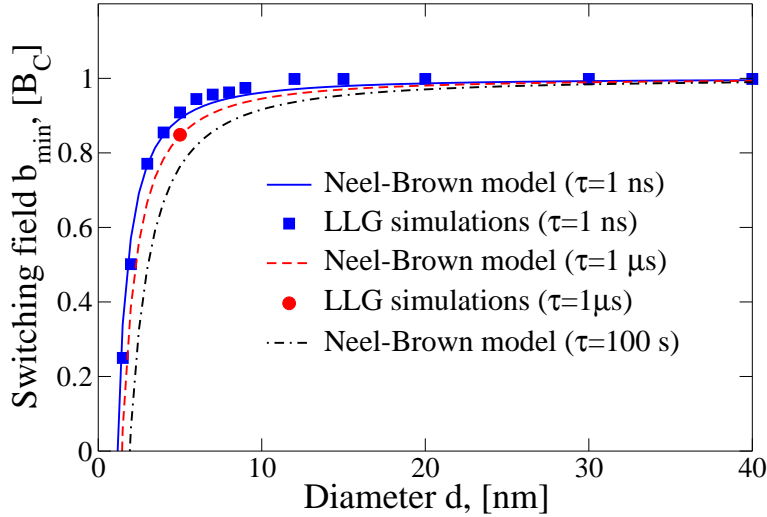


Figure 3.6: Minimal switching field expressed in units of the coercive field as a function of the diameter of a nanoparticle. Squares or circles represent numerical simulations based on the LLG, whereas the curves are calculated using formula (3.57). The time τ denotes the total time of calculations.

MC is a purely numerical method and can not be reproduced analytically.

The FP equation associated with the LLG equation is widely discussed in the literature [51]. Some analytical solutions are available especially in the stationary situation [51]. Alternatively, the FP equation should be solved numerically by use of methods known for solving the partial differential equations.

Numerical procedure. All of the three methods can be numerically implemented. The advantage of the stochastic LLG arises when one aims to acquire the whole dynamics, i.e. for all time moments. Additionally, since the LLG is in this sense a Langevin type equation it can include in the energy and hence in the effective field all possible types of interactions, like exchange, anisotropy etc. Knowing all these effects, the LLG is a very powerful tool for study the magnetization dynamics, magnetization control as well as for more complicated analysis, e.g. response functions.

However, when one is merely interested in the equilibrium properties of a system, such as the averaged magnetization then the MC methods appear to be a more effective recipe due to the higher allowed temporal steps of implementation and hence a lower calculation time.

The FP equation associated with the LLG can serve as a supplementary tool for finding different characteristic parameters.

Results obtained with the methods. The key point of the LLG equation is that it permits us to know all states of the magnetization for the whole of the propagation time. This can be of advantage when the control properties are addressed. The MC method yields a fast information for the averaged states. And finally, from solving the FP equation one can find all information about the system. However, the FP is usually used to analytically characterize the stochastic time scale of the system.

3.3 Comparison of the static and the dynamic Approaches

A quantitative comparison of the statical (using the Néel-Brown model) and dynamical (using the stochastic LLG equation) methods is illustrated in Fig. 3.6. For this, the minimal switching field b_{\min} of a single-domain magnetic nanoparticle is studied as a function of a particle's diameter d . An analytical expression for the minimal switching field might be given by formula (3.11) transformed for b_{\min} and expressed in units of the coercive field B_C

$$b_{\min} = 1 - \sqrt{\frac{6k_B T}{K \pi d^3} \ln \left(\frac{\tau}{\tau_0} \right)}. \quad (3.57)$$

Numerical simulations were performed using the stochastic LLG implemented as described in Chapter 5 for a Co-nanoparticle. The following parameters were used in simulations: $\alpha = 0.25$, $\mu_{\text{per atom}} = 1.8 \cdot \mu_B$, $K = 1.0 \cdot 10^6 \text{ J/m}^3$, $T = 8.3 \text{ K}$ [79–81]. The parameter τ_0 was calculated using formula (3.12). Co-nanoparticles with high damping provided a faster relaxation towards the desirable state. The minimal switching field was obtained numerically as the minimal field at which the magnetic moment changed from a parallel to an antiparallel state.

Fig. 3.6 reveals that the analytical and the numerical results coincide, proving the correctness of both static and dynamic approaches. For high waiting times $\tau > 1 \mu\text{s}$ only one numerical result is given due to the dramatic increase in calculation time by a factor of 1000.

4 Relaxation in ferromagnetic Systems

This chapter deals with the magnetization damping, which enters the phenomenological treatment proposed by Landau, Lifshitz and Gilbert which is popular nowadays. After a discussion the experimental evidence (e.g. [82–84]) and theoretical microscopic treatment of damping [85] is presented.

4.1 Review of Experiments for the Measurement of the Damping Parameter

Experimental techniques for the measurement of magnetization damping are based on the LL or the LLG equations, (3.25) or (3.28) respectively. The damping parameter can be measured either in the dimensionless units (λ in the Landau-Lifshitz form or α in the Gilbert form) or in units of the field free precessional frequency $\omega = \gamma B_C$ in [rad/s] as described in Ref. [82]. In our calculations we will use the dimensionless damping α in the Gilbert form.

One of the most well known techniques in this respect is the Ferromagnetic Resonance technique (FMR) [86, 87]. By applying a static and perpendicular to it a time-dependent magnetic field to a ferromagnetic sample the response function is measured as a function of the strength of the static field. The absorbed power is proportional to the imaginary part of the transverse susceptibility. The measured absorbed power signal is of a Lorentzian type with a maximum at a certain field B_{res} which refers to the resonance frequency $\omega_{\text{res}} = \gamma B_{\text{res}}$. The applied static field creates a splitting of the energy levels, whereas the oscillating field induces a transition between the levels when the frequency of the oscillating field coincides with the one associated with the splitting. In a perfect sample without dissipation the absorbed power is a delta function with the absorption at only one frequency. Damping leads to a width broadening and is measured as a function of resonance frequency of the broadened curves [82]. This technique has been performed for a wide range of temperatures and revealed [88, 89] that damping has a different behavior for iron, cobalt and nickel and shows an increase in it at low and high temperatures. Typical values of damping measured with the FMR are in the range from 0.01 to 0.3 [90–93] and are very material specific.

Recently, further techniques like Magneto Optical Kerr Effect (MOKE) [83, 94] were employed for the measurement of the magnetization damping. Here, the MOKE-signal is related to the time propagation of the magnetization. Usually, one fits the measured signal with the solution of the LLG equation for a chosen damping parameter. The best fit to the measurement yields the value of damping. Generally, measured values of damping here [83, 94–96] are in agreement with those obtained from FMR.

Similarly, X-Ray Magnetic Circular Dichroism (XMCD) allows for measurements of

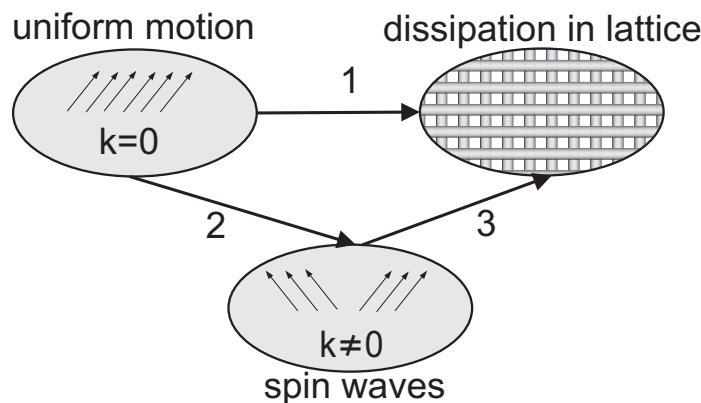


Figure 4.1: Schematic illustration of possibilities for damping in a ferromagnetic body. Path 1 presents a direct relaxation to the lattice. Paths 2 and 3 show an indirect damping into nonuniform motions of the magnetization and then into the lattice.

the damping parameter [84, 97] with element specification which is advantageous for heterostructures.

The effect of doping on the damping was extensively studied experimentally by mixing to NiFe alloys rare earths [98] or transition metals [99]. As a result, damping rate can accurately be tuned up to 0.8. Additionally, doping iron with vanadium resulted in a decreased damping [100]. All these findings hint on complicated mechanisms of damping and a demand for a microscopic understanding of the processes.

4.2 Mechanisms and Models of the Magnetization Damping

The fact that there is a number of mechanisms for damping (see review in Ref. [85, 101]) implies that no one model is able to explain all the experimental findings. In Ref. [102] the author points out two main channels for the energy dissipation in ferromagnetic materials: Direct and indirect damping (see Fig. 4.1). As direct damping an energy dissipation from the uniform motion of the magnetic moment (or a magnon with the wave vector $\mathbf{k} \approx 0$) to the thermal bath is understood. It is shown that this irreversible damping mechanism can be considered in fact as a viscous damping of the magnetic moment coupled to shear distortions of the lattice. This scenario might be realized in small samples with sizes lower than the domain wall thickness.

For sufficiently large samples such a uniform motion can populate states in the magnetic subsystem, i.e. the energy transfers into the spin waves ($\mathbf{k} \neq 0$). This process is reversible, however, on the long time scale the energy will flow into the thermal bath as well. That is what is called indirect damping, which is also experimentally observable [103].

Since in this study we focus on small ferromagnetic nanoparticles the damping mechanism is supposed to be direct. For practical purposes, however, one aims to calculate a material specific damping parameter to be able to compare it with the associated experiment. Below the main steps of the so called "breathing" Fermi surface model [104, 105] are presented. This model usually serves as the basis for *ab initio* techniques to calculate

damping.

The Spin Orbit Coupling (SOC) causes changes of electronic states $\epsilon_{\mathbf{k},j}$ during the precession of the magnetic moment \mathbf{S}_i . Here, index j denotes a particular electronic state and i stands for the Cartesian component of the normalized magnetic moment. The total electronic energy is then

$$E = \sum_{\mathbf{k},j} \epsilon_{\mathbf{k},j} n_{\mathbf{k},j}, \quad (4.1)$$

where $n_{\mathbf{k},j}$ is defined below.

Quasistatic changes of \mathbf{S}_i during the precession produce small variation of Fermi surface which is equivalent to the action of the effective field

$$H_i^{\text{eff}} = -\frac{1}{\mu_S} \sum_{\mathbf{k},j} n_{\mathbf{k},j} \frac{\partial \epsilon_{\mathbf{k},j}}{\partial S_i}. \quad (4.2)$$

The summation runs over the first Brillouin zone. Those nonequilibrium states that are close to the Fermi level relax due to collisions with lattice defects. Thus, for the nonequilibrium populations we may write

$$n_{\mathbf{k},j} = f(\epsilon_{\mathbf{k},j}) - \tau_j \frac{df(\epsilon_{\mathbf{k},j})}{dt}, \quad (4.3)$$

where $f(\epsilon_{\mathbf{k},j})$ is the Fermi function and τ_j is the lifetime of the state j . Therefore, the damping consists in the phase lag between the changes in S_i and the population response. Mathematical illustration of the phase lag may be obtained by inserting of (4.3) into (4.2) and applying the chain rules to the out-of-phase part

$$H_i^{\text{eff}} = -\frac{1}{\mu_S} \sum_{\mathbf{k},j} f(\epsilon_{\mathbf{k},j}) \frac{\partial \epsilon_{\mathbf{k},j}}{\partial S_i} - \frac{1}{\mu_S} \sum_{\mathbf{k},j} \tau_{\mathbf{k},j} \left(-\frac{\partial f_{\mathbf{k},j}}{\partial \epsilon_{\mathbf{k},j}} \right) \frac{\partial \epsilon_{\mathbf{k},j}}{\partial S_i} \frac{\partial \epsilon_{\mathbf{k},j}}{\partial S_l} \frac{dS_l}{dt}. \quad (4.4)$$

Comparing now the out-of-phase part of (4.4) with the Gilbert-like relaxation expression

$$H_i^{\text{eff}} = -\frac{\alpha}{\gamma} \frac{dS_i}{dt} \quad (4.5)$$

and recalling that at low temperatures $-\frac{\partial f(\epsilon_{\mathbf{k},j})}{\partial \epsilon_{\mathbf{k},j}} \approx \delta(\epsilon_F - \epsilon_{\mathbf{k},j})$ one finally finds

$$\alpha_{il} = \frac{\tau\gamma}{\mu_S} \sum_{\mathbf{k},j} \left(\frac{\partial \epsilon_{\mathbf{k},j}}{\partial S_i} \right) \left(\frac{\partial \epsilon_{\mathbf{k},j}}{\partial S_l} \right) \delta(\epsilon_F - \epsilon_{\mathbf{k},j}). \quad (4.6)$$

Here, the assumption is made, that the lifetimes are equal for all states j , i.e. $\tau = \tau_j$. It should be noted that damping in the "breathing" Fermi surface model is a tensor. Moreover, this result is very similar to the Drude conductivity tensor which is also proportional to the relaxation time. It is known that the relaxation time scales with temperature as $\sim T^{-2}$. Hence, at low temperatures the model predicts $\alpha \sim T^{-2}$ behavior and explains experimental results [88].

Calculations of damping tensor can be found in [106]. In particular, it was shown that damping may completely vanish in some directions.

Further improvements of this model like *ab initio* calculations on the basis of the torque correlation model [107] succeeded to explain high temperature regime of damping. Within this model damping splits into conductivity-like term at low temperatures and a resistivity-like term for high temperatures.

In the calculations presented in this work the results will be presented as a variation of damping with the values of damping being appropriate for low and high temperatures.

5 Numerical Procedure

The LLG equation can be solved analytically only in the very low damping regime, i.e. in a nearly linear case. In the completely nonlinear regime some analytical solutions are available in certain limits only. For example, in the low energy regime of the damped magnetic moment [108–110] as a spin wave propagation or a solution with a very restricted geometry [77].

The fact that the LLG equation which is to be solved is a stochastic differential equation entails the use of numerical integration methods.

5.1 Stochastic Calculus for the Langevine Type Equations

The LLG equation can be written as a stochastic Langevine equation for three Cartesian components denoted by i in equation (3.45). Expressions (3.48) and (3.49) decipher coefficients $A_i(S_i, t)$ and $B_{ik}(S_i, t)$. Suppose, we are interested in finding small changes of $\Delta S_i(t)$ in the time interval $t \in [t; t + \Delta t]$. Then, from (3.45) we deduce

$$\begin{aligned} \Delta S_i(t) &= S_i(t + \Delta t) - S_i(t) \\ &= \int_t^{t+\Delta t} A_i(S_i, t') dt' + \int_t^{t+\Delta t} \sum_k B_{ik}(S_i, t') \zeta_k(t') dt'. \end{aligned} \quad (5.1)$$

For the times close to the beginning of the time interval, i.e. $\Delta t \rightarrow 0$, $A_i(S_i, t + \Delta t) \approx A_i(S_i, t)$ and $B_{ik}(S_i, t + \Delta t) \approx B_{ik}(S_i, t)$. With these considerations we obtain from (3.45)

$$\Delta S_i(t) = A_i(S_i, t) \Delta t + \sum_k B_{ik}(S_i, t) \int_t^{t+\Delta t} \zeta_k(t') dt'. \quad (5.2)$$

Assuming that the noise function $\zeta_k(t)$ is a Markov process we infer from (3.32)

$$\left\langle \int_t^{t+\Delta t} \zeta_k(t') dt' \int_t^{t+\Delta t} \zeta_l(t'') dt'' \right\rangle \sim \int_t^{t+\Delta t} dt' \int_t^{t+\Delta t} \delta_{kl} \delta(t'' - t') dt'' = \delta_{kl} \Delta t. \quad (5.3)$$

Thus, we find for (5.2)

$$\Delta S_i(t) \Big|_{\Delta t \rightarrow 0} = A_i(S_i, t) \Delta t + \sum_k B_{ik}(S_i, t) \zeta_k(t) \sqrt{\Delta t}. \quad (5.4)$$

When aiming to find $\bar{S}_i(t)$ for any time moment from the interval $t \in [t; t + \Delta t]$ $\bar{S}_i(t)$ reads as

$$\begin{aligned} \bar{S}_i(t) &= (1 - \nu) S_i(t) + \nu S_i(t + \Delta t) = (1 - \nu) S_i(t) + \nu (S_i + \Delta S_i(t)) \\ &= S_i(t) + \nu \Delta S_i(t). \end{aligned} \quad (5.5)$$

With the last equation the expression for $\Delta S_i(t)$ converts into

$$\Delta S_i(t) = A_i(\bar{S}_i(t), t)\Delta t + \sum_k B_{ik}(S_i(t) + \nu\Delta S_i(t), t)\zeta_k(t)\sqrt{\Delta t}. \quad (5.6)$$

For the second term the following expression is valid

$$\begin{aligned} & B_{ik}(S_i(t) + \nu\Delta S_i(t), t)\zeta_k(t)\sqrt{\Delta t} \\ = & B_{ik}(S_i(t), t)\zeta_k(t)\sqrt{\Delta t} + \nu\frac{\partial B_{ik}(S_i(t), t)}{\partial S_i(t)}\Delta S_i(t)\zeta_k(t)\sqrt{\Delta t} + \dots \\ = & B_{ik}(S_i(t), t)\zeta_k(t)\sqrt{\Delta t} + \nu\frac{\partial B_{ik}(S_i(t), t)}{\partial S_i(t)}\left(\sum_k B_{ik}(S_i(t), t)\zeta_k(t)\right)\Delta t + O(\Delta t^{\frac{3}{2}}). \end{aligned} \quad (5.7)$$

Inserting the expression (5.7) into (5.6) finally yields

$$\begin{aligned} \Delta S_i(t) = & \left[A_i(\bar{S}_i(t), t) + \nu\left(\sum_k \frac{\partial B_{ik}(S_i(t), t)}{\partial S_i(t)}\zeta_k(t)\right)\left(\sum_k B_{ik}(S_i(t), t)\zeta_k(t)\right) \right] \Delta t \\ & + \sum_k B_{ik}(S_i(t), t)\zeta_k(t)\sqrt{\Delta t}. \end{aligned} \quad (5.8)$$

This is a general expression for the time propagation of the reduced magnetic moment. Various definitions of the stochastic integral are known from the literature [72, 111]. They differ only in the drift term (see the expression in square brackets). An *Itô interpretation* [72] is obtained when $\nu = 0$, i.e.

$$\Delta S_i(t) = A_i(\bar{S}_i(t), t)\Delta t + \sum_k B_{ik}(S_i(t), t)\zeta_k(t)\sqrt{\Delta t}. \quad (5.9)$$

For $\nu = 1/2$ a *Stratonovich interpretation* [72] is acquired

$$\begin{aligned} \Delta S_i(t) = & \left[A_i(\bar{S}_i(t), t) + \frac{1}{2}\left(\sum_k \frac{\partial B_{ik}(S_i(t), t)}{\partial S_i(t)}\zeta_k(t)\right)\left(\sum_k B_{ik}(S_i(t), t)\zeta_k(t)\right) \right] \Delta t \\ & + \sum_k B_{ik}(S_i(t), t)\zeta_k(t)\sqrt{\Delta t}. \end{aligned} \quad (5.10)$$

It can be shown [76] that the dynamical properties within the two integral interpretations are totally different. The Itô integral interpretation is usually used for pure mathematical purposes, whereas the Stratonovich interpretation leads to correct physical results. In particular, the trajectories of the magnetic moment created by the stochastic LLG equation coincide with those yielded by the corresponding FP equation only when the stochastic integral is interpreted in the Stratonovich sense. This interpretation underlies the present study throughout.

5.2 Numerical Integration Scheme

For the numerical integration of stochastic differential equations of the Langevine type a proper numerical scheme is required, since the stochastic integral, in contrast to the

deterministic case has to converge to the Stratonovich solution.

In all the numerical simulations presented in this work the *Heun* or *improved Euler* method is employed [72, 111] which is a predictor corrector method. A rather simple *Euler* method [111] can not be used here since it yields the Itô solution and omits the noise-induced drift. This integration scheme is shown to be inconsistent [112, 113]. On the other hand, a rigorous numerical treatment can be achieved by means of the *Runge-Kutta* method [114]. However, a high precision provided by the Runge-Kutta method is not needed in the stochastic case. Hence, the Heun method is a good compromise between a low accuracy and an enormous calculation time.

The Heun integration scheme works as follows. For a given initial condition determined by a set of $S_i(t=0)$ a recursive predictor step for discretization time interval $t^{n+1} - t^n = \Delta t$ is made according to

$$\bar{S}_i^{n+1} = S_i^n + A_i(S_i^n, t^n)\Delta t + \sum_k B_{ik}(S_i^n, t^n)\zeta_k(t^n)\sqrt{\Delta t}. \quad (5.11)$$

A corrector part is calculated according to

$$\begin{aligned} S_i^{n+1} = S_i^n &+ \frac{1}{2} [A_i(\bar{S}_i^n, t^{n+1}) + A_i(S_i^n, t^n)] \Delta t \\ &+ \frac{1}{2} \sum_k [B_{ik}(\bar{S}_i^n, t^{n+1}) + B_{ik}(S_i^n, t^n)] \zeta_k(t^n)\sqrt{\Delta t}. \end{aligned} \quad (5.12)$$

The characteristics of the white multiplicative noise are given by expressions (3.32). The deterministic part within the Heun scheme is calculated with the second order of accuracy in Δt . Local discretization errors given by the method are of the order three in Δt [111]. The integration time step is commonly chosen such that it is at least 1/1000 of the field-free precessional period. The random numbers $\zeta_k(t)$ are generated according to the Box-Müller algorithm [115] and the period of them is around 2^{31} ($> 10^9$). Therefore, artifacts associated with repetition of random numbers are avoided.

The stochastic LLG equation is evaluated numerically in reduced units, where the effective field is expressed in units of the anisotropy field and the time is reduced to the field-free precessional period.

Comparison with other numerical procedures is widely presented in the literature [111, 116, 117]. In contrast to the Milstein method, the Heun method allows for larger integration steps (approximately ten times larger) with the same precision.

6 Dynamical Properties of the Magnetization in the Presence of continuous Fields

In this chapter results of the magnetization switching are presented. Several techniques for the magnetization switching are known in the meantime in the literature: Via short laser pulses [118], spin-polarized electric currents [119, 120] or the use of conventional magnetic fields ([10–12] and references therein). It was recently shown both experimentally [121] and theoretically [122, 123] (mostly numerical studies) and [124, 125] (fully analytical based on the FP equation solution) that a microwave time-dependent field synchronized with the magnetic moment of a ferromagnetic nanoparticle is capable to switch it. Moreover, the amplitudes of applied fields turned out to be even smaller than those for a static field. Additionally, switching occurred on a much faster time scale as compared to static fields.

In the context of the switching properties of ferromagnetic nanoparticles the quantities of interest are *critical switching field amplitudes* and the *corresponding reversal times* depending on damping parameters, temperature and the type of anisotropy.

It should be stressed that the term *continuous* for the applied fields means that the envelope is longer than the field-free precessional period.

All the results presented in this chapter are obtained mostly using numerical simulations details of which are described in Chapter 5.

6.1 Static magnetic Fields

6.1.1 Analytical Study at Zero Temperature

Assume a ferromagnetic nanoparticle at zero temperature in a single domain state (Stoner particle [38, 122, 126, 127]) with the uniaxial anisotropy axis being parallel to the Z direction (Fig. 3.1). If a static field \mathbf{b} is applied antiparallel to the initial state of the magnetic moment \mathbf{S} , i.e. $\theta_b = \pi$, then for the total energy expressed in units of the anisotropy energy we may write

$$\tilde{\mathcal{H}} = -\frac{1}{2} \cos^2 \theta + b \cos \theta. \quad (6.1)$$

Since the energy is only dependent on the polar angle θ , the equation for θ , as follows from expression (3.30), can be exactly analytically solved. For the conditions with the start angle $\theta_0 = \pi/360$ and $\theta_e = \pi$ at the end, this equation reads

$$\int_{\theta_0}^{\pi} \frac{d\theta}{\sin \theta (b - \cos \theta)} = \frac{\alpha}{1 + \alpha^2} \int_0^{t_{\text{rev}}} dt'. \quad (6.2)$$

From (6.2) for the time of complete reversal t_{rev} we find

$$t_{\text{rev}} = \frac{1 + \alpha^2}{\alpha} \frac{1}{\omega_A} \frac{1}{b^2 - 1} \ln \left(\frac{\tan \left(\frac{\theta}{2} \right)^b \sin \theta}{b - \cos \theta} \right) \Big|_{\theta_0}^{\pi}, \quad (6.3)$$

with $\omega_A = \gamma B_A = 2\gamma D/\mu_S$ (with $B_A = B_C$). Here we obtained results similar to those reported in [77].

From expression (6.3) the following conclusions can be drawn. Apart from the SW model (Section 3.1.1) the result obtained using the LLG equation is the same: Switching can only occur on the finite time scale when the static field applied exceeds the anisotropy field ($b > 1$). Moreover, this formula reveals a dependence on the damping parameter α and the start angle θ_0 . In particular, an interesting feature of the nonstochastic LLG equation shows up: Starting from $\theta_0 = 0$ no switching can be achieved. Noteworthy is the fact that the volume dependence is missing in equation (6.3), since due to the zero temperature dynamics of the LLG equation, no coupling to the thermal bath is present. The pronounced dependence of t_{rev} on damping is shown in Fig. (6.4) as a dashed curve. This dependence can be explained as a dominant precessional motion in a low damping regime and an enhanced damping term in the LLG equation in case of high damping. A certain balance between the two motion types is observed for a moderate damping parameter. Neglecting the weaker altering logarithmic dependence, equation (6.3) takes the following form for minimal fields needed for switching

$$b \approx \sqrt{\frac{1}{t_{\text{rev}}\omega_A} \frac{1 + \alpha^2}{\alpha} + 1}. \quad (6.4)$$

This expression shows the field strength dependence on t_{rev} which might be interpreted as a measuring time. For infinite t_{rev} we end up with the SW result, whereas a rather complicated dependence on damping arises when approaching $t_{\text{rev}} \rightarrow 1/\omega_A$. Typically, the measuring times which will be demonstrated in the next sections are close in spirit to those measured using the microwave spectroscopy methods (e.g. FMR) and are around 1000 or more of the precessional period.

6.1.2 Numerical Study for Nanoparticles with a uniaxial Anisotropy at Nonzero Temperatures

The analytical results reported above provide an insight into the dynamics of the magnetic moment at zero Kelvin. The question of how finite temperatures will assist the dynamics can be addressed by employing the stochastic LLG equation. For this purpose nanoparticles with a uniaxial anisotropy are chosen (e.g. $\text{Fe}_{50}\text{Pt}_{50}$, Table 2.1). To clearly address the issue with the finite temperatures we chose temperatures high enough to demonstrate their effect on the one hand, by paying attention to the point of losing the ferromagnetic properties on the other hand. Three finite temperatures are $T_1 = 56$ K, $T_2 = 280$ K and $T_3 = 560$ K. For the last temperature the net magnetic moment is still not completely lost due to critical phenomena (see Fig. 3.4). As was pointed out in section (3.1.2) the magnetic moment can also vanish due to the dynamical effect of superparamagnetism. For this reason for the measurement time to be approximately equal to 5 ns the following escape times associated with the above temperatures were calculated, $\tau_{T_1} = 2 \cdot 10^{217}$ s, $\tau_{T_2} = 1 \cdot 10^{75}$ s and $\tau_{T_3} = 7 \cdot 10^{31}$ s, respectively (further details see in [128]).

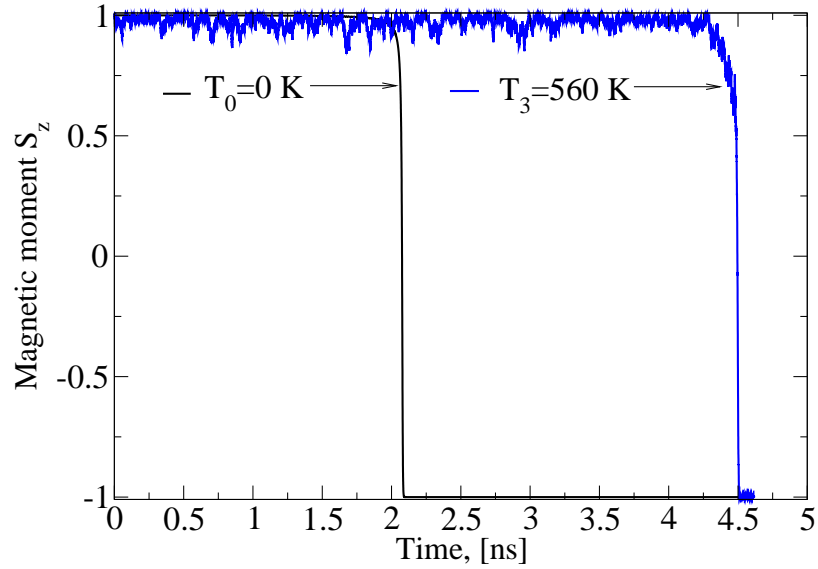


Figure 6.1: Magnetization reversal of a nanoparticle when a static field is applied for two temperatures $T_0 = 0$ K and $T_3 = 560$ K with the strengths of the field $b = 1.01$ and 0.74 , respectively. The damping parameter is $\alpha = 0.1$. Start angle of the magnetic moment is $\theta_0 = \pi/360$.

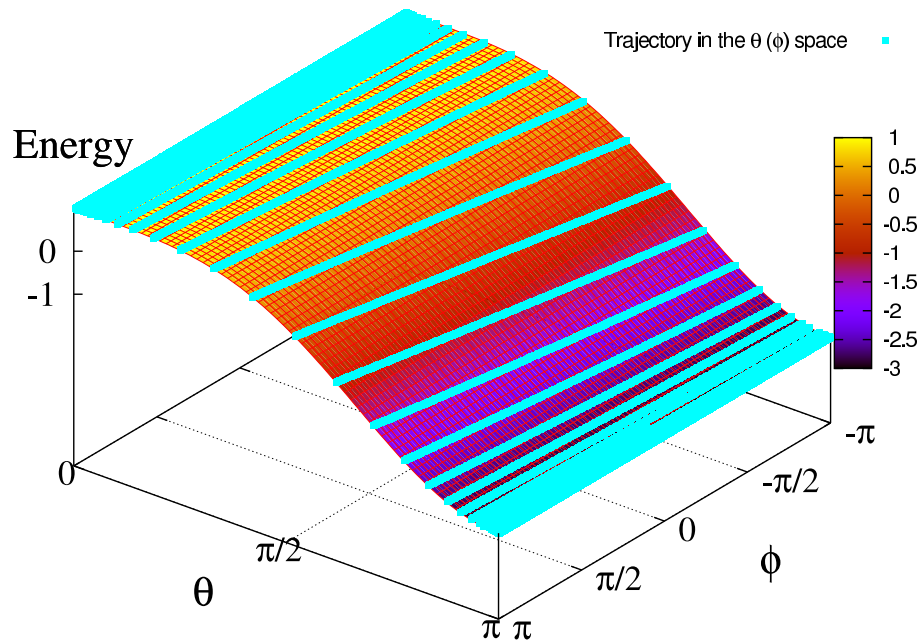


Figure 6.2: Trajectories of the magnetic moment in the $E(\theta, \phi)$ space. The motion starts at $\theta \rightarrow 0$ and arrives at $\theta \rightarrow \pi$. Other parameters are $T_0 = 0$ K, $b = 1.01$ and $\alpha = 0.1$.

The procedure of finding the critical fields is as follows. Antiparallel to the magnetic moment of the nanoparticle a static field is applied in small steps starting from small values. When a magnetization reversal is realized, the values of the last field applied and the corresponding reversal times are recorded (Fig. 6.1). Note that in contrast to the situation described in [122] we define the reversal as a magnetization switching from a parallel to the antiparallel state, since at finite temperatures the state with $S_z = 0$ may be not stable. Thermal fluctuations may lead to a switching back to the original state.

Fig. 6.2 illustrates how the switching occurs in the energy space $E(\theta, \phi)$. Static magnetic field changes the energy profile by elevating the initial and lowering the target states at the same time. Hence, the initial state becomes energetically not favorable and the magnetic moment switches.

The behavior of minimal fields needed for switching for a given measurement time and temperature is shown in Fig. 6.3. The zero temperature curve approves the results of SW model. Indeed, for zero Kelvin and a high measurement time damping is insufficient, hence, there is no dependence on it (the same what equation (6.4) implies in the limit of large t_{rev}). High temperatures assist the switching by lowering the required minimal static fields (Direct Current, DC-fields).

Inset of Fig. 6.3 shows data not averaged over many realizations. As can be seen, the averaging is not relevant for the critical fields, however, becomes very reasonable in calculations of the corresponding reversal times (see Fig. 6.4). The temperature effect eliminates the pronounced dependence on damping as it was for $T = 0$ K and the reversal times occur on the nanosecond time scale. For these results it should be stressed that the reversal times shown in Fig. 6.4 are continuously associated with the calculated critical fields. The reversal times might be essentially reduced by keeping the static field amplitude to be the same for all temperatures.

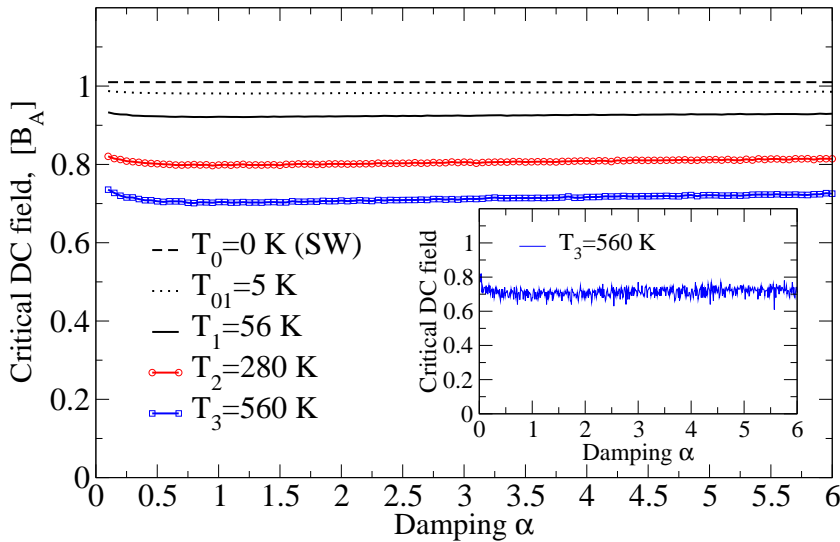


Figure 6.3: Critical field amplitudes expressed in units of the uniaxial anisotropy field as a function of damping parameter for a static field. Each curve is averaged over 500 cycles. Inset shows as-calculated data for $T_3 = 560$ K.

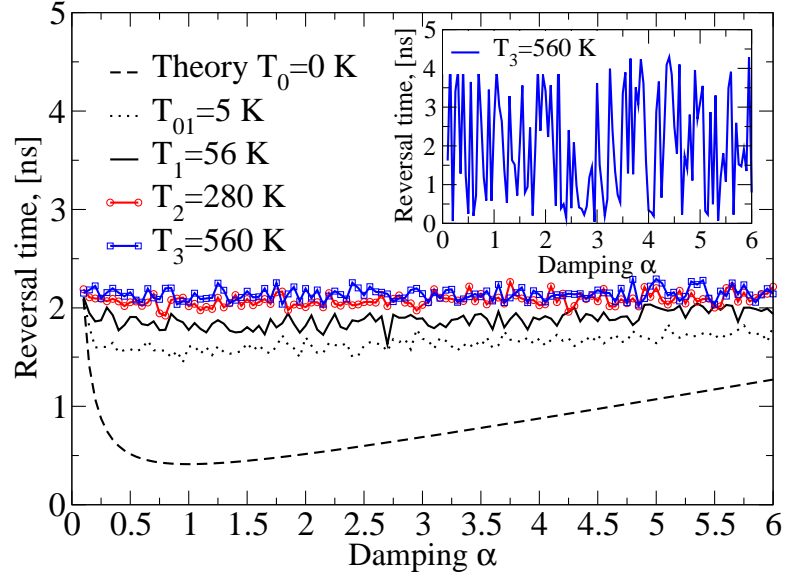


Figure 6.4: Reversal times corresponding to the critical fields in Fig. 6.3 as a function of damping parameter. Inset shows not averaged data for $T_3 = 560$ K.

6.1.3 Numerical Study for Nanoparticles with a cubic Anisotropy at Nonzero Temperatures

The issue of a cubic anisotropy arises since it is not captured by the analytical solution (Section 6.1.1) as well. For the role of a ferromagnetic nanoparticle with a cubic anisotropy we choose $\text{Fe}_{70}\text{Pt}_{30}$ nanoparticles with the parameters listed in Table 2.2. Similarly to $\text{Fe}_{50}\text{Pt}_{50}$ nanoparticles the temperatures of calculations are $T_4 = 0.3$ K, $T_5 = 0.9$ K and $T_6 = 1.9$ K. The corresponding escape times are $\tau_{T_4} = 1 \cdot 10^{34}$ s, $\tau_{T_5} = 2 \cdot 10^5$ s and $\tau_{T_6} = 2 \cdot 10^{-2}$ s, respectively. Note that the temperatures for the both types of nanoparticles were calculated as the same ratio of the thermal energy to the anisotropy energy $k_B T/D$, whereas in the case of cubic anisotropy the smallest energy barrier were taken (see Fig. 2.3).

An additional issue for cubic anisotropy crystals is how to define switching. Since there are more than two stable orientations (see Fig. 2.2), there exist more possibilities for the reversal. In this chapter the switching for the cubic anisotropy is defined similarly to that for the uniaxial anisotropy, namely as a switching from a parallel to the antiparallel state.

The total energy of a nanoparticle with a cubic anisotropy in an external static field is

$$\tilde{\mathcal{H}} = -\frac{1}{2}(\cos^2 \phi \sin^2 \phi \sin^4 \theta + \cos^2 \theta \sin^2 \theta) - \mathbf{S} \cdot \mathbf{b}. \quad (6.5)$$

At first we let the magnetic moment relax to the state close to $\phi_0 = \pi/4$ and $\theta_0 = \arccos(1/\sqrt{3})$. The target state is thus $\phi_e = 3\pi/4$ and $\theta_e = \pi - \arccos(1/\sqrt{3})$. To achieve switching we apply the magnetic field as

$$\mathbf{b} = -\frac{b}{\sqrt{3}}(\mathbf{e}_x + \mathbf{e}_y + \mathbf{e}_z). \quad (6.6)$$

To be consistent with the results reported for the uniaxial anisotropy we plot the Z projections of the magnetic moment S_z for different temperatures (Fig. 6.5). This, however, does not yield a full picture of the three-dimensional motion. The trajectories of this motion are shown in the $E(\theta, \phi)$ -space for the static field and for small damping. Similar to the uniaxial anisotropy, the initial state lies higher than the target one and a slow motion towards the target state happens (Fig. 6.6). The dynamics of this motion is, however, totally different compared with the uniaxial one.

The procedure of determining the critical fields (these fields we denote as Alternate Current (AC) fields) despite the completely different geometry of the system is the same: Reaching the target state the minimal fields and the corresponding reversal times are recorded and plotted as a function of damping parameter and temperature.

One general feature should be commented upon in Fig. 6.7. All fields, expressed in units of the maximum anisotropy field, turn out to be smaller than those for the uniaxial anisotropy. The reason is that the cubic anisotropy with the same constant in expression (6.5) is generally lower than the uniaxial (see Fig. 2.3). Hence, smaller reversal fields appear to be sufficient for switching.

The corresponding reversal times shown in Fig. 6.8 indicate that, due to the low measurement time chosen for a better comparison with the results for the uniaxial anisotropy constant, jumps for t_{rev} appear even for $T = 0$ K. The reason of the lower temperature-assisted reversal times is as follows. Due to the initial states to which the magnetic moment relaxes, a switching not assisted by the temperature, takes a longer time.

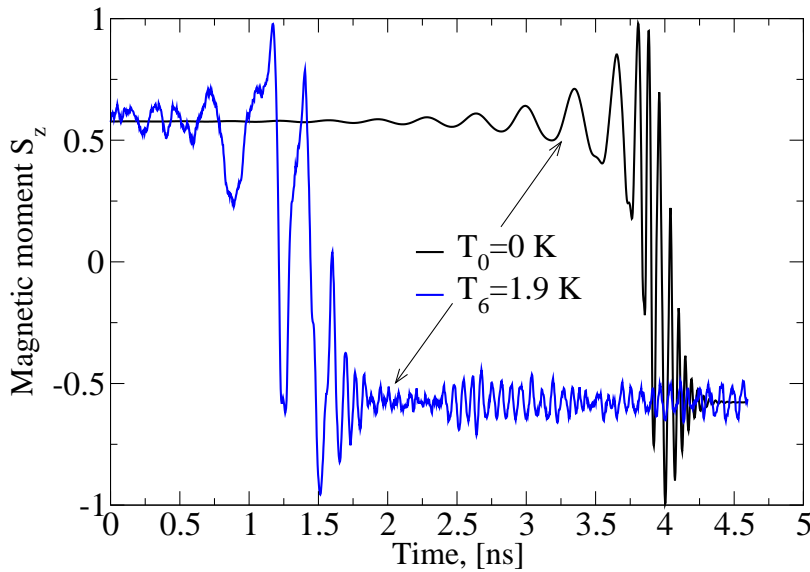


Figure 6.5: Magnetization reversal of a nanoparticle with a cubic anisotropy when a static field is applied for two temperatures $T_0 = 0$ K and $T_6 = 1.9$ K with the strengths of the field of $b = 0.82$ and 0.22 , respectively. The damping parameter is $\alpha = 0.1$. The magnetic moment starts its motion from $\phi_0 = \pi/4$, $\theta_0 = \arccos(1/\sqrt{3})$ and finally arrives at $\phi_e = 3\pi/4$, $\theta_e = \pi - \arccos(1/\sqrt{3})$.

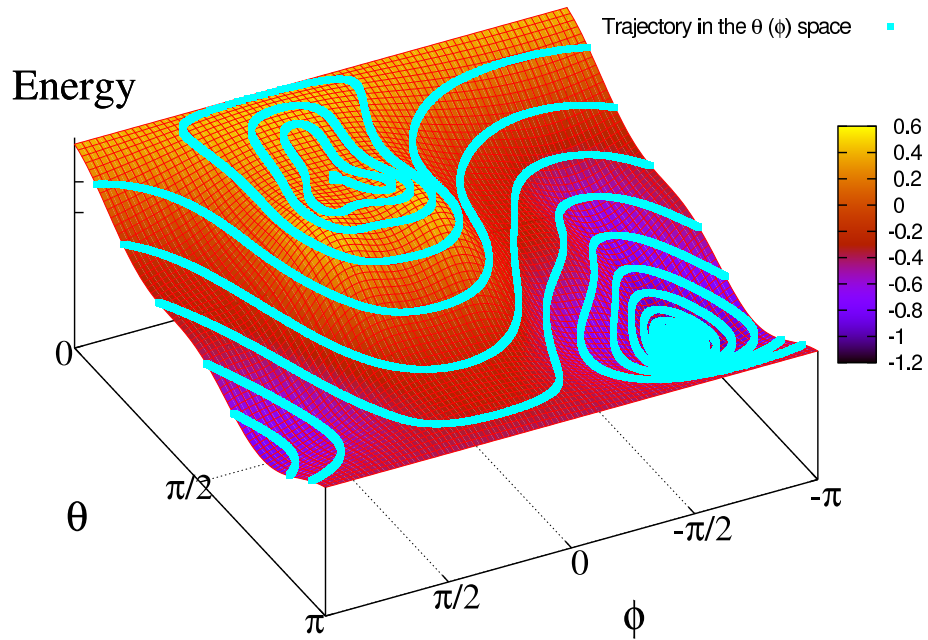


Figure 6.6: Trajectories of the magnetic moment in the $E(\theta, \phi)$ space for $b = 0.82$ and $\alpha = 0.1$. The initial and target states are the same as those indicated in Fig. 6.5.

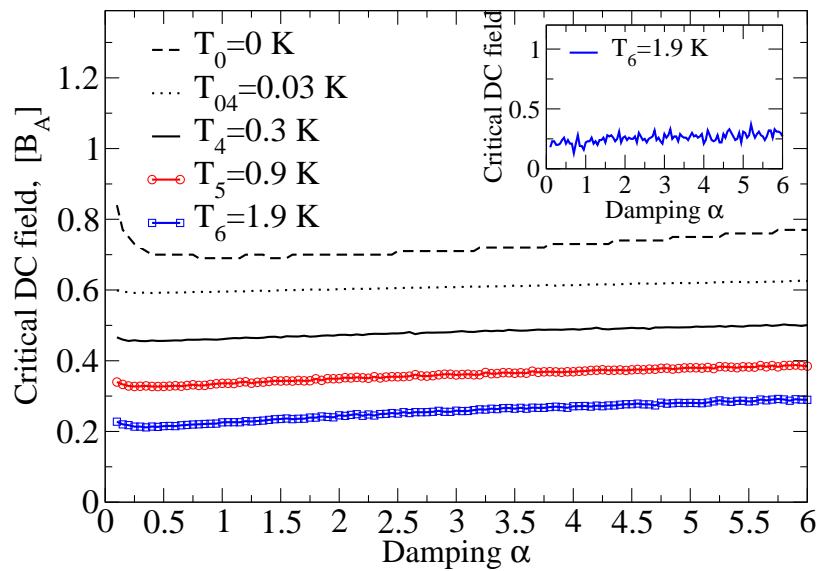


Figure 6.7: Critical field amplitudes expressed in units of the uniaxial anisotropy field as a function of the damping parameter for a static field applied. Each curve is averaged over 500 cycles. Inset shows as-calculated data for $T_6 = 1.9$ K.

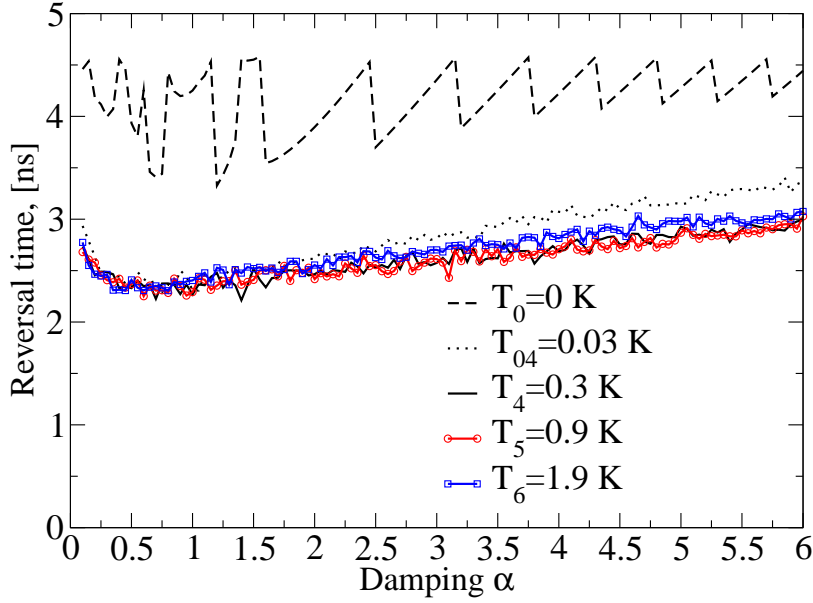


Figure 6.8: Reversal times corresponding to the critical fields shown in Fig. 6.7 as a function of damping.

6.2 Continuous Time-Dependent magnetic Fields

6.2.1 New Strategy for Switching

Experimental findings [121] revealed the possibility of magnetization switching of small magnetic nanoparticles in the absence of a strong static field merely by usage of time-dependent field with a frequency close to the precessional frequency. Here we depict the main steps to understand the process of magnetization excitation on the basis of the LLG equation (3.28) [122, 127].

The effective field \mathbf{H}^{eff} is separated into the internal and the external (Zeemann) one

$$\mathbf{H}^{\text{eff}} = -\frac{1}{\mu_S} \frac{\partial \mathcal{H}}{\partial \mathbf{S}} = \mathbf{H}^{\text{int}} + \mathbf{H}^{\text{ext}}. \quad (6.7)$$

Consider an energy change rate using the continuity equation

$$\frac{d\mathcal{H}}{dt} = \frac{\partial \mathcal{H}}{\partial t} + \dot{\mathbf{H}}^{\text{ext}} \cdot \frac{\partial \mathcal{H}}{\partial \mathbf{H}^{\text{ext}}}. \quad (6.8)$$

For the external field we obtain from the definition

$$\frac{\partial \mathcal{H}}{\partial \mathbf{H}^{\text{ext}}} = -\mu_S \mathbf{S}. \quad (6.9)$$

$\partial \mathcal{H} / \partial t$ can be found from the definition of the effective field (6.7) as

$$\mathbf{H}^{\text{eff}} = -\frac{1}{\mu_S} \frac{\partial \mathcal{H}}{\partial \mathbf{S}} = -\frac{1}{\mu_S} \frac{\partial \mathcal{H}}{\partial t} \frac{1}{\frac{\partial \mathbf{S}}{\partial t}}, \quad (6.10)$$

from which we finally deduce

$$\frac{\partial \mathcal{H}}{\partial t} = -\mu_S \mathbf{H}^{\text{eff}} \cdot \frac{\partial \mathbf{S}}{\partial t}. \quad (6.11)$$

The last scalar product can be found by multiplying the LLG equation (3.28) with \mathbf{H}^{eff}

$$\begin{aligned} \mathbf{H}^{\text{eff}} \cdot \frac{\partial \mathbf{S}}{\partial t} &= -\frac{\gamma}{1+\alpha^2} \left(\mathbf{H}^{\text{eff}} \cdot [\mathbf{S} \times (\mathbf{H}^{\text{eff}} + \alpha [\mathbf{S} \times \mathbf{H}^{\text{eff}}])] \right) \\ &= \frac{\gamma}{1+\alpha^2} \left(\mathbf{H}^{\text{eff}} + \alpha [\mathbf{S} \times \mathbf{H}^{\text{eff}}] \right) \cdot [\mathbf{S} \times \mathbf{H}^{\text{eff}}] \\ &= \frac{\alpha\gamma}{1+\alpha^2} \left| [\mathbf{S} \times \mathbf{H}^{\text{eff}}] \right|^2. \end{aligned} \quad (6.12)$$

Finally, inserting the last expression into equation (6.8) we arrive at

$$\frac{d\mathcal{H}}{dt} = -\frac{\alpha\gamma\mu_S}{1+\alpha^2} \left| [\mathbf{S} \times \mathbf{H}^{\text{eff}}] \right|^2 - \mu_S \mathbf{S} \cdot \dot{\mathbf{H}}^{\text{ext}}. \quad (6.13)$$

Equation (6.13) makes the process of energy absorption in the presence of a time-dependent field clear. In particular, when the system is solely subjected to a static field, i.e. $\dot{\mathbf{H}}^{\text{ext}} = 0$, the energy can only decrease due to damping. The presence of a time-dependent field enables a balance in the energy decrease and increase. Nevertheless, not all fields are able to pump the system with an energy. It is shown [127] that choosing $\mathbf{H}^{\text{ext}} \sim \dot{\mathbf{S}}$ and keeping in mind the relation $\mathbf{S} \cdot \dot{\mathbf{S}} = -\dot{\mathbf{S}} \cdot \dot{\mathbf{S}}$ the second term can be positive and depending on the field amplitude can exceed the losses in the system.

In the following a similar strategy will be employed for the magnetization reversal.

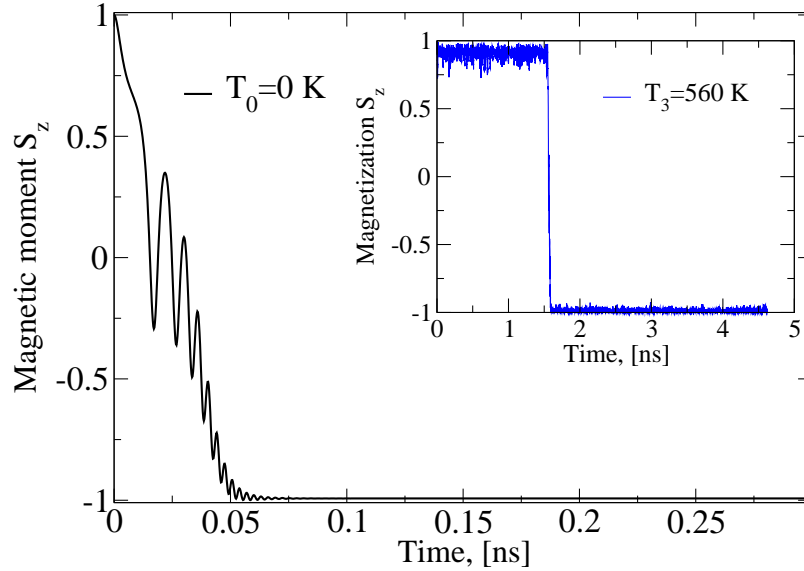


Figure 6.9: Magnetization reversal of a nanoparticle when a time-dependent field is applied for zero Kelvin and $\alpha = 0.1$. The field strength and the frequency in reduced units are $b_0 = 0.18$ and $\omega = \omega_A/1.93$, respectively. The inset shows the reversal at $T_3 = 560$ K and $b_0 = 0.17$.

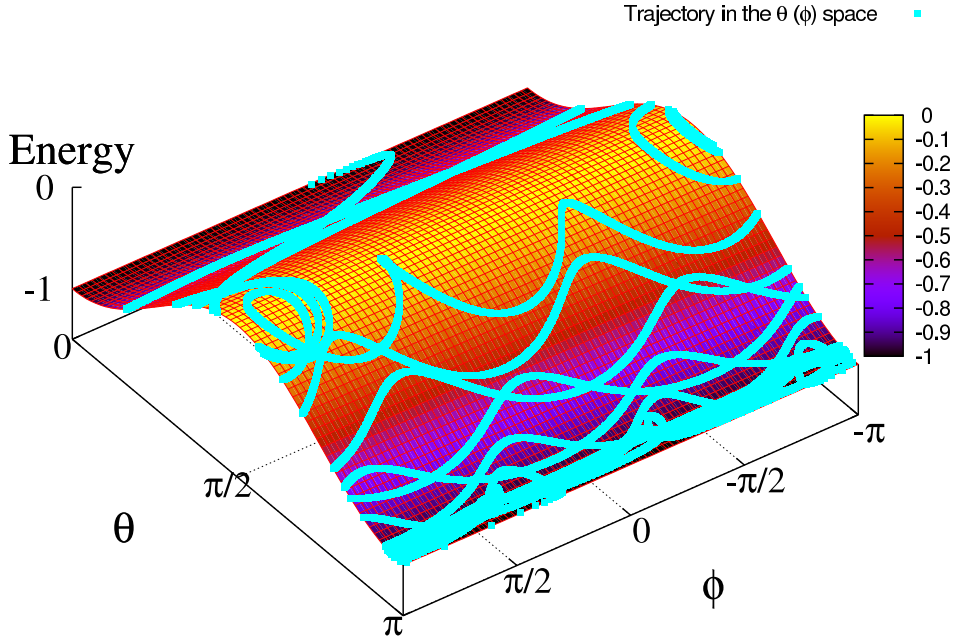


Figure 6.10: Trajectories of the magnetic moment in the $E(\theta, \phi)$ space. Other parameters are $T_0 = 0$ K, $b_0 = 0.18$, $\omega = \omega_A/1.93$, $\alpha = 0.1$.

6.2.2 Numerical Study for Nanoparticles with a uniaxial Anisotropy at Nonzero Temperatures

Since the experimental realization of the strategy with $\mathbf{H}^{\text{ext}} \sim \dot{\mathbf{S}}$ is a difficult task involving a tracking of the magnetization on a very short time scale, another strategy with a modified version of the field is presented. We focus on a nanoparticle with a uniaxial anisotropy. All parameters used in the simulations are the same as mentioned in Subsection 6.1.2. The total energy of the nanoparticle expressed in $\mu_S B_A$ is given by

$$\tilde{\mathcal{H}} = -\frac{1}{2} \cos^2 \theta + \mathbf{S} \cdot \mathbf{b}(t), \quad (6.14)$$

with the field applied in the XY -plane (Fig. 3.1)

$$\mathbf{b}(t) = b_0 \cos \omega t \mathbf{e}_x + b_0 \sin \omega t \mathbf{e}_y. \quad (6.15)$$

Fig. 6.9 illustrates the present strategy for the reversal process for two different temperatures. It is important to note that due to oscillating field the switching occurs on a faster time scale of approximately ten picoseconds for each oscillation at zero Kelvin. Temperature assists the switching with the effect of increasing of switching time.

Trajectories of the magnetic moment illustrated in Fig. 6.10 supplement the fact that all in all the dynamics for a time-dependent field is more complicated. This figure has to be understood as an immediate snapshot since the energy landscape oscillates alone with the field applied. However, for small amplitudes which is the case for Fig. 6.10 this effect is negligible.

The main effect induced by the time-dependent fields is that the field amplitudes expressed in units of the anisotropy fields (Fig. 6.11) have a very pronounced dependence on damping parameter in contrast to the static case. In particular, switching fields for low damping are much smaller than the SW limit indicated on this scale as one. For extremely

high damping this strategy is not advantageous since the minimal fields exceed the SW limit. Such behavior can be explained qualitatively via a resonant energy absorption mechanism when the frequency of the oscillating field matches the precessional one. Note that temperature does not influence these results much for small and moderate damping since the energy landscape oscillates with a high frequency (compared to the static fields shown in Fig. 6.2).

The reversal times associated with these switching fields show qualitatively similar behavior as those for a static field.

A quantitative understanding of the dependencies plotted in Fig. 6.11 and Fig. 6.12 can be found via the solution of the LLG equation in spherical coordinates (system of equations (3.30)) with the field applied as in expression (6.15). The last expression should be presented, however, in spherical coordinates which yields

$$\mathbf{b}(t) = b_0 \left(\sin \theta \sin(\phi - \omega t) \mathbf{e}_r + \cos \theta \cos(\phi - \omega t) \mathbf{e}_\theta + \sin(\omega t - \phi) \mathbf{e}_\phi \right). \quad (6.16)$$

Assuming equation (6.16) and $\mathbf{S} = \mathbf{e}_r$ we find for the total energy

$$\tilde{\mathcal{H}} = -\frac{1}{2} \cos^2 \theta - b_0 \sin \theta \sin(\phi - \omega t), \quad (6.17)$$

from where we deduce for the derivatives needed in equations (3.30)

$$\frac{\partial \tilde{\mathcal{H}}}{\partial \phi} = -b_0 \sin \theta \cos(\phi - \omega t) \quad \text{and} \quad \frac{\partial \tilde{\mathcal{H}}}{\partial \theta} = \cos \theta \sin \theta - b_0 \cos \theta \sin(\phi - \omega t). \quad (6.18)$$

Finally, for the altering of θ we find

$$\dot{\theta} = \frac{1}{1 + \alpha^2} [b_0 \cos(\phi - \omega t) - \alpha \cos \theta (\sin \theta - b_0 \sin(\phi - \omega t))]. \quad (6.19)$$

On this stage the assumption of the field and the magnetic moment synchronization is made which is the case in the vicinity of the energy minima as our dynamical simulations show [129]. Therefore, for the synchronized motion we obtain

$$\dot{\theta} = \frac{1}{1 + \alpha^2} \left[b_0 - \frac{\alpha}{2} \sin 2\theta \right]. \quad (6.20)$$

In principle, from equation (6.20) it follows that $\dot{\theta} > 0$ remains for $b_0 > \alpha/2$. This is a rough estimate of the critical fields needed for the magnetization reversal. The exact solution of equation (6.20) for the initial and target conditions θ_0 and θ_e , respectively, yields

$$b_{0\text{cr}} = \frac{1}{2} \sqrt{\frac{4C^2(1 + \alpha^2)^2}{\omega^2_A t_{\text{rev}}^2} + \alpha^2}, \quad (6.21)$$

with

$$C = \arctan \left[\frac{\alpha - 2b_0 \tan \theta_e}{\sqrt{4b_0^2 - \alpha^2}} \right] - \arctan \left[\frac{\alpha - 2b_0 \tan \theta_0}{\sqrt{4b_0^2 - \alpha^2}} \right]. \quad (6.22)$$

Note that C is small, nonzero and α -independent for $\theta_0 \rightarrow 0$ and $\theta_e \rightarrow \pi$. This relation explains qualitatively and quantitatively the behavior shown in Fig. 6.11 obtained numerically for variation of damping, however, only for low and moderate damping.

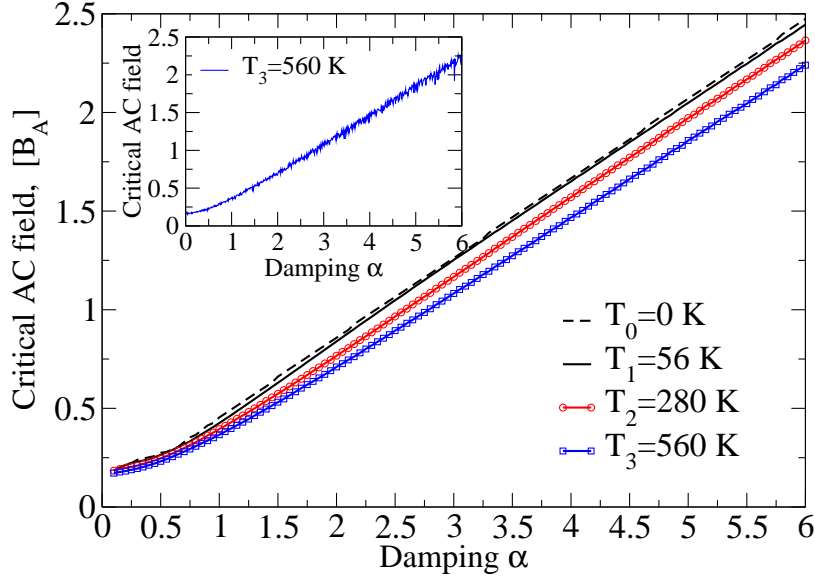


Figure 6.11: Critical field amplitudes expressed in units of the uniaxial anisotropy field as a function of damping parameter for a time-dependent field applied. Each curve is averaged over 500 cycles. Inset shows as-calculated data for $T_3 = 560$ K.

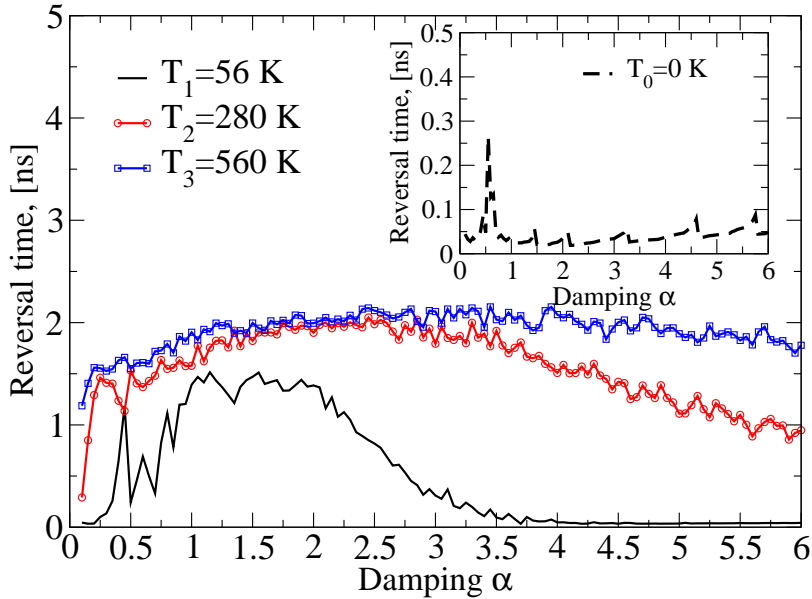


Figure 6.12: Reversal times corresponding to the critical fields plotted in Fig. 6.11. Inset shows not averaged data for $T_0 = 0$ K.

6.2.3 Numerical Study for Nanoparticles with a cubic Anisotropy at Nonzero Temperatures

Finally we study the dynamics and the behavior of switching fields and reversal times of the oscillating field on a nanoparticle with a cubic anisotropy. We take the same nanoparticles and parameters for calculation as described in Subsection 6.1.3. To interpret the results

in a similar way with those reported above we apply the oscillating fields in the plane which is perpendicular to the initial state of the magnetic moment given by $\phi_0 = \pi/4$ and $\theta_0 = \arccos(1/\sqrt{3})$. This implies that the field which enters equation (6.5) can be written as

$$\begin{aligned} \mathbf{b}(t) = & + b_0(\cos \omega_1 t \cos \phi_0 + \sin \omega_1 t \sin \phi_0 \cos \theta_0) \mathbf{e}_x \\ & + b_0(-\cos \omega_1 t \sin \phi_0 + \sin \omega_1 t \cos \phi_0 \cos \theta_0) \mathbf{e}_y \\ & + b_0 \sin \omega_1 t \sin \theta_0 \mathbf{e}_z, \end{aligned} \quad (6.23)$$

with b_0 being the strength and ω_1 the frequency of the oscillating field.

The procedure of determining the field amplitudes is the same as before (see Fig. 6.13 for Z -projection of the magnetization). A three dimensional trajectories of the magnetic moment projected on the energy landscape reveal an interesting behavior (Fig. 6.14): Switching occurs mostly close to the local minima.

Finally, minimal switching fields (Fig. 6.15) and their reversal times (Fig. 6.16) demonstrate the same qualitative behavior as that for the uniaxial anisotropy.

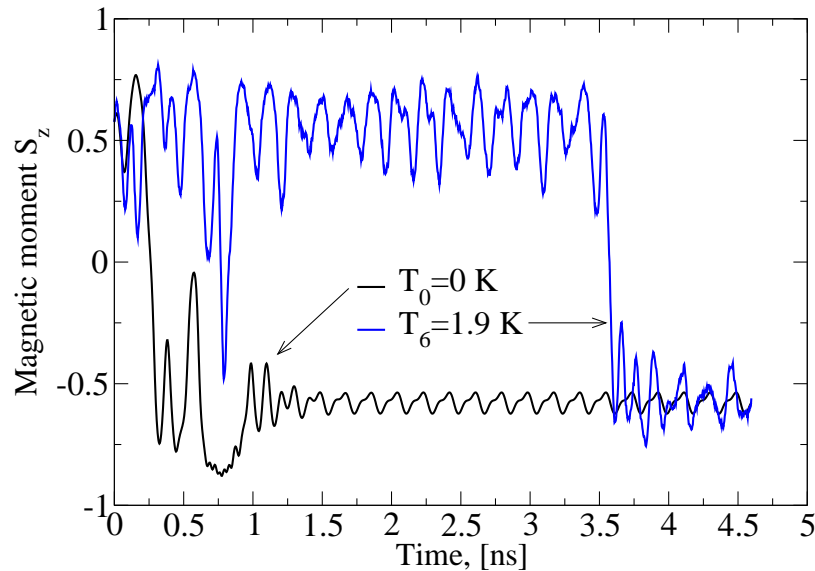


Figure 6.13: Magnetization reversal of a nanoparticle when a time-dependent field is applied for $\alpha = 0.1$ and at $T_0 = 0$ K and $T_6 = 1.9$ K. Parameters chosen in simulations are $b_0 = 0.055$ and $\omega_1 = \tilde{\omega}_A/1.93$ with $\tilde{\omega}_A = (2/3)\omega_A$.

6.3 Discussion and Interpretation of the Results obtained

In this chapter the dynamical properties of mainly two kinds of systems using the analytical LLG equation and the one numerically extended for finite temperatures were studied. The most attention was paid to the study of the minimal switching fields as a function of the damping parameter, temperature and the type of anisotropy. The corresponding reversal times should be considered as complementary data since they turned out to be very sensitive functions of the applied fields and hence thermal fluctuations (see equation (6.3)).

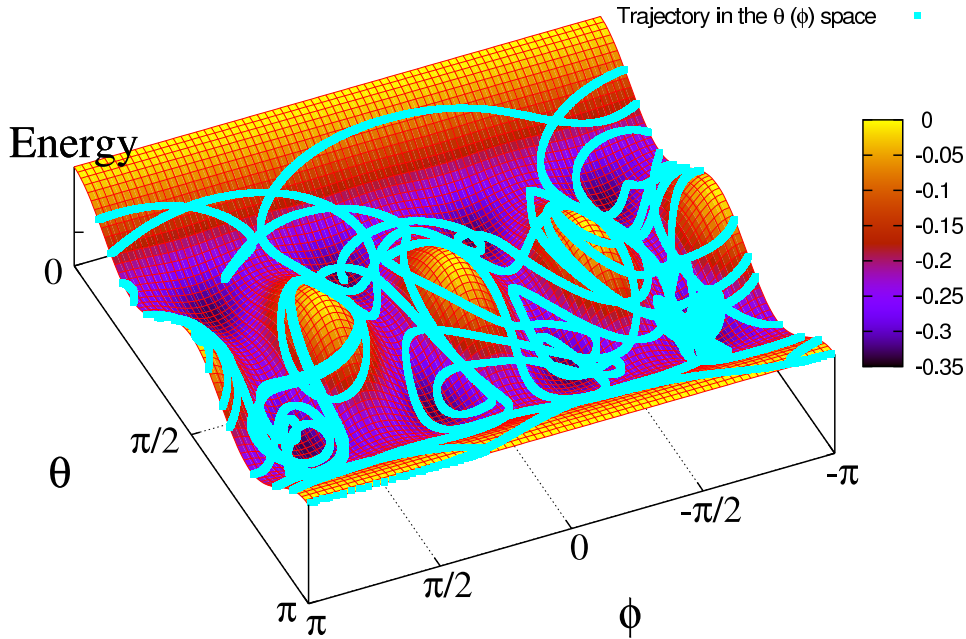


Figure 6.14: Trajectories of the magnetic moment in the $E(\theta, \phi)$ space. Other parameters are as those listed in Fig. 6.13 for zero Kelvin. The start and target states are as those shown in Fig. 6.5.

These numerical "experiments" are similar in spirit to those captured by the microwave spectroscopy, where the oscillating fields with frequencies in the range of some hundred Gigahertz are used. The main similarity concerns the time window or the measurement time which was fixed to some nanoseconds. However, there are significant principle differences between the numerical results and the conventional experiments. In particular, we explicitly contrasted the cases of static (DC) and time-dependent (AC) fields. As inferred from Figures 6.2 and 6.10 e.g., the mechanisms of transition between the states for a DC and an AC field have totally various nature. Indeed, in case of a static field switching occurs due to the change of the heights in the energy landscape between the initial and the target states. When applying a field oscillating with a frequency of the same order of magnitude with the field-free precessional frequency one observes a resonant-like energy absorption followed by a magnetization switching when the field strength is large enough. As a result of the different mechanisms the dependencies of critical fields on damping and temperature for DC and AC fields show a different behavior. Once the measurement time is set to be large enough for switching critical DC fields do not depend on damping. This phenomenon is explained due to a quasi equilibrium change of the state of the magnetic moment where a certain equilibrium between the supplied energy and the dissipated one is set. This is also reflected in the corresponding reversal times that all regardless the temperature are of the order of picoseconds. This becomes especially important for an AC field applied which is a more dynamical process in the sense that the $T = 0$ K reversal times are on the time scale of some tens to hundred picoseconds.

Various anisotropy types are important as the potential systems for information storage units. Their dynamical properties are generally more complicated and even the issue of switching becomes questionable. This will be additionally addressed in the next chapter. Moreover, systems with a cubic anisotropy demonstrate lower switching fields due to the geometry of the crystal.

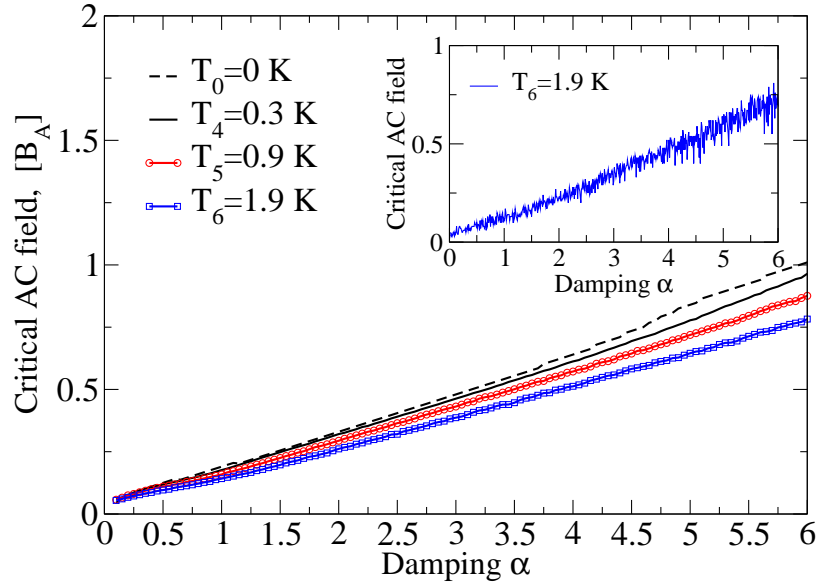


Figure 6.15: Critical field amplitudes expressed in units of the uniaxial anisotropy field as a function of damping parameter for a time-dependent field. Each curve is averaged over 500 cycles. Inset shows as-calculated data for $T_6 = 1.9$ K.

As a final point to this chapter the relatively high range of damping variation should be addressed. Usually, the values of damping for ferromagnetic thin films range from 0.01 to 0.3. Doping of ferromagnets with rare earths or transition metals can enhance the values up to 0.8 (see references in Chapter 4).

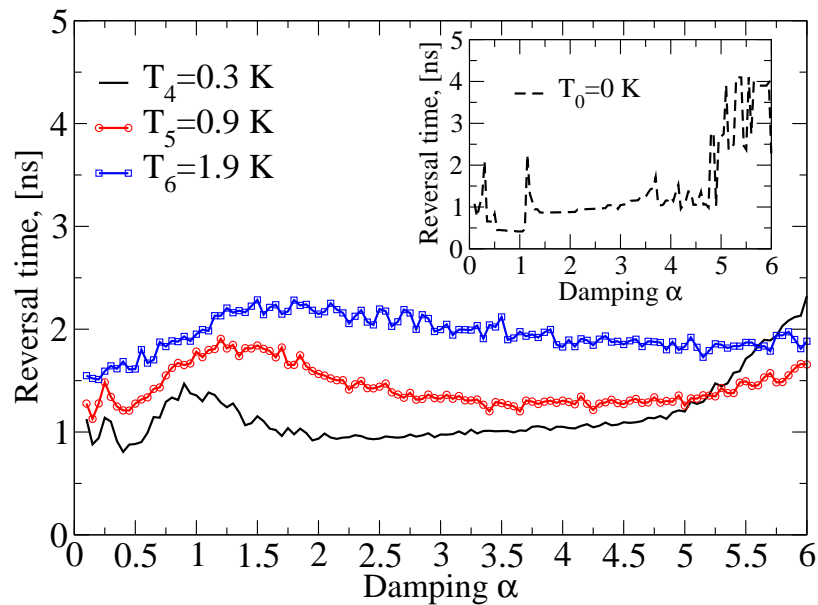


Figure 6.16: Reversal times corresponding to the critical fields plotted in Fig. 6.15. Inset shows not averaged data for $T_0 = 0$ K.

7 Dynamical Properties of the Magnetization in the Presence of pulsed Fields

In this chapter properties of magnetization dynamics are studied when short magnetic pulses are applied. The key point is an impulsive excitation which populates states with higher energies within times much shorter than the field-free precessional period.

The interest in such type of magnetization excitation is driven by possible applications in data storage devices as well as fast magnetic sensors [10–13] on the one hand, and by the fundamentally different physical properties of these systems on the other hand. Recent experiments [90, 91, 130, 131] revealed the usage of a finely focused electron beam producing magnetic pulses with durations of several picoseconds and field strengths of up to several tesla for the magnetization switching. We require the pulses to be even shorter than those in the experiments and in contrast to the numerical simulations [132] develop an analytical scheme for the magnetization reversal, "freezing" and numerically extend the proposed model for finite temperatures. The scheme relies on the Local Control Theory (LCT) [19–21] widely used in the quantum chemistry [133]. The controlled conditions within the LCT are derived from the response of the system providing a clear physical interpretation for the control mechanism.

First, the analytical model with the main assumptions and approximations is presented. Then, we demonstrate that the properties of the magnetic moment evolution mainly depend on the angle shift $\delta\phi$ between the magnetization and the pulse. Note, that the main assumption, namely the shortness of the pulse, allows to decouple the LLG equations with respect to the Cartesian components and to proceed with subsequent analytical findings. Further analytical and numerical results are illustrated by contrasting two cases with different angles shifts $\delta\phi = 3\pi/2$ and $\delta\phi = 0$. Numerical methods serve additionally for illustrating the magnetization dynamics for nanoparticles with a cubic anisotropy.

7.1 Analytical Model

7.1.1 Theory

For demonstration of the proposed scheme we chose $\text{Fe}_{50}\text{Pt}_{50}$ nanoparticles (see Chapter 2 for their internal parameters), whereas the results for a cubic anisotropy will be addressed for $\text{Fe}_{70}\text{Pt}_{30}$ small particles.

Similarly to the previous chapter the dynamics of the magnetic moment of the nanoparticle is governed by a system of the LLG equations (3.30) with the zero Kelvin effective field in the form of equation (3.26). The total energy of the nanoparticle is given by

$$\tilde{\mathcal{H}} = \tilde{\mathcal{H}}_A + \tilde{\mathcal{H}}_F = \tilde{\mathcal{H}}_A - \mathbf{S} \cdot \mathbf{b}_0(t), \quad (7.1)$$

where the energy is measured in units of $\mu_S B_A$ with $B_A = 2D/\mu_S$. D is the strength of the anisotropy energy. Time in the system of equations (3.30) is expressed in units of the field-free precessional period T^{prec} . The magnetic field pulse $\mathbf{b}_0(t)$ is realized as a superposition of two perpendicular pulses \mathbf{b}_x and \mathbf{b}_y lying in the XY -plane (see Fig. 3.1) with the mock angle $\phi_0 = \arctan(|b_y|/|b_x|)$. Note, that for the pulse with duration ε we may write

$$\mathbf{b}_0(t) = \begin{cases} \frac{f(t)b_0}{2\varepsilon}(\cos \phi_0 \mathbf{e}_x + \sin \phi_0 \mathbf{e}_y), & t_0 - \varepsilon < t < t_0 + \varepsilon \\ 0, & \text{elsewhere.} \end{cases} \quad (7.2)$$

The total energy change under the influence of such a pulse becomes

$$\begin{aligned} \frac{\partial \tilde{\mathcal{H}}}{\partial \phi} &= \frac{\partial \tilde{\mathcal{H}}_A}{\partial \phi} + \frac{\partial \tilde{\mathcal{H}}_F}{\partial \phi} = \frac{\partial \tilde{\mathcal{H}}_A}{\partial \phi} + \frac{b_0 f(t)}{2\varepsilon} \sin \theta \sin(\phi - \phi_0), \\ \frac{\partial \tilde{\mathcal{H}}}{\partial \theta} &= \frac{\partial \tilde{\mathcal{H}}_A}{\partial \theta} + \frac{\partial \tilde{\mathcal{H}}_F}{\partial \theta} = \frac{\partial \tilde{\mathcal{H}}_A}{\partial \theta} - \frac{b_0 f(t)}{2\varepsilon} \cos \theta \cos(\phi - \phi_0). \end{aligned} \quad (7.3)$$

Rewriting the LLG system of equation with the expressions (7.3) and with new dimensionless variable $\tau(t)$

$$\tau(t) = \frac{t - (t_0 + \varepsilon) + 2\varepsilon}{2\varepsilon}, \quad \frac{d\tau}{dt} = \frac{1}{2\varepsilon}, \quad (7.4)$$

with properties

$$\begin{aligned} \tau &= 0 \text{ for } t = t_0 - \varepsilon, \\ \tau &= 1 \text{ for } t = t_0 + \varepsilon, \end{aligned} \quad (7.5)$$

yields

$$\begin{aligned} \frac{1}{2\varepsilon} \frac{d\phi}{d\tau} &= p \left[\frac{1}{\sin \theta} \frac{\partial \tilde{\mathcal{H}}_A}{\partial \theta} - \frac{\alpha}{\sin^2 \theta} \frac{\partial \tilde{\mathcal{H}}_A}{\partial \phi} \right] \\ &\quad - \frac{pb_0 f(t(\tau))}{2\varepsilon} \left[\frac{\cos \theta}{\sin \theta} \cos \delta\phi + \alpha \frac{\sin \delta\phi}{\sin \theta} \right], \\ \frac{1}{2\varepsilon} \frac{d\theta}{d\tau} &= p \left[-\frac{1}{\sin \theta} \frac{\partial \tilde{\mathcal{H}}_A}{\partial \phi} - \alpha \frac{\partial \tilde{\mathcal{H}}_A}{\partial \theta} \right] \\ &\quad + \frac{pb_0 f(t(\tau))}{2\varepsilon} [-\sin \delta\phi + \alpha \cos \theta \cos \delta\phi], \end{aligned} \quad (7.6)$$

where the new notations $\delta\phi = \phi - \phi_0$ for the angle shift and $p = 1/(1 + \alpha^2)$ were introduced.

We require for the pulses to be much shorter than the precessional period, i.e. $\varepsilon \ll T^{\text{prec}}$. Hence, as it follows from equations (7.6) the effect of the anisotropy becomes negligible during the pulse application and the dynamics of the magnetic moment can be separately considered during the pulse application (excitation) and directly after the pulse application (relaxation).

In the absence of the field, i.e. $b_0 = 0$, the dynamics is only influenced by the type of the anisotropy. For instance, for a uniaxial anisotropy

$$\tilde{\mathcal{H}}_A^U = -\frac{1}{2} \cos^2 \theta \quad (7.7)$$

for the initial conditions $\phi_f(t = \bar{t}_0)$ and $\theta_f(t = \bar{t}_0)$ the solution is known [76, 77] and reads

$$\begin{aligned}\phi_f(t) &= \phi(\bar{t}_0) \pm \frac{t - \bar{t}_0}{1 + \alpha^2} \\ &\pm \frac{1}{\alpha} \ln \left| \frac{\cos \theta_f(\bar{t}_0) \left(1 + \sqrt{1 + \tan^2 \theta_f(\bar{t}_0) \cdot e^{-\frac{2\alpha(t - \bar{t}_0)}{1 + \alpha^2}}} \right)}{1 + \cos \theta_f(\bar{t}_0)} \right|, \\ \tan \theta_f(t) &= \tan \theta_f(\bar{t}_0) \cdot e^{-\frac{\alpha}{1 + \alpha^2}(t - \bar{t}_0)},\end{aligned}\tag{7.8}$$

where \pm refer to the area $0 < \theta < \pi/2$ or $\pi/2 < \theta < \pi$, respectively. This solution indicates that the magnetic moment relaxes either to $\theta_{f,\min 1} = 0$ or to $\theta_{f,\min 2} = \pi$.

When no field is applied and the dynamics is governed by a cubic anisotropy with energy

$$\tilde{\mathcal{H}}_A^C = -\frac{1}{2}(\cos^2 \phi \sin^2 \phi \sin^4 \theta + \cos^2 \theta \sin^2 \theta),\tag{7.9}$$

the solution of the system

$$\begin{aligned}\frac{d\phi}{dt} &= -\frac{1}{1 + \alpha^2} \cos \theta \left(\frac{1}{2} \sin^2 2\phi \sin^2 \theta + \cos 2\theta \right) \\ &+ \frac{1}{4} \frac{\alpha}{1 + \alpha^2} \sin^2 \theta \sin 4\phi, \\ \frac{d\theta}{dt} &= \frac{1}{4} \frac{1}{1 + \alpha^2} \sin^3 \theta \sin 4\phi \\ &+ \frac{1}{2} \frac{\alpha}{1 + \alpha^2} \sin 2\theta \left(\frac{1}{2} \sin^2 2\phi \sin^2 \theta + \cos 2\theta \right),\end{aligned}\tag{7.10}$$

becomes nontrivial and only in certain limiting cases like for a thin film approximation, an analytical solution can be obtained.

Now we focus on the issue concerning the state of the magnetic moment directly after the pulse application. The system of equations (7.6) in approximation $\varepsilon \ll T^{prec}$ yields

$$\begin{aligned}\frac{d\phi}{d\tau} &= -\frac{1}{\sin \theta} \frac{b_0 f(t(\tau))}{1 + \alpha^2} [\cos \theta \cos \delta\phi + \alpha \sin \delta\phi], \\ \frac{d\theta}{d\tau} &= \frac{b_0 f(t(\tau))}{1 + \alpha^2} [-\sin \delta\phi + \alpha \cos \theta \cos \delta\phi].\end{aligned}\tag{7.11}$$

Introducing the notations for before the pulse $\theta(t^-)$, $\phi(t^-)$ ($t^- := t_0 - \varepsilon$) and directly after the pulse $\theta(t^+)$ and $\phi(t^+)$ ($t^+ := t_0 + \varepsilon$), we demand for a stroboscopic evolution of the magnetic moment

$$\theta(t^+) > \theta(t^-) \quad \forall t^+, t^-, \tag{7.12}$$

which leads to switching when θ increases always upon the pulse application.

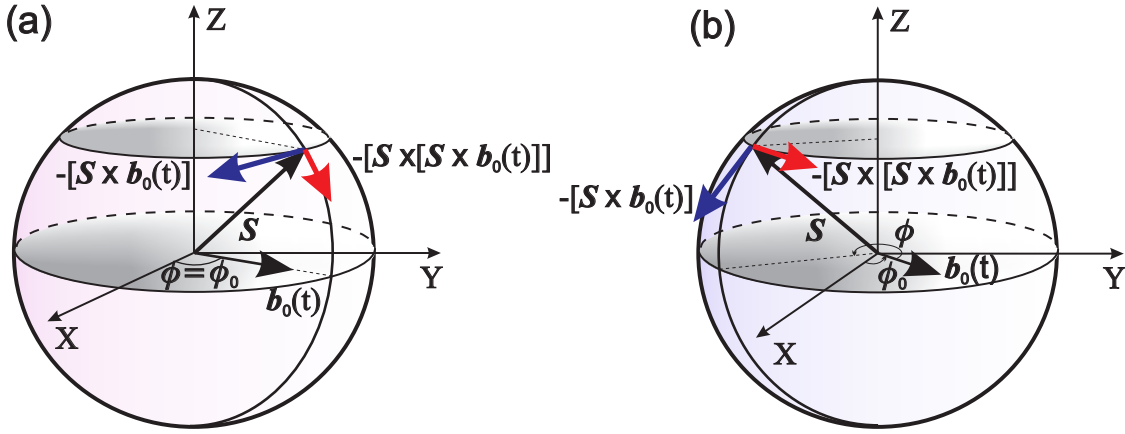


Figure 7.1: Graphical illustration of torques exerted by a magnetic pulse for two different angle shifts: $\delta\phi = 0$ (a) and $\delta\phi = 3\pi/2$ (b). For $\delta\phi = 3\pi/2$ the precessional torque becomes more favorable for switching, whereas for $\delta\phi = 0$ this is the case when the relaxation term is dominant.

Solution for $\delta\phi = 0$

For a sequence of pulses (7.2) each applied with the same duration and angle shift $\delta\phi_i = 0$ and centered at times $t_{0,i}$ we find from the system (7.11) the following changes of azimuthal and polar angles

$$\begin{aligned} \phi(t_i^+) &= \phi(t_i^-) - \ln \left| \tan \left(\frac{\theta(t_i^+)}{2} \right) \cdot \frac{\tan \left(\frac{\theta(t_i^-)}{2} + \frac{\pi}{4} \right) + 1}{\tan \left(\frac{\theta(t_i^-)}{2} + \frac{\pi}{4} \right) - 1} \right|, \\ \tan \left(\frac{\theta(t_i^+)}{2} \right) &= \frac{\tan \left(\frac{\theta(t_i^-)}{2} + \frac{\pi}{4} \right) \cdot e^{\frac{\alpha b_0 f(t_{0,i})}{1+\alpha^2}} - 1}{\tan \left(\frac{\theta(t_i^-)}{2} + \frac{\pi}{4} \right) \cdot e^{\frac{\alpha b_0 f(t_{0,i})}{1+\alpha^2}} + 1}. \end{aligned} \quad (7.13)$$

Two features of this solution should be mentioned. The changes of θ are not uniform and depend on the prior-pulse angle $\theta(t_i^+)$. Moreover, the changes of the angles strongly depend on damping. In particular, for low damping the switching becomes not effective since θ is not altered. For high damping we get $\theta(t_i^+) \rightarrow \pi/2$ and $\phi(t_i^+)$ strongly depends on $\theta(t_i^-)$. For the condition $d\theta/d\tau > 0$ which enables the switching, the sign of $\cos \theta$ should be taken into account, since it is different for $0 < \theta < \pi/2$ and $\pi/2 < \theta < \pi$.

Solution for $\delta\phi = 3\pi/2$

Similar to the solutions for $\delta\phi_i = 0$ one can also derive those for $\delta\phi_i = 3\pi/2$

$$\begin{aligned} \phi(t_i^+) &= \phi(t_i^-) + \alpha \ln \left| \frac{\tan \left(\frac{\theta(t_i^-)}{2} + \frac{1}{2} \frac{b_0 f(t_{0,i})}{1+\alpha^2} \right)}{\tan \left(\frac{\theta(t_i^-)}{2} \right)} \right|, \\ \theta(t_i^+) &= \theta(t_i^-) + \frac{b_0 f(t_{0,i})}{1+\alpha^2}. \end{aligned} \quad (7.14)$$

This solution reveals totally different properties of θ variation. They are uniform and essentially depend on the field strength b_0 and less on damping. An additional property is that for small α angle ϕ remains almost the same. In view of a very low damping parameter to be measured and calculated for nanoparticles this strategy provides a quasi ballistic switching.

Fig. 7.1 sketches the directions of the torques acting on the magnetic moment when the pulse is applied for both $\delta\phi = 0$ and $\delta\phi = 3\pi/2$. The main feature for the $\delta\phi = 0$ pulse is that both the precessional and the relaxation terms written for the applied pulse point in the opposite directions as compared to the relaxation motion (Fig. 3.5). Therefore, every time the pulse is applied its precessional torque compensates for the precessional term caused by the anisotropy and its relaxation term can compensate for the damping term in the case of field-free motion in the case when the appropriate field strength is chosen. The situation becomes completely different for the $\delta\phi = 3\pi/2$ pulses. Every time when the $\delta\phi = 3\pi/2$ pulses are applied their precessional torque acts against the field-free relaxation motion and their damping torque is aligned parallel to the field-free precessional moment.

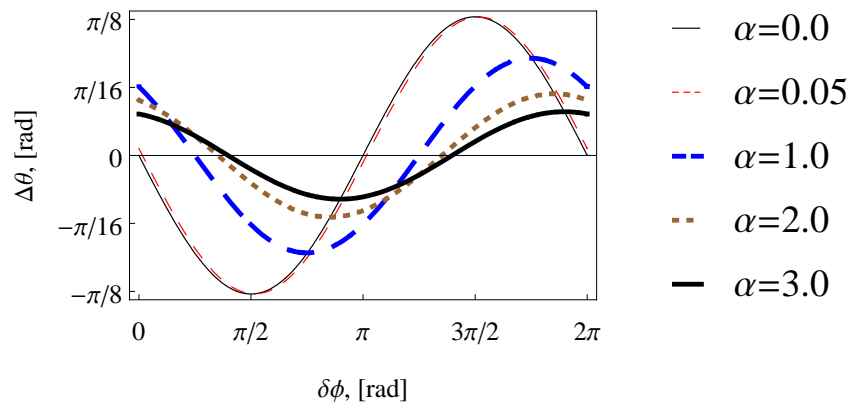


Figure 7.2: Change of angle θ directly after the i th pulse as a function of $\delta\phi$ plotted for different values of damping α ($b_0 = 0.4$, $\theta(t_i^-) = \pi/180$, $f(t_{0,i}) = 1$).

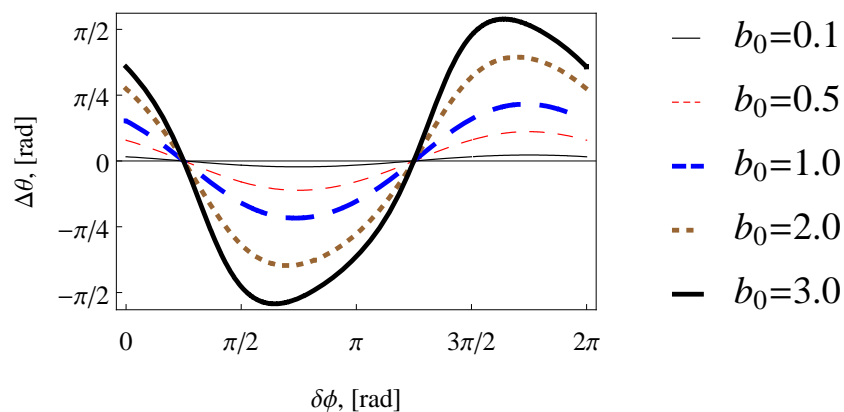


Figure 7.3: Change of angle θ directly after the i th pulse as a function of $\delta\phi$ plotted for different values of the field amplitude b_0 ($\alpha = 1.0$, $\theta(t_i^-) = \pi/180$, $f(t_{0,i}) = 1$).

Solution for general $\delta\phi$

It has to be stressed that the second equation in system (7.11) can be solved exactly. We are interested in the quantity $\Delta\theta_i = \theta(t_i^+) - \theta(t_i^-)$ as a function of $\delta\phi$ which might be found from

$$\begin{aligned} & \left| 2\sqrt{2} \operatorname{arctanh} \left[\frac{\frac{\sqrt{1+\cos 2\delta\phi_i}}{\cos \delta\phi_i} (\alpha \cos \delta\phi_i + \sin \delta\phi_i) \tan \frac{\theta}{2}}{\sqrt{\alpha^2 - 1 + (\alpha^2 + 1) \cos 2\delta\phi_i}} \right] \right|_{\theta(t_i^-)}^{\theta(t_i^+)} \\ &= \frac{b_0 f(t_{0,i})}{1 + \alpha^2} \cdot \sqrt{\alpha^2 - 1 + (\alpha^2 + 1) \cos 2\delta\phi_i}. \end{aligned} \quad (7.15)$$

Fig. 7.2 shows the dependency (7.15) with a variation of damping. Due to a high moment (see the LLG equation) exerted to the system one achieves a maximum positive change in θ for $\delta\phi = 3\pi/2$ at small α (black thin curve). The figure also supplements the fact that the switching might be effective for $\delta\phi = 0$, however, in a high damping regime.

Besides damping, the field strengths can also strongly influence the dynamics of the magnetic moment subjected to such short magnetic pulses. Change $\Delta\theta_i$ upon the field strength is shown in Fig. 7.3, where for a more contrast we increased damping to $\alpha = 1.0$. For sufficiently high field amplitudes one can even obtain switching by using one single field pulse.

A general observation from both Fig. 7.2 and Fig. 7.3 is that upon no variation of damping or field amplitudes it is not possible to change the period of $\delta\phi$, which has always positive and negative changes of $\Delta\theta$.

An independent solution for the variation of angles θ and ϕ might be directly obtained from the system (7.11) by assuming α to be zero. The solution obtained is

$$\begin{aligned} \phi(t_i^+) &= \phi(t_i^-) - \frac{\cos \delta\phi}{\sin \delta\phi} \ln \left| \frac{\tan(\theta(t_i^-) - b_0 f(t_{0,i}) \sin \delta\phi)}{\sin \theta(t_i^-)} \right|, \\ \theta(t_i^+) &= \theta(t_i^-) - b_0 f(t_{0,i}) \sin \delta\phi. \end{aligned} \quad (7.16)$$

The solution is basically presented by the black thin curves in Fig. 7.2 and Fig. 7.3 which clearly affirms the idea of the most effective switching for $\delta\phi_i = 3\pi/2$.

Regarding the change of ϕ for general $\delta\phi$, it becomes impossible to deduce it from equations (7.11) using the general solution (7.15). Thus, further purely analytical realization of switching is not available and will be supported by a recursive numerical procedure described in Subsection 7.1.2.

Critical Field Amplitudes needed for Reversal for a Sequence of Pulses with fixed $\delta\phi$

Above the shift angle $\delta\phi$ was addressed to mainly determine the switching behavior. Obviously, the strength of the applied pulses plays a significant role for switching. Here, we discuss the conditions under which the minimum field amplitudes can be derived. For the steady increase of θ it is natural to demand that the change during the excitation $\Delta\theta_i^{\text{excit}} = \theta(t_i^+) - \theta(t_i^-)$ is at least not less than the rate of θ decrease during the relaxation process $\Delta\theta_i^{\text{relax}} = \theta(t_i^-) - \theta(t_{i-1}^+)$ or

$$\Delta\theta_i^{\text{excit}} \geq |\Delta\theta_i^{\text{relax}}|. \quad (7.17)$$

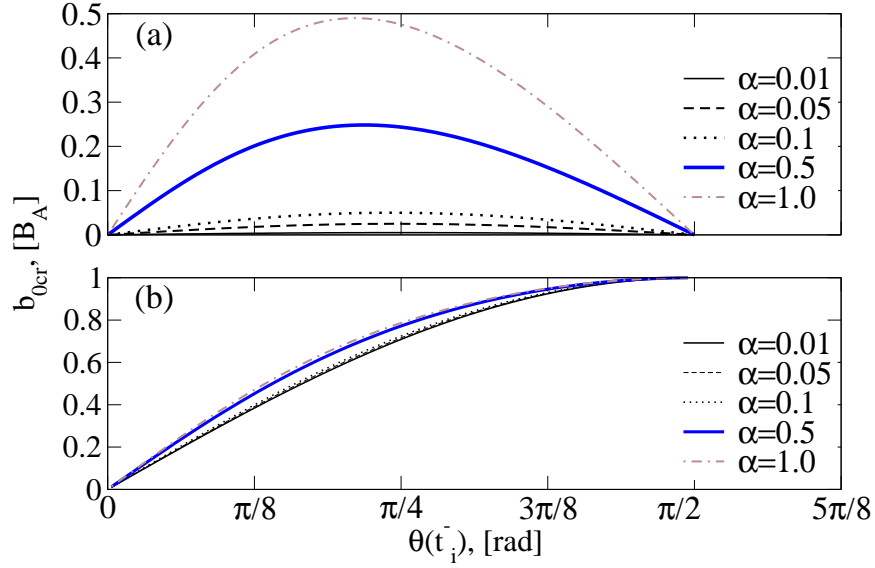


Figure 7.4: Dependence of critical field amplitude b_{0cr} expressed in units of the uniaxial anisotropy field on the angle $\theta(t_i^-)$ at the beginning of the pulse application for $\delta\phi_i = 3\pi/2$ (a) and $\delta\phi_i = 0$ (b). The pulses are applied with a time interval equal to the precessional period.

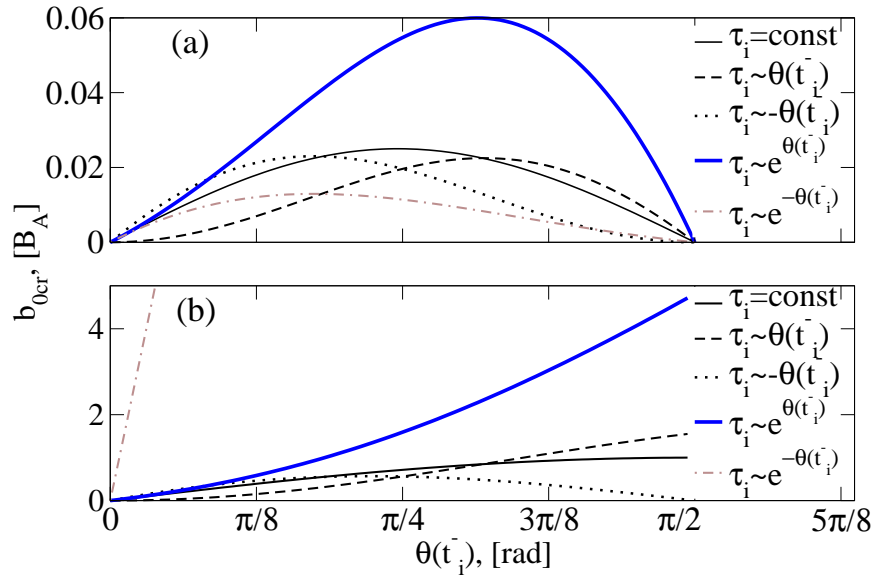


Figure 7.5: Dependence of critical field amplitude b_{0cr} on the angle $\theta(t_i^-)$ at the beginning of the pulse application for $\delta\phi_i = 3\pi/2$ (a) and $\delta\phi_i = 0$ (b) for $\alpha = 0.05$. Pulses are applied with various time lags τ_i .

The relaxation rate is known from the field-free solution contained in equation (7.8) and can be expressed as

$$\Delta\theta_i^{\text{relax}} = \arctan\left(\tan(\theta(t_i^-)) \cdot e^{\frac{\alpha\tau_i}{1+\alpha^2}}\right) - \theta(t_i^-), \quad (7.18)$$

where τ_i denotes the i th relaxation until the $i + 1$ th excitation. Assuming expressions (7.18) and (7.14) and keeping in mind the condition (7.17) we determine for the critical

field amplitudes all applied with $\delta\phi_i = 3\pi/2$

$$b_{0\text{cr}}^{(\delta\phi_i=3\pi/2)} = (1 + \alpha^2) \left(\arctan \left(\tan(\theta(t_i^-)) \cdot e^{\frac{\alpha\tau_i}{1+\alpha^2}} \right) - \theta(t_i^-) \right). \quad (7.19)$$

In a similar manner one can find the critical fields for the pulses all applied with $\delta\phi_i = 0$

$$b_{0\text{cr}}^{(\delta\phi_i=0)} = - \frac{1 + \alpha^2}{\alpha} \ln \left| \tan \left(\frac{\theta(t_i^-)}{2} + \frac{\pi}{4} \right) \right| + \frac{1 + \alpha^2}{\alpha} \ln \left| \frac{1 + \tan\left(\frac{1}{2} \arctan \left(\tan(\theta(t_i^-)) \cdot e^{\frac{\alpha\tau_i}{1+\alpha^2}} \right)\right)}{1 - \tan\left(\frac{1}{2} \arctan \left(\tan(\theta(t_i^-)) \cdot e^{\frac{\alpha\tau_i}{1+\alpha^2}} \right)\right)} \right|. \quad (7.20)$$

Both equation (7.19) and (7.20), i.e. the minimal field amplitudes expressed in units of the anisotropy field and leading to switching, are plotted in Fig. 7.4. For the constant lag time between the pulses the procedure of pulse applications with $\delta\phi_i = 3\pi/2$ turns out to be more advantageous for all values of damping since due to more effective switching the field amplitudes to be applied have lower values. For the nonconstant time lag between the pulses these dependencies change their forms. In particular, upon the time lag function this may lead to either decrease or increase of minimal switching fields. Nevertheless, for the damping chosen to be small the strategy with the pulses all applied with $\delta\phi_i = 3\pi/2$ we obtained smaller field amplitudes.

Our further numerical simulations will show that the scenario with the fixed lag time during relaxation is valid during the stabilization of the magnetic moment in equilibrium. This means that out of equilibrium, i.e. when the excitation is not completely balanced by the relaxation, the time lag is not a constant.

7.1.2 Principle of controlled Switching

Based on the results obtained from the solution of the nonstochastic LLG equation we attempt to demonstrate how the scheme is capable for switching (Fig. 7.6) when all short magnetic pulses are applied with the shift angle $\delta_i = 3\pi/2$. Starting from a given equilibrium state of the magnetic moment given by $\phi = \phi(0)$ and $\theta = \theta(0)$ the first pulse centered at $t_{0,1}$ is applied when condition $\phi(0) - \phi_0 = 3\pi/2$ is fulfilled. Equation (7.14) yields a condition for the tilt angle after the pulse application. Thereafter, the field-free propagation comes about according to equation (7.8) with the initial values $\phi_f(\bar{t}_0) = \phi(t_1^+)$ and $\theta_f(\bar{t}_0) = \theta(t_1^+)$. Then, at the time moment $t = t_{0,2}$ a second pulse is applied with the same angle shift $\phi_f(t_1^+ + \tau_1) - \phi_0 = 3\pi/2$. The procedure of the controlled pulse applications is repeated until the state with $\theta = \pi/2$ is reached by a subsequent relaxation to the target state $\theta \rightarrow \pi$.

Figs. 7.7 and 7.8 demonstrate the described scheme for two limits of damping parameter, 0.05 and 1.0, respectively. Interesting fact is that in low relaxation regime (see Fig. 7.7) switching is observed for both angle shifts, where surprisingly for $\delta\phi_i = 0$ the switching occurs earlier. Switching is completely not achievable for high values of damping for the same field strengths as for small α when $\delta\phi_i = \pi/2$ (Fig. 7.8 (a)). Also in the limit of high damping the switching occurs for $\delta\phi_i = 0$. From these illustrations we conclude that not only θ change after the pulse, also ϕ altering plays a significant role and should be taken into account.

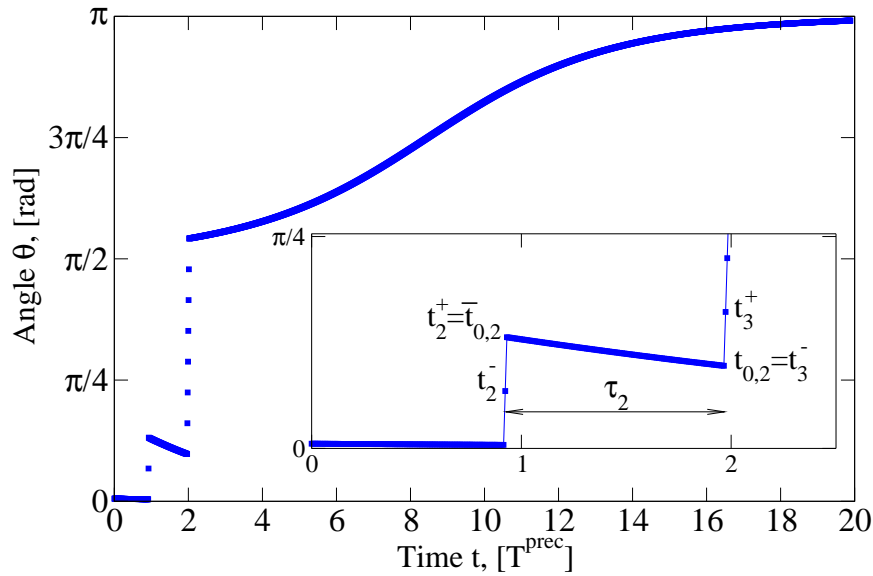


Figure 7.6: Evolution of θ according to the proposed control scheme and for $\phi_f(t=0) = \pi/180 = \theta_f(t=0)$, $\phi_0 = \arctan(b_y/b_x) = 2\pi/3$, $\alpha = 0.05$, $f = 1$, $b_0 = 0.2$. Inset shows the short-time behavior (pulses are switched off for $\theta > \pi/2$).

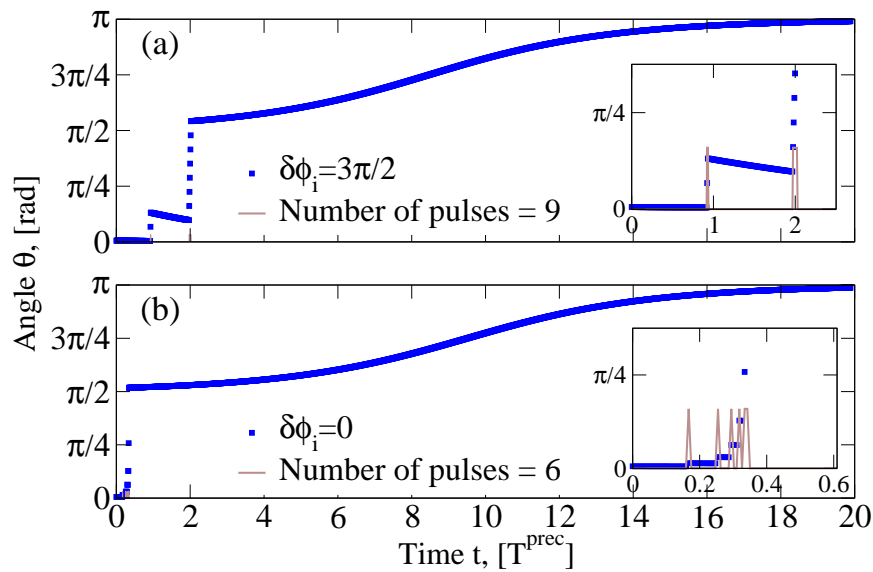


Figure 7.7: Evolution of θ for two angle shifts $\delta\phi_i = 3\pi/2$ (a) and $\delta\phi_i = 0$ (b) and for $\phi_f(0) = \pi/180$, $\theta_f(0) = \pi/180$, $\phi_0 = \pi/3$, $\alpha = 0.05$, $b_0 = 0.2$, $f(t_{0,i}) = 1$. Insets show the detailed motion at the beginning of the pulse application (field amplitudes enlarged x5).

7.2 Numerical Illustrations

7.2.1 Rectangular shaped magnetic Pulses

The results shown above have uncovered many interesting issues needed for the magnetization switching and control, the questions of pulse duration and its form together with temperature and different anisotropy effects, however, were all not captured by the analyt-

ical procedure. Hence, further numerical simulations are required to supplement, approve and also extend the analytical results. The analytical results reported in Section 7.1 remain important since they state the range of parameters used in numerics. Concerning the damping parameter it is known that the typical values are from 0.001 to approximately 0.05 (Chapter 4). We deliberately decide to take the maximum of these values to speed up the relaxation process.

The numerical stochastic LLG was implemented according to the description given in Chapters 5 and 6. Further details can be found in [128].

In this subsection we choose rectangular shaped short magnetic pulses having a duration T^R for which we can write

$$\mathbf{b}_0^R(t) = \begin{cases} b_0^R(\cos \phi_0 \mathbf{e}_x + \sin \phi_0 \mathbf{e}_y), & t_0 - T^R < t < t_0 + T^R \\ 0, & \text{elsewhere.} \end{cases} \quad (7.21)$$

Duration of the Pulses

To decide which duration of the pulses is the most appropriate for the scheme proposed we numerically model switching starting from a state $\theta \rightarrow 0$ (see Fig. 7.9). All pulses are applied at zero Kelvin when the ϕ -angles of the magnetic moment and of the field differ in $3\pi/2$ (both (a) cases in Fig. 7.7 and 7.8). In particular, a very effective way to apply pulses is when a certain balance between the strength and the duration of the pulse is set, which is the case for $T^R = T^{\text{prec}}/6$. Additional feature is that when reaching equilibrium between the relaxation and the excitation a magnetic moment stabilization (θ stabilization) is achievable. DC or AC continuous magnetic fields mentioned in Chapter 6 are not capable to provide such a stabilization, to the knowledge of the author. Figures 7.4 and 7.5 (both (a) cases) depict the reason for the stabilization: Choosing a certain constant field amplitude it is enough to reach further state where this field lies higher than the critical one. At the crossing of the critical fields curve with the chosen field the balance in the relaxation and excitation sets in and for the magnetic moment it means a spacial θ stabilization. As

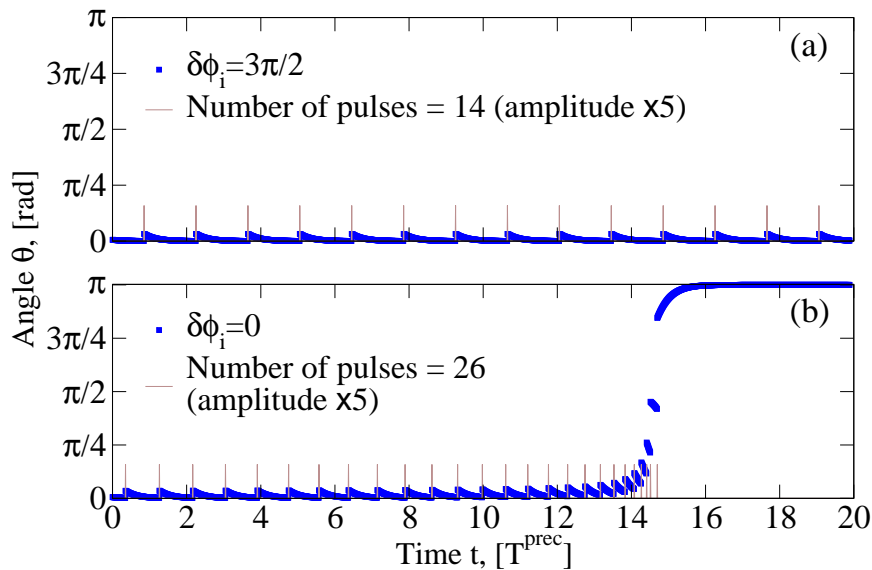


Figure 7.8: Evolution of θ for two angle shifts $\delta\phi_i = 3\pi/2$ (a) and $\delta\phi_i = 0$ (b) and for $\phi_f(0) = \pi/180$, $\theta_f(0) = \pi/180$, $\phi_0 = \pi/3$, $\alpha = 1.0$, $b_0 = 0.2$, $f(t_{0,i}) = 1$.

inferred from Fig. 7.9 the magnetic moment can be well controlled for the durations below T^{prec} and no special pulse duration tuning is required as long as the duration is shorter than the precessional period.

For the later results we choose the duration of $T^{\text{R}} < T^{\text{prec}}/100$ to avoid an overlapping of the pulses.

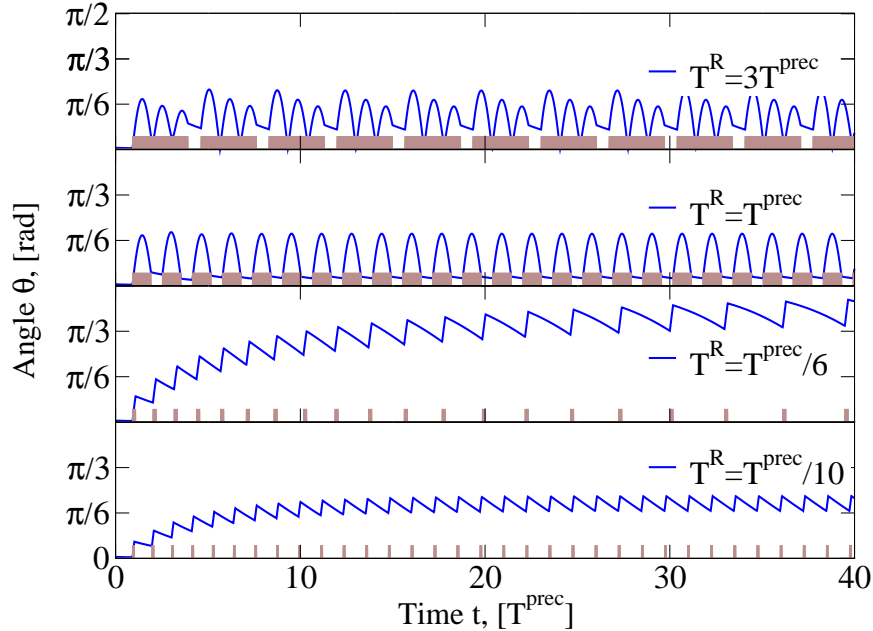


Figure 7.9: $\theta(t)$ for different pulse durations. The pulses are shown as solid rectangles. T^{prec} is the precessional period and $b_0 = 0.3$, $\alpha = 0.05$.

Controlled Switching

When an exact control is required to achieve switching what will happen when only the first pulse is applied with a fixed angle shift and the rest with an arbitrary angle shift? This question is relevant for an experimental realization of this scheme. This point we address by simulating the evolution of θ of the magnetic moment subjected to short pulses when all the pulses are applied strictly with $\delta\phi_i = 3\pi/2$ (Fig. 7.10 (a)) and only the first pulse is strictly followed to this scheme, i.e. $\delta\phi_1 = 3\pi/2$ (Fig. 7.10 (b)). Obviously, when the magnetic moment is not controlled no switching can be seen regardless of the strength of the fields applied. Only a small θ -stabilization is reached around a certain θ . At the same time, for a strict control we observe both the θ -stabilization (amplitudes below $b_0 = 10$) and the switching for higher amplitudes. Similar behavior concerning the control properties is observable from Fig. 7.11 where the angle difference was fixed at $\delta\phi = 0$. However, θ stabilization is only obtained for the smallest field amplitude and further increase in fields resulted in switching. These findings are consistent with the analytical one for $\delta\phi = 0$ (compare Fig. 7.8). This behavior is explained due to the change which the angle ϕ experiences directly after the pulse for $\delta\phi = 0$ (equation (7.13)): After the pulse application the condition where $\delta\phi = 0$ is reached earlier than for $\delta\phi = 3\pi/2$. Hence, switching occurs on the time scale of several and not as in the case of $\delta\phi = 3\pi/2$ ten precessional periods.

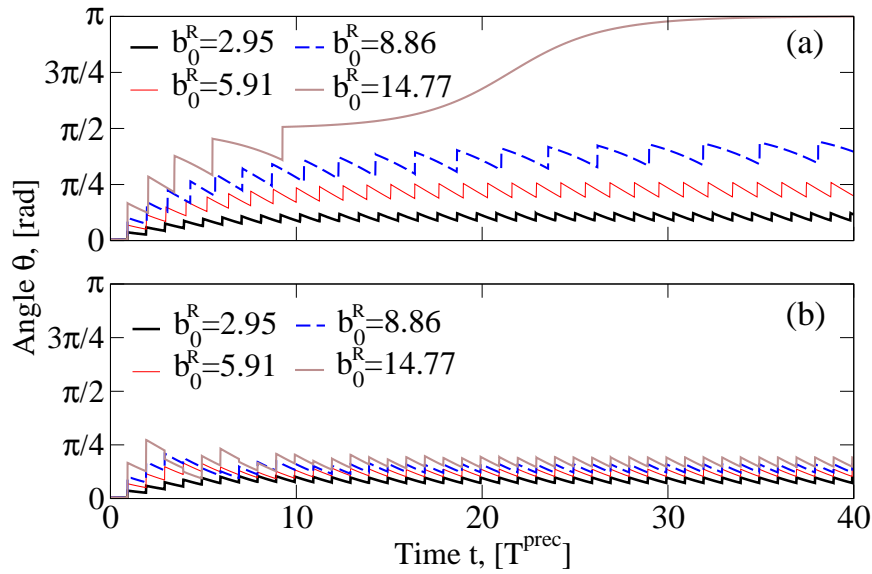


Figure 7.10: Evolution of angle θ for different strategies of the pulse application: Every time the rectangular pulses are applied when $\delta\phi_i = 3\pi/2$ (a); Only the first pulse is applied when $\delta\phi_1 = 3\pi/2$, the rest after a time lag of the precessional period (b). Other parameters are: $\alpha = 0.05$, $T_0 = 0K$.

The representation which is chosen for the θ evolution turns out to be universal for various systems in so far as θ is expressed in radians and time in units of the precessional pe-

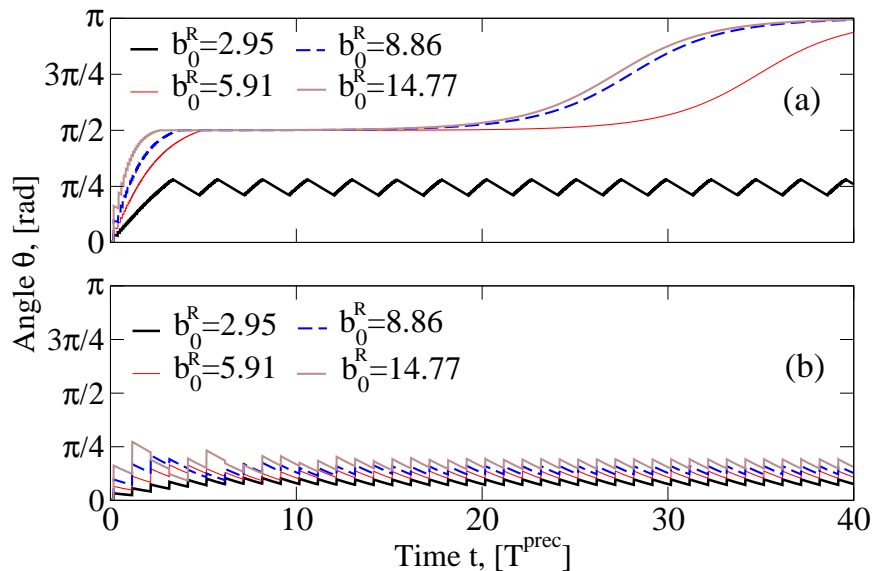


Figure 7.11: Evolution of angle θ for different strategies of pulse application: Every time the rectangular pulses are applied when $\delta\phi_i = 0$ (a); Only the first pulse is applied when $\delta\phi_1 = 0$, the rest after a time lag of the precessional period (b). Other parameters are: $\alpha = 0.05$, $T_0 = 0K$.

riod. In this respect the only parameter which can influence the dynamics of such systems in reduced dimensions is damping, which is dimensionless as well. Co-nanoparticles are therefore modeled in a similar way as FePt. Damping was taken as $\alpha = 0.25$ and further parameters were extracted from [79]. The statement that only damping significantly influences the dynamics in such representation is clearly illustrated in Fig. 7.12. Compared to the simulations made on $\text{Fe}_{50}\text{Pt}_{50}$ -nanoparticles switching demands higher pulse strengths, since the magnetic moment faster relaxes to the original state.

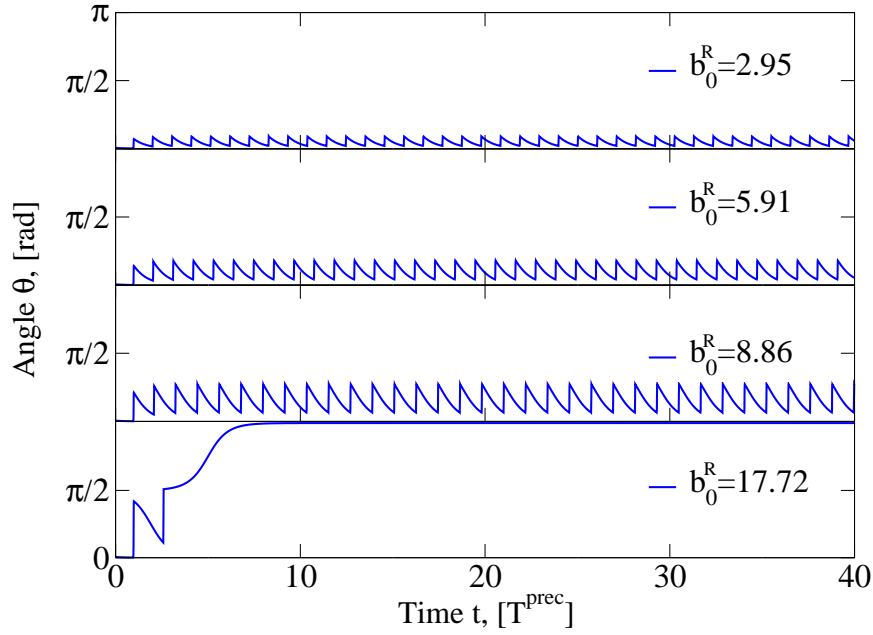


Figure 7.12: Evolution of angle θ for a Co-nanoparticle for $\delta\phi_i = 3\pi/2$ and different field strengths. Other parameters are: $\alpha = 0.25$, $T_0 = 0K$.

Temperature effects we illustrate in Figures 7.13 and 7.14. Since the time scale of excitation is comparable with that of thermal fluctuations no observable changes can be seen during the application of a pulse. Temperature causes changes of the relaxation. More attention should be paid to the relaxation process. In particular, as inferred from Fig. 7.13 (b) the application of pulses should be performed for angles higher than $\pi/2$, since thermal fluctuations may drive the magnetic moment back to the initial state.

A shown comparison of the analytical and fully numerical results of stabilization and switching demonstrated in figures 7.7, 7.8 and 7.10, 7.11 yields different amplitudes of the applied fields needed for switching. However, this discrepancy can be explained due to a time-dependent analytical field amplitude. Hence, the following time integrals should be compared: Analytically

$$\int_{-\infty}^{\infty} \frac{b_0}{2\varepsilon} dt = b_0 \int_0^1 \frac{2\varepsilon}{2\varepsilon} d\tau = b_0$$

and numerically

$$\int_{-\infty}^{\infty} b_0^R dt = \int_{t_i^-}^{t_i^+} b_0^R dt = b_0^R (t_i^+ - t_i^-),$$

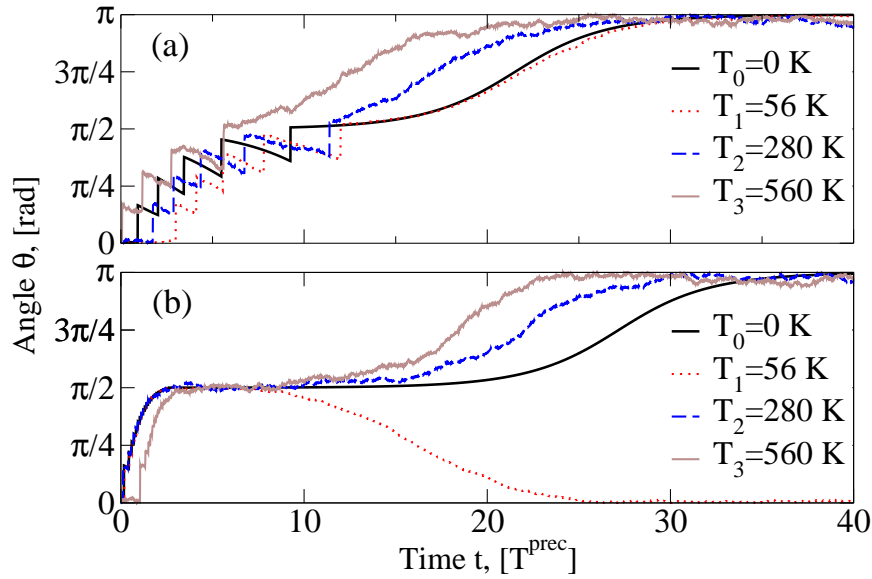


Figure 7.13: Temperature-dependent evolution of angle θ for $\delta\phi_i = 3\pi/2$ (a) and $\delta\phi_i = 0$ (b). The pulses are applied only when $\theta < \pi/2$. Other parameters are: $\alpha = 0.05$, $b_0^R = 14.77$.

from those the relation between the amplitudes can be found as

$$b_0^R = \frac{b_0}{t_i^+ - t_i^-}. \quad (7.22)$$

Using equation (7.19) and Fig. 7.4 we find a critical field for e.g. $\delta\phi_i = 3\pi/2$, $\alpha = 0.05$ to be equal to $b_{0\text{cr}} = 0.05$. The numerical value corresponding to it, according to expression (7.21), is $0.05/(6/1000) \approx 8.3$. Starting from approximately this value the numerical switching occurs, however, on much longer time scale (see Fig. 7.10).

Magnetization Freezing

θ stabilization or freezing was depicted in Fig. 7.11 for $b_0^R = 2.95$ for which the ϕ stabilization for short periods is shown in Fig. 7.15. Stabilization of both angles θ and ϕ was not, however, achieved.

Thermal-Assisted controlled Switching

Field-assisted magnetization freezing can be used for fast field-assisted thermal switching. First, the magnetic moment is finely stabilized near the state $\theta \approx \pi/2$ (Fig. 7.16). Temperatures on this time scale is unable to switch the magnetic moment as inset of Fig. 7.16 reveals. The presence of the field at finite temperatures assists a fast magnetization reversal. This effect is achievable only within a stabilization procedure. Such a thermal-assisted switching can be used for fast temperature monitoring as a thermal sensor.

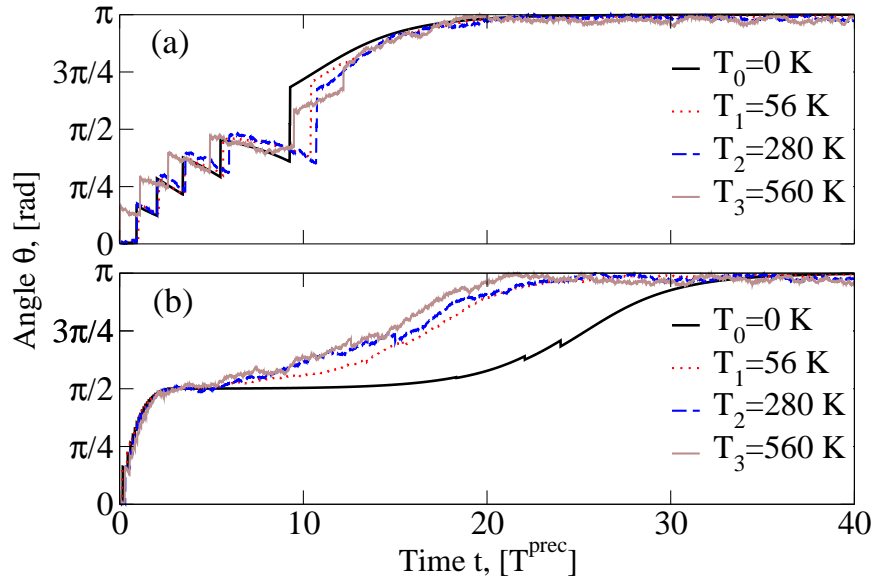


Figure 7.14: Temperature-dependent evolution of angle θ for $\delta\phi_i = 3\pi/2$ (a) and $\delta\phi_i = 0$ (b). The pulses are applied even when $\theta > \pi/2$. Other parameters are: $\alpha = 0.05$, $b_0^R = 14.77$.

Some Aspects for Nanoparticles with a cubic Anisotropy

The present scheme can also be extended for the case of a cubic anisotropy. As was pointed out in Chapter 2 a crystal with a cubic anisotropy possess more than two stable orientations. Hence, switching can be defined either as a reversal from a parallel to the antiparallel state or as a change of the magnetization from one stable orientation to another one. We understand under switching the second scenario which is demonstrated in Fig. 7.17. Black curve shows a relaxation from a state close to the energy minimum. Increasing the field amplitude and applying the pulses for $\delta\phi = 3\pi/2$ the neighbor state is populated (green curve). Further increase of the field strength results in the switching close to the antiparallel states (cyan curve).

It can also be shown that the effect of magnetization freezing functions in the case of a cubic anisotropy. As was shown in [134] the stabilization within the present scheme can be realized by freezing the magnetic moment on the top of the potential barrier.

7.2.2 Gaussian shaped magnetic Pulses

Final issue which is to be addressed in this section is another form of the pulses. Pulses of a Gaussian-like form ($f(t) = 2\varepsilon e^{-(t-t_0)^2/T^2}$ in equation (7.2)) applied in the XY -plain

$$\mathbf{b}_0^G(t) = b_0^G e^{-\frac{(t-t_0)^2}{T^2}} (\cos \phi_0 \mathbf{e}_x + \sin \phi_0 \mathbf{e}_y), \quad (7.23)$$

and having the following absolute values in units of rectangular-like pulses

$$b_0^G = b_0^R \frac{t_i^+ - t_i^-}{\sqrt{\pi}T} \quad (7.24)$$

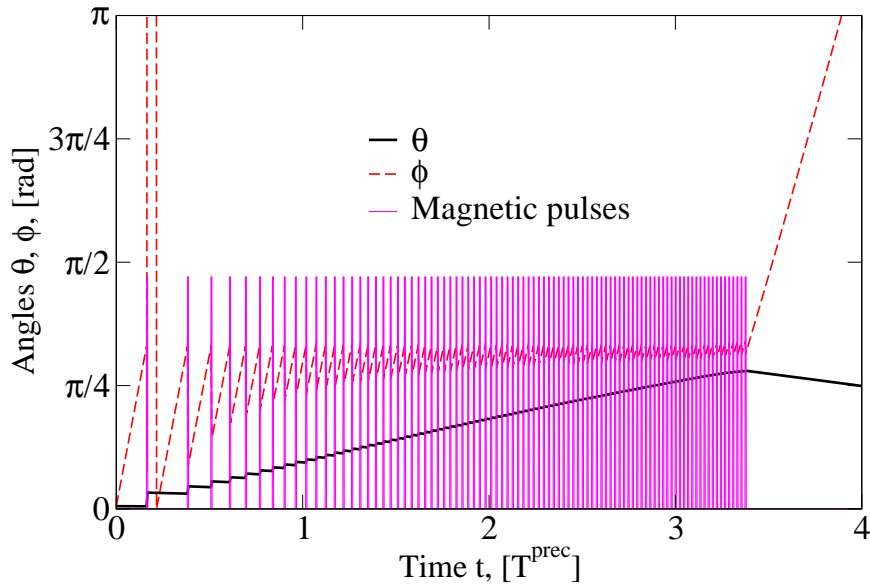


Figure 7.15: Evolution of angles θ and ϕ for $\delta\phi_i = 0$ and for the parameters of the black curve shown in Fig. 7.11 where $b_0^R = 2.95$. This figure indicates the ϕ stabilization. The short pulses are shown as pink straight lines having the same amplitude.

are useful for the magnetization stabilization and switching as Fig. 7.18 clearly shows. One should remark here that the main attention was focused on a very short pulses for which independently of their form the dynamics is the same (for the durations shorter than the precessional period, Fig. 7.18).

7.3 Discussion

The analytical and numerical results demonstrated in this chapter stated the usefulness of the scheme where two perpendicular magnetic fields with a duration shorter than the precessional period can be used for the magnetization switching and its stabilization (freezing). The requirement of the pulse shortness is insofar important since it provides a rapid excitation of the system to a certain state with a subsequent relaxation on a much longer time scale. Mathematically, the short excitation enabled to decouple the LLG equation giving rise to a variety of analytical predictions. These are the dependencies of the θ changes on the angle shift $\delta\phi$ (figures 7.2 and 7.3), critical field amplitudes for a constant (Fig. 7.4) and a changing (Fig. 7.5) lag time during the relaxation. Full numerical simulations extended for finite temperatures confirmed quantitatively and qualitatively the analytical results and supplemented them in questions of the pulse form and the duration variations as well as for a cubic anisotropy.

The results presented in this chapter contrasted two limiting cases of the angle shift between the magnetic moment and the field, namely $\delta\phi = 0$ and $\delta\phi = 3\pi/2$. As inferred from Fig. 7.1 the main difference consists in various torques that are exerted on the magnetic moment during the application of the magnetic pulses with given $\delta\phi$. In particular, for $\delta\phi = 3\pi/2$ the switching is realized easier since the torque acting towards the target

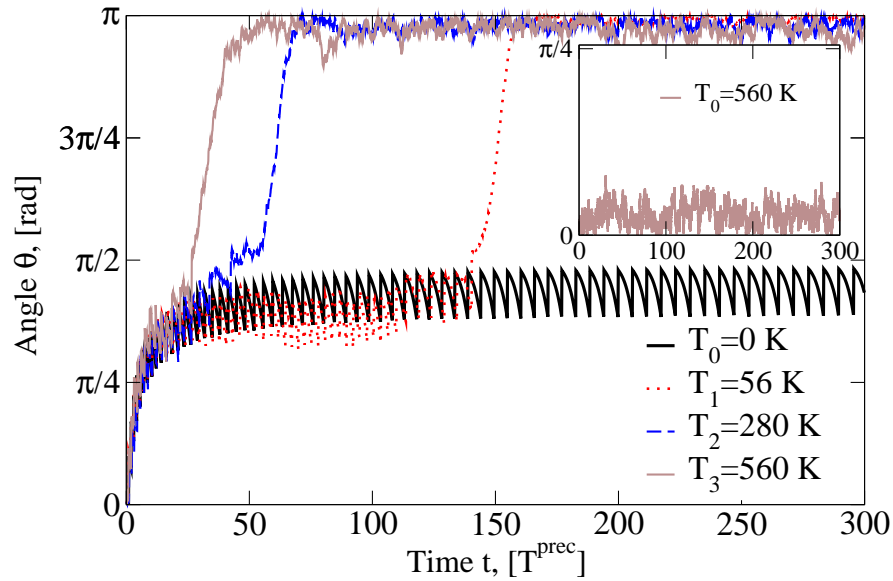


Figure 7.16: Thermal-assisted controlled switching in the presence of short pulses with an amplitude $b_0 = 8.86$. Inset shows that switching is not possible for $b_0 = 0$.

state (negative Z in Fig. 7.1) is not damping-dependent and is only a function of the pulse field strength (equation (7.14)). Additionally, we have also demonstrated the effect of θ freezing (Fig. 7.10, e.g.) which was realized for the $\delta\phi = 3\pi/2$ pulses.

The $\delta\phi = 0$ pulses are interesting since they allow for the ϕ freezing (Fig. 7.15). Switching is realizable within these angle shifts as well.

The scheme proposed in this chapter also allowed for thermally assisted switching. As demonstrated in Fig. 7.16 it is enough to steer the magnetic moment to a state in the vicinity of $\theta = \pi/2$ and then thermal fluctuations can cause switching. Note that this scenario is realizable due to a strong control of the magnetization. The control becomes possible since the time scale of the pulse changes is nearly the same as that for thermal fluctuations.

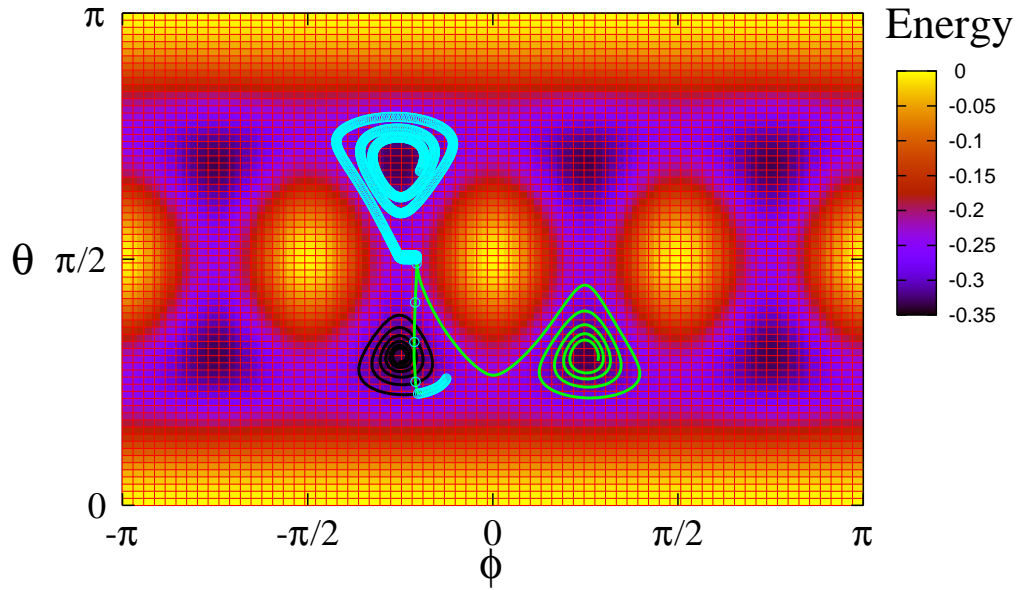


Figure 7.17: Trajectories of the magnetization on the energy landscape dependent on ϕ and θ for three various amplitudes of magnetic pulses: $b_0^R = 0$ (black curve), $b_0^R = 2.07$ (green curve) and $b_0^R = 4.14$ (cyan open points). Start conditions are: $\phi_f(0) = 15\pi/8$, $\theta_f(0) = 0.81$, $\phi_0 = \pi/4$. $T_0 = 0$ K, $\alpha = 0.05$.

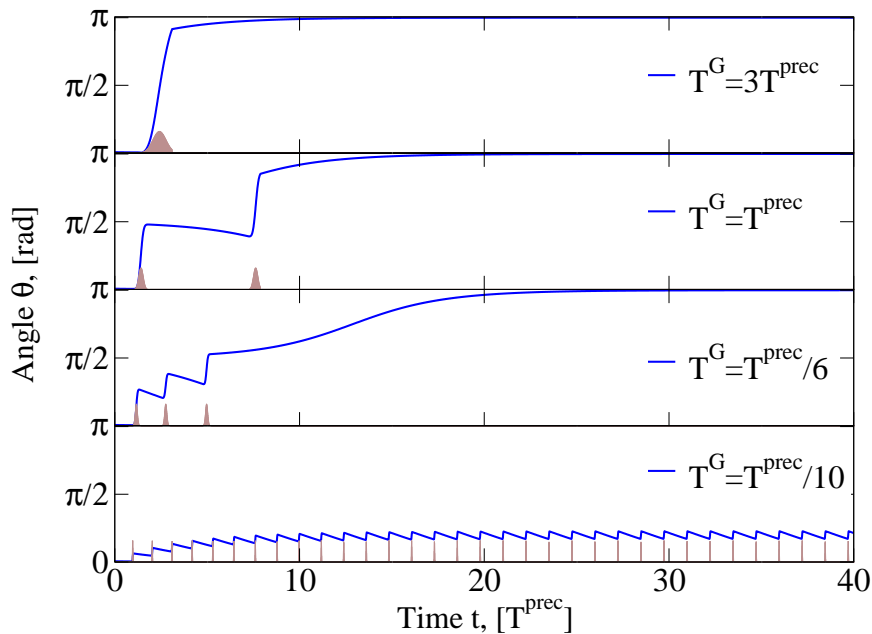


Figure 7.18: Time evolution of θ for different pulse durations expressed in units of the precessional period. Applied pulses are shown as solid bell-shaped curves. Other parameters are: $b_0^G = 1.0$, $\alpha = 0.05$.

8 Concluding Remarks and future Perspectives

8.1 Summary

The stochastic LLG equation provides a powerful tool for studying the magnetization dynamics. The main advantage of the LLG equation is that it explicitly highlights and allows us to separately study the main sources of the magnetization perturbations, namely the precessional motion, the relaxation motion and the thermal fluctuations. Additionally, the effect of the spin-torque can be taken into account by adding the torque induced term (see the next section of this chapter). This would not be possible using the MC method presented in Chapter 3, whereas the FP equation could lead to a highly complicated solutions. Another advantage of the LLG is that it yields the magnetization properties for all moments of the time propagation. This makes the LLG very powerful for the investigation of the control properties. As shown in Chapter 7, for sufficiently short magnetic pulses the LLG allows for a direct comparison of the analytical and the numerical predictions. Furthermore, one can state that only using the stochastic LLG equation the effects of controlled switching, θ or ϕ freezing and thermal assisted switching can be studied.

The main disadvantage of the stochastic LLG equation is that it does not allow for high steps in time propagation. By increasing the time steps wrong physical results may be obtained. This disadvantage results in a high computational time when the numerical results should be compared with the experimental data especially for the experiments with high measuring times like SQUID. However, even for continuous magnetic fields we used the stochastic LLG since it allowed for a flexible tuning of the damping. Additionally, the dynamics in the presence of the oscillating continuous fields could be compared directly with that for the static fields.

The main purpose of this study is the investigations of controlled dynamics of the magnetic moment of a ferromagnetic nanoparticle within the possible shortest times by applying as small excitations as possible. In Chapter 1 we specified the total energy of a ferromagnetic nanoparticle and identified the relevant parts.

To this end we assumed that nanoparticles considered are isolated. This excluded the dipole-dipole interactions. The size of ferromagnetic nanoparticles was from several to hundred nanometers. The high magnetic anisotropy energies known in particular for FePt alloys make the nanoparticles stable against thermal excitations which might lead to superparamagnetism. The small size of the nanoparticles leads to further simplifications in the total energy. Since a noncollective motion of the spins within the particle entails too much of the exchange energy, its contributions become negligible (Stoner-particle).

The classical spin dynamics is justified by the huge value of the magnetic moment.

Effects of thermal fluctuations for the nanoparticles are important and should be taken into account as we demonstrated by explicit calculations.

Both the continuous and the pulsed magnetic fields enabled switching. However, the

application of the continuous and the pulsed magnetic fields resulted in different critical field amplitudes and different reversal times. In case of static fields the switching occurred on the cost of the reversal time, allowing thus for a relatively low switching fields around the SW limit for the static fields. The reversal times are some nanoseconds. Application of oscillating fields resulted in the reduction of switching fields up to ten times and the lowering of switching times. This was due to the resonant absorption of the energy of the oscillating field. The effect of temperatures modified strongly the critical static fields and their reversal times.

Switching with magnetic pulses occurred within ten to twenty precessional periods, i.e. around several tens of picoseconds for Fe₅₀Pt₅₀-nanoparticles. Temperatures do not strongly modify the magnetization dynamics since the time scales of excitations and thermal fluctuations are approximately the same.

Pulsed magnetic excitations revealed a more transparent analytical scheme and established besides the switching the effects of magnetization freezing around a certain direction and the effect of thermal-assisted switching. The freezing effect was due to a controlled balance in the excitation and the relaxation energies. Although the effects of θ and ϕ freezing were separately demonstrated, the complete freezing or fixing of the magnetization was not achieved.

The effect of thermal-assisted switching is only due to the controlled excitation of the magnetization and is not observable for continuous fields.

8.2 Perspectives for future Studies

8.2.1 Spin-Torque Effect

Independently Slonczewski [119] and Berger [120] both predicted that a spin-polarized electric current flowing into a ferromagnetic layer can exert a torque on the magnetization. This effect is known as a *spin-torque transfer*. The nature of it is the $s-d$ exchange interaction [135] between the $4s$ itinerant electrons and the $3d$ localized electrons of the ferromagnet [120]. Usually, it is assumed that the current propagates perpendicularly to the interface of the metallic and ferromagnetic layers (Current Perpendicular Plane, CPP). However, for the effect to be observable relatively high current densities are required ($> 10^7$ A/cm²) [136, 137]. For such current densities flowing through the ferromagnet a current induced magnetization switching is expected to occur.

Experimental Observations

Inspired by the predictions of Slonczewski and Berger a number of experiments have been done in order to evidence the spin-torque effect. An experimental setup of one of the first of such experiments [138] is sketched in Fig. 8.1 (a). A thin ferromagnetic layer of cobalt (Co1) is separated from another thick ferromagnetic cobalt layer (Co2) by a copper (Cu) spacer. All lengths of the layers including the diameter of the pillar are of the order of some nanometers to provide a high current density. The orientation of the magnetization in this experiment can be detected via the GMR effect [139, 140] for the Co1/Cu/Co2 trilayer system. For a negative bias between the electrodes the direction of the current is stabilized from the thick layer with a fixed magnetization to the thin layer with a free magnetization. The magnetization of the Co1 layer is then aligned parallel to that of the second ferromag-

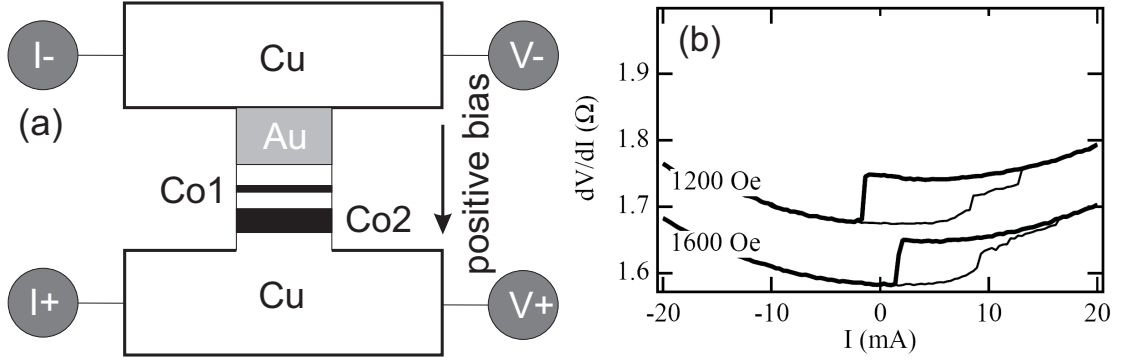


Figure 8.1: (a) Experimental setup for measurement of the current-induced switching in a pillar system described in Ref. [138]. (b) $dV/dI(I)$ measurements obtained via the GMR effect [138].

netic layer (see dV/dI -curve of Fig. 8.1 (b)). For a negative bias the parallel orientation changes to the antiparallel one and dV/dI increases. The hysteresis like behavior depicted on the dV/dI -curve demonstrates that the magnetization of the free layer switches back upon decreasing the current.

Oersted fields created by moving electrons of the current might be responsible for the switching. However, these fields have a wrong symmetry and favor a vortex-like magnetization state with a helicity depending on the current direction. Hence, this experiment manifests a new way of magnetization switching via spin-polarized currents.

Microscopic Origin of the Effect

In order to understand the microscopic origin of the spin torque let us consider a nonmagnetic and a ferromagnetic layers connected together as illustrated in Fig. 8.2. We also assume the spin quantization axis to be parallel to the magnetization of the ferromagnet (Z -direction). Then, in the nonmagnetic film the normalized wave function of an electron whose spin points in an arbitrary direction with angles θ and ϕ can be written using the rotation matrix [141] as a superposition of spin up (\uparrow) and spin down (\downarrow) states

$$\psi_{\text{in}} = e^{ik_x x} \left[\cos \frac{\theta}{2} e^{-i\frac{\phi}{2}} |\uparrow\rangle + \sin \frac{\theta}{2} e^{i\frac{\phi}{2}} |\downarrow\rangle \right]. \quad (8.1)$$

k_x denotes the wave vector along the X -direction. We have also assumed the direction of the incident electron to be perpendicular to the interface. For simplicity, ϕ is set to zero since in experiments the shape anisotropy causes altering of the magnetization in the plane of the film. In contrast to the studies reported in [119, 120] and based on the $s-d$ exchange interaction model a more simple physical problem is considered here. The consideration is based on the Stoner model which tells that there is an exchange splitting Δ for an electron in the ferromagnetic layer. The splitting shifts the down electron states higher in energy than the up electrons. Hence, the physical properties can be modeled as a simple scattering problem from a rectangular potential displayed in Fig. 8.2 (below). Thus, the transmitted and reflected parts of the scattered wave function for spin up ($t_{\uparrow}, r_{\uparrow}$) and spin down ($t_{\downarrow}, r_{\downarrow}$)

configurations read [142]

$$\begin{aligned}\psi_{\text{trans}} &= e^{ik_x x} \left[t_{\uparrow} \cos \frac{\theta}{2} | \uparrow \rangle + t_{\downarrow} \sin \frac{\theta}{2} | \downarrow \rangle \right], \\ \psi_{\text{ref}} &= e^{ik_x x} \left[r_{\uparrow} \cos \frac{\theta}{2} | \uparrow \rangle + r_{\downarrow} \sin \frac{\theta}{2} | \downarrow \rangle \right],\end{aligned}\quad (8.2)$$

or for the case when wave functions and their derivatives of the both layers are equal at the interface [143]

$$\begin{aligned}\psi_{\text{trans}} &= e^{ik_{\uparrow} x} \cos \frac{\theta}{2} | \uparrow \rangle + e^{ik_{\downarrow} x} \sin \frac{\theta}{2} | \downarrow \rangle, \\ \psi_{\text{ref}} &= e^{-ik_x x} \sin \frac{\theta}{2} | \downarrow \rangle.\end{aligned}\quad (8.3)$$

New variables are $k_{\uparrow} = k_x = k$ and $k_{\downarrow} = \sqrt{2m(E - \Delta)}/\hbar$ with $E = \hbar^2 k^2 / (2m)$ and m to be the electron mass.

To calculate the torque exerted on the localized magnetic moment \mathbf{S} by a single itinerant electron the spin current density should first be defined [143]

$$\mathbf{Q} = \frac{\hbar^2}{2m} \text{Im}(\psi^* \boldsymbol{\sigma} \otimes \nabla \psi), \quad (8.4)$$

where $\boldsymbol{\sigma}$ denotes the pauli matrices σ_x , σ_y and σ_z and \otimes stands for the outer product. As can be seen from this definition \mathbf{Q} is a tensor.

For a normalized spinor plane-wave wave-function of the form

$$\psi = e^{ik_x x} \left[a | \uparrow \rangle + b | \downarrow \rangle \right] \quad (8.5)$$

the components of the current density for an x spatial and the three x, y, z spin directions are

$$\begin{aligned}Q_{xx} &= \frac{\hbar^2 k}{2m} 2\text{Re}(ab^*), \\ Q_{xy} &= \frac{\hbar^2 k}{2m} 2\text{Im}(ab^*), \\ Q_{xz} &= \frac{\hbar^2 k}{2m} (|a|^2 - |b|^2).\end{aligned}\quad (8.6)$$

Using expressions (8.6) the spatial components $\hat{\mathbf{x}}$, $\hat{\mathbf{y}}$, $\hat{\mathbf{z}}$ of \mathbf{Q} transform to

$$\begin{aligned}Q_{\text{in}} &= \frac{\hbar^2 k}{2m} \left[\sin \theta \hat{\mathbf{x}} + \cos \theta \hat{\mathbf{z}} \right], \\ Q_{\text{trans}} &= \frac{\hbar^2}{2m} \sin \theta \frac{2kk_{\downarrow}}{k+k_{\downarrow}} \left(\cos[(k_{\uparrow} - k_{\downarrow})x] \hat{\mathbf{x}} + \sin[(k_{\uparrow} - k_{\downarrow})x] \hat{\mathbf{y}} \right) \\ &\quad + \frac{\hbar^2}{2m} k_{\downarrow} \left(\cos^2 \frac{\theta}{2} - \left(\frac{2k}{k+k_{\downarrow}} \right)^2 \sin^2 \frac{\theta}{2} \right) \hat{\mathbf{z}}, \\ Q_{\text{ref}} &= \frac{\hbar^2}{2m} k \left(\frac{k - k_{\downarrow}}{k + k_{\downarrow}} \right)^2 \hat{\mathbf{z}}.\end{aligned}\quad (8.7)$$

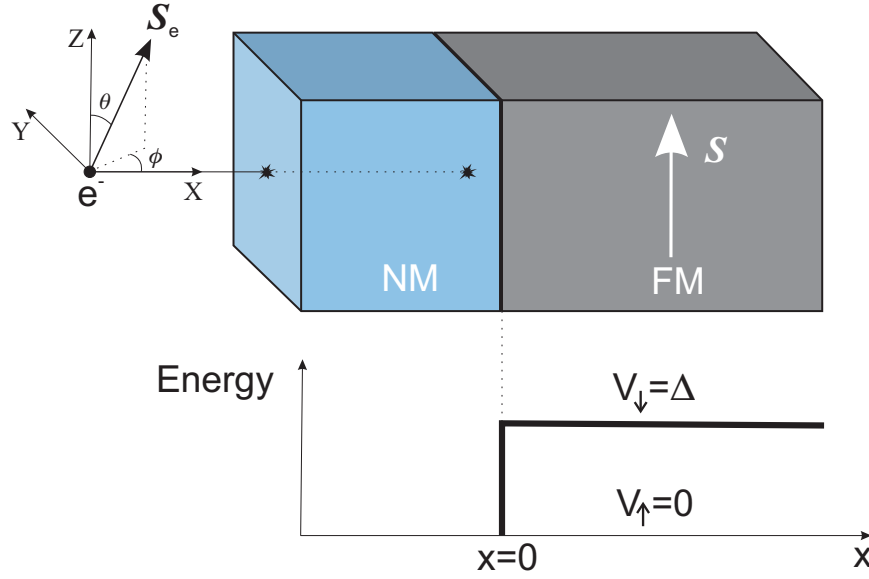


Figure 8.2: Incident spin wave is shown for a single electron having a spin projection with θ and ϕ on the X , Y , Z axes. The nonmagnetic metallic layer is denoted with blue color (NM) and the ferromagnetic layer is shown in gray (FM).

Finally, since the total angular momentum is conserved the torque exerted on the volume near the interface can be determined as a net flux of the nonequilibrium current density

$$\mathbf{N}_{\text{ST}} = - \int_{\text{surface}} d^2R \hat{\mathbf{n}} \cdot \mathbf{Q} = A \hat{\mathbf{x}} (\mathbf{Q}_{\text{in}} + \mathbf{Q}_{\text{refl}} - \mathbf{Q}_{\text{trans}}), \quad (8.8)$$

where A is the area of the ferromagnet on which the torque is exerted. The last equation simply means that the torque \mathbf{N}_{ST} is equal to the incoming flux $\mathbf{Q}_{\text{in}} A \hat{\mathbf{x}}$ minus the outgoing flux $\mathbf{Q}_{\text{trans}} A \hat{\mathbf{x}}$ and $\mathbf{Q}_{\text{refl}} A \hat{\mathbf{x}}$.

Transmitted and reflected current densities summed over all states on the Fermi surface are collinear with the magnetic moment of the ferromagnetic layer. Thus, the origin of the spin-torque effect is the absorption of the transverse spin current density on the interface [142] and

$$\mathbf{N}_{\text{ST}} \approx A \hat{\mathbf{x}} \cdot \mathbf{Q}_{\text{in}\perp} = A \frac{\hbar^2 k}{2m} \sin \theta \hat{\mathbf{x}}. \quad (8.9)$$

$\sin \theta$ entering the equation (8.9) is indeed proportional to the double vector product of the itinerant and localized magnetic moment directions. Using the notation \mathbf{S}_e as the polarization of the incoming electrons and \mathbf{S} as the magnetic moment of the localized magnetic moment, the change of \mathbf{S} is (with coefficients assumed in [68, 144])

$$\left(\frac{d\mathbf{S}}{dt} \right)_{\text{ST}} = \gamma \frac{\beta}{1 + \eta \mathbf{S} \cdot \mathbf{S}_e} [\mathbf{S} \times [\mathbf{S} \times \mathbf{S}_e]], \quad (8.10)$$

where γ is a gyromagnetic ratio and β , η are model dependent dimensionless parameters; current or current density enters in β (for details see [145]).

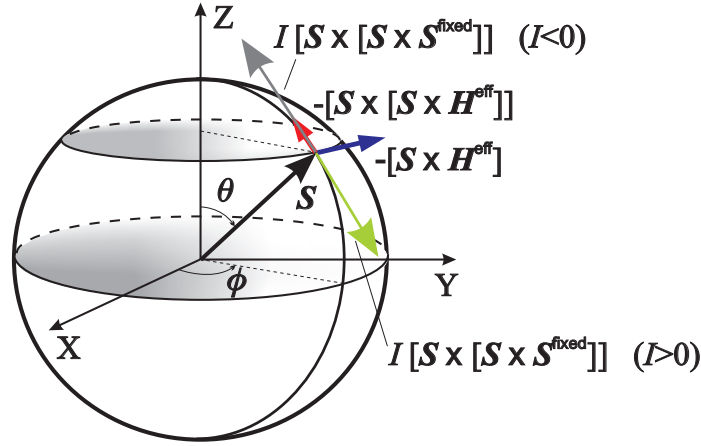


Figure 8.3: Demonstration of the torque directions exerted on the magnetization by a spin-current. Direction of the torque strongly depends on the direction of the current. The gray arrow indicates the situation for a negative current. The green arrow shows in turn the torque for a positive current.

Current-induced Magnetization Dynamics

Due to the fact that torques acting on the magnetic moment are additive quantities we can simply add the spin-torque term to the LLG equation (3.28). For the resulting equation we have

$$\frac{d\mathbf{S}}{dt} = -\frac{\gamma}{1+\alpha^2} [\mathbf{S} \times \mathbf{H}^{\text{eff}}] - \frac{\alpha\gamma}{1+\alpha^2} [\mathbf{S} \times [\mathbf{S} \times \mathbf{H}^{\text{eff}}]] + \gamma \frac{\beta}{1+\eta\mathbf{S} \cdot \mathbf{S}_e} [\mathbf{S} \times [\mathbf{S} \times \mathbf{S}_e]]. \quad (8.11)$$

Each term of this equation is illustrated in Fig. 8.3. The precessional motion is weakly affected by the spin-torque term. The relaxation motion in turn can be fully compensated by the current induced torque. In case when the spin-torque term has a positive current ($I > 0$) and is higher than the relaxation in the system, then the current-induced switching can take place.

Interesting dynamical properties arise when applying the proposed scheme for ultra short magnetic pulses (Chapter 7) for spin currents alone or combined with ultrashort magnetic pulses.

Despite the similar geometrical structure of the damping and the spin-torque terms they are different. In particular, the effective field around which the magnetic moment precesses changes upon temperature fluctuations or anisotropy contributions, whereas the orientations of \mathbf{S}_e is fixed. Interesting behavior is expected for the case when the damping and the spin torques are compensated.

Considering an extension of the calculations proposed here, equation (8.11) can also be applied for continuous media to study the effect of spin torque on the propagation of domain walls. Despite a huge amount of recent works in this area [146–149], to name but a few, the proposed scheme for ultrashort spin-torque pulses can also be used for studying the domain walls propagation. This becomes exciting in view of existing experiments for spin-torques pulses [150–152]. Interesting is the application of this approach to studying the magnetization dynamics of small objects (nanoislands) in the vicinity of the blocking temperature (see experiments reported in [153]).

Bibliography

- [1] J. C. Maxwell. *Treatise of Electricity and Magnetism*. Dover Publications, New York, reprint of the 3rd edition, 1954.
- [2] V. K. Arkad'ev. Absorption of electric Waves in parallel Wires. *Zh. Russk. Fiz.-Khim. Obshchestva, Otdel Fiz.*, 44:165–200, 1912.
- [3] J. H. E. Griffiths. Anomalous High-Frequency Resistance of ferromagnetic Metals. *Nature*, 158:670–671, 1946.
- [4] E. K. Zavoiskii. Paramagnetic Absorption in some Salts in perpendicular magnetic Fields. *J. Phys. (U. S. S. R.)*, 10:170, 1946.
- [5] W. Gerlach, O. Stern. Das magnetische Moment des Silberatoms. *Z. Phys.*, 9:353–355, 1922.
- [6] W. Heisenberg. Merkörperproblem und Resonanz in der Quantenmechanik. *Z. Phys.*, 38:411–426, 1926.
- [7] P. A. M. Dirac. On the Theory of Quantum Mechanics. *Proceedings of the Royal Society of London, Series A* 112:661–677, 1926.
- [8] W. H. Meiklejohn, C. P. Bean. New magnetic Anisotropy. *Phys. Rev.*, 105:904–913, 1957.
- [9] C. Kittel. *Introduction to Solid State Physics*. John Wiley & Sons, Inc., 8th edition, 2005.
- [10] B. Hillebrands, K. Ounadjela (Eds.). *Spin Dynamics in confined magnetic Systems I*. Springer, Berlin, 2001.
- [11] B. Hillebrands, K. Ounadjela (Eds.). *Spin Dynamics in confined magnetic Systems II*. Springer, Berlin, 2003.
- [12] B. Hillebrands, A. Thiaville (Eds.). *Spin Dynamics in confined magnetic Systems III*. Springer, Berlin, 2006.
- [13] B. Heinrich, J. A. C. Bland. *Ultrathin magnetic Structures IV*. Springer, Berlin, 2005.
- [14] R. C. O'Handley. *Modern magnetic Materials: Principles and Applications*. John Wiley & Sons, Inc., New York, 2000.
- [15] U. Nowak. Thermally activated Reversal in magnetic Nanostructures. *Ann. Rev. Comp. Phys.*, 9:105–153, 2001.

- [16] L. Landau. Zur Theorie der Energieübertragung. *Phys. Z. Sowjet.*, 2:46–51, 1932.
- [17] C. Zener. Non-Adiabatic Crossing of Energy Levels. *Proceedings of the Royal Society of London*, A 137:696–702, 1932.
- [18] S. Miyashita. Dynamics of the Magnetization with an Inversion of the magnetic Field. *J. Phys. Soc. Jpn.*, 64:3207–3214, 1995.
- [19] M. Shapiro, P. Brumer. *Principles of the Quantum Control of molecular Processes*. John Wiley & Sons, Inc., Hoboken, 2003.
- [20] R. Kosloff and A. D. Hammerich. Excitation without Demolition: Radiative Excitation of Ground-Surface Vibration by impulsive stimulated Raman Scattering with Damage Control. *Phys. Rev. Lett.*, 69:2172–2175, 1992.
- [21] S. Gräfe, C. Meier, V. Engel. Instantaneous Dynamics and quantum Control Fields: Principle and Numerical Applications. *J. Chem. Phys.*, 122:184103–1–8, 2005.
- [22] B. Aktas, L. Tagirov, F. Mikailov (Eds.). *Magnetic Nanostructures (Springer Series in Materials Science)*, volume 94. Springer, Berlin, 2007.
- [23] C. B. Murray, S. Sun, W. Gaschler, H. Doyle, T. A. Betley, C. R. Kagan. Colloidal Synthesis of Nanocrystals and Nanocrystal Superlattices. *IBM J. Res. & Dev.*, 45:47–55, 2001.
- [24] S. Sun, C. B. Murray, D. Weller, L. Folks, A. Moser. Monodisperse FePt Nanoparticles and ferromagnetic FePt Nanocrystal Superlattices. *Science*, 287:1989–1992, 2000.
- [25] C. Antoniak, A. Trunova, M. Spasova, M. Farle, H. Wende, F. Wilhelm, A. Rogalev. Lattice Expansion in nonoxidized FePt Nanoparticles: X-ray Absorption Measurements. *Phys. Rev. B*, 78:041406–1–4, 2008.
- [26] S. Sun, E. E. Fullerton, D. Weller, C. B. Murray. Compositionally controlled FePt Nanoparticle Materials. *IEEE Trans. Magn.*, 37:1239–1243, 2001.
- [27] J. B. Staunton, S. Ostanin, S. S. A. Razee, B. L. Gyorffy, L. Szunyogh, B. Ginatempo, E. Bruno. Temperature-Dependent magnetic Anisotropy in metallic Magnets from an *Ab Initio* electronic Structure Theory: $L1_0$ -Ordered FePt. *Phys. Rev. Lett.*, 93:257204–1–4, 2004.
- [28] O. N. Mryasov, U. Nowak, K. Y. Guslienko, R. W. Chantrell. Temperature-dependent magnetic Properties of FePt: Effective Spin Hamiltonian Model. *Europhys. Lett.*, 69:805–811, 2005.
- [29] C. Antoniak, J. Lindner, M. Farle. Magnetic Anisotropy and its Temperature Dependence in iron-rich $\text{Fe}_x\text{Pt}_{1-x}$ Nanoparticles. *Europhys. Lett.*, 70:250–256, 2005.
- [30] C. Antoniak, J. Lindner, V. Salgueiriño-Maceira, M. Farle. Multifrequency magnetic Resonance and blocking Behavior of $\text{Fe}_x\text{Pt}_{1-x}$ Nanoparticles. *Phys. Stat. Sol.*, 203:2968–2973, 2006.

- [31] S. Chikazumi. *Physics of Ferromagnetism*. Oxford University Press Inc., New York, 2nd edition, 2002.
- [32] P. Bruno. Tight-binding Approach to the orbital magnetic Moment and magnetocrystalline Anisotropy of Transition-metal Monolayers. *Phys. Rev. B*, 39:865–868, 1989.
- [33] C. Uiberacker, J. Zabludil, P. Weinberger, L. Szunyogh, C. Sommers. Lattice Relaxation driven Reorientation Transition in Ni_n/Cu(100). *Phys. Rev. Lett.*, 82:1289–1292, 1999.
- [34] A. B. Shick, O. N. Mryasov. Coulomb Correlations and magnetic Anisotropy in ordered L1₀ CoPt and FePt Alloys. *Phys. Rev. B*, 67:172407–1–4, 2003.
- [35] J. H. Van Vleck. On the Anisotropy of cubic ferromagnetic Crystals. *Phys. Rev.*, 52:1178–1198, 1937.
- [36] S. Ostanin, S. S. A. Razee, J. B. Staunton, B. Ginatempo, E. Bruno. Magnetocrystalline Anisotropy and compositional Order in Fe_{0.5}Pt_{0.5} : Calculations from an *Ab initio* electronic Model. *J. Appl. Phys.*, 93:453–457, 2003.
- [37] C. Antoniak, J. Lindner, M. Spasova, D. Sudfeld, M. Acet, M. Farle, K. Fauth, U. Wiedwald, H.-G. Boyen, P. Ziemann, F. Wilhelm, A. Rogalev, S. Sun. Enhanced orbital Magnetism in Fe₅₀Pt₅₀ Nanoparticles. *Phys. Rev. Lett.*, 97:117201–1–4, 2006.
- [38] E. C. Stoner, E. P. Wohlfarth. A Mechanism of magnetic Hysteresis in heterogeneous Alloys. *Phil. Trans. Roy. Soc. London A*, 240:599–642, 1948.
- [39] E. C. Stoner, E. P. Wohlfarth. A Mechanism of magnetic Hysteresis in heterogeneous Alloys. *IEEE Trans. Magn.*, 27:3475–3518, 1991.
- [40] L. Néel. Theorie du trainage magnetique des ferromagnetiques en grains fins avec applications aux terres cuites. *Ann. Geophys.*, 5:99–136, 1949.
- [41] L. Néel. Influence des fluctuations thermiques sur l’aimantation de grains ferromagnétiques très fins. *Compt. Rend. Acad. Scien.*, 228:664–666, 1949.
- [42] L. Néel. Some theoretical Aspects of Rock-Magnetism. *Adv. Phys.*, 4:191–243, 1955.
- [43] W. F. Brown. Thermal Fluctuations of a Single-Domain Particle. *Phys. Rev.*, 130:1677–1686, 1963.
- [44] L. D. Landau and E. M. Lifshitz. *Statistical Physics*, volume 5. Elsevier, Amsterdam, 3rd edition, 2007.
- [45] F. Reif. *Statistische Physik und Theorie der Wärme*. Walter de Gruyter, Berlin, 3rd edition, 1987.
- [46] L. D. Landau, E. M. Lifshitz. On the Theory of the Dispersion of magnetic Permeability in ferromagnetic Bodies. *Phys. Z. Sowjet.*, 8:153–169, 1935.

- [47] T. L. Gilbert, J. M. Kelly. Anomalous rotational Damping in ferromagnetic Sheets. In *Proceedings of the Pittsburgh Conference on Magnetism and magnetic Materials*, pages 253–263, Pittsburgh, PA, June 14 - 16, 1955. American Institute of Electrical Engineers.
- [48] T. L. Gilbert. A phenomenological Theory of Damping in ferromagnetic Materials. *IEEE Trans. Magn.*, 40:3443–3449, 2004.
- [49] R. J. Glauber. Time-Dependent Statistics of the Ising Model. *J. Math. Phys.*, 4:294–307, 1963.
- [50] N. Metropolis, A. R. Rosenbluth, M. N. Rosenbluth, A. H. Teller, E. Teller. Equation of State Calculations by fast computing Machines. *J. Chem. Phys.*, 21:1087–1092, 1953.
- [51] H. Risken. *The Fokker-Planck Equation*. Springer, Berlin, 2nd edition, 1989.
- [52] J. M. Thijssen. *Computational Physics*. Cambridge University Press, 2nd edition, 2007.
- [53] I. N. Bronshtein, K. A. Semendyayev. *Handbook of Mathematics*. Springer, Berlin, 3rd edition, 1998.
- [54] J. C. Slonczewski. Research Memorandum. volume 003.111.224. IBM Research Center, 1956.
- [55] L. He, W. D. Doyle, H. Fujiwara. High Speed coherent Switching below the Stoner-Wohlfarth Limit. *IEEE Trans. Magn.*, 30:4086–4088, 1994.
- [56] A. Thiaville. Extensions of the geometric Solution of the two dimensional coherent Magnetization Rotation Model. *J. Magn. Magn. Mater.*, 182:5–18, 1998.
- [57] A. Thiaville. Coherent Rotation of Magnetization in three Dimensions: A geometrical Approach. *Phys. Rev. B*, 61:12221–12232, 2000.
- [58] M. Jamet, W. Wernsdorfer, C. Thirion, D. Mailly, V. Dupuis, P. Mélinon, A. Pérez. Magnetic Anisotropy of a Single Cobalt Nanocluster. *Phys. Rev. Lett.*, 86:4676–4679, 2001.
- [59] C. Vouille, A. Thiaville, J. Miltat. Thermally activated Switching of Nanoparticles: A numerical Study. *J. Magn. Magn. Mater.*, 272-276:e1237–e1238, 2004.
- [60] I. Klik, L. Gunther. First-Passage-Time Approach to Overbarrier Relaxation of Magnetization. *J. Stat. Phys.*, 60:473–484, 1990.
- [61] H. -B. Braun. Kramers’s Rate Theory, broken Symmetries, and Magnetization Reversal. *J. Appl. Phys.*, 76:6310–6315, 1994.
- [62] D. A. Garanin, E. C. Kennedy, D. S. F. Crothers, W. T. Coffey. Thermally activated Escape Rates of uniaxial Spin Systems with transverse Field: Uniaxial Crossovers. *Phys. Rev. E*, 60:6499–6502, 1999.

- [63] R. W. Chantrell, N. Y. Ayoub, J. Popplewell. The low Field Susceptibility of a textured superparamagnetic System. *J. Magn. Magn. Mater.*, 53:199–207, 1985.
- [64] O. Fruchart, P.-O. Jubert, C. Meyer, M. Klaua, J. Barthel, J. Kirschner. Vertical Self-Organization of epitaxial magnetic Nanostructures. *J. Magn. Magn. Mater.*, 239:224–227, 2002.
- [65] T. L. Gilbert. A Lagrangian Formulation of the gyromagnetic Equation of the Magnetization Field. *Phys. Rev.* 100:1243. Abstract only; Full report, Armor Research Foundation Project No. A059, 1955.
- [66] A. G. Gurevich, G. A. Melkov. *Magnetization Oscillations and Waves*. CRC Press, Boca Raton, 1996.
- [67] R. Zivieri, L. Giovannini, P. Vavassori. *Magnetic Nanostructures*. American Scientific Publishers, Stevenson Ranch, 2002 (p. 219).
- [68] Y. Tserkovnyak, A. Brataas, G. E. W. Bauer. Theory of current-driven Magnetization Dynamics in inhomogeneous Ferromagnets. *J. Magn. Magn. Mater.*, 320:1282–1292, 2008.
- [69] H. B. Callen. A ferromagnetic dynamical Equation. *J. Phys. Chem. Solids*, 4:256–270, 1958.
- [70] D. A. Garanin. Fokker-Planck and Landau-Lifshitz-Bloch Equations for classical Ferromagnets. *Phys. Rev. B*, 55:3050–3057, 1997.
- [71] N. Bloembergen. On the Ferromagnetic Resonance in Nickel and Supermalloy. *Phys. Rev.*, 78:572–580, 1950.
- [72] N. G. Van Kampen. *Stochastic Processes in Physics and Chemistry*. Elsevier, Amsterdam, 3rd edition, 2007.
- [73] E. Ising. Beitrag zur Theorie des Ferromagnetismus. *Z. Phys.*, 31:253–258, 1925.
- [74] U. Nowak, R. W. Chantrell, E. C. Kennedy. Monte Carlo Simulation with Time Step Quantification in Terms of Langevin Dynamics. *Phys. Rev. Lett.*, 84:163–166, 2000.
- [75] A. D. Fokker. Die mittlere Energie rotierender elektrischer Dipole im Strahlungsfeld. *Z. Phys.*, 43:810–820, 1914.
- [76] J. L. García-Palacios, F. J. Lázaro. Langevin-Dynamics Study of the dynamical Properties of small magnetic Particles. *Phys. Rev. B*, 58:14937–14958, 1998.
- [77] R. Kikuchi. On the Minimum of Magnetization Reversal Time. *J. Appl. Phys.*, 27:1352–1357, 1956.
- [78] R. Z. Sagdeev, D. A. Usikov, G. M. Zaslavskii. *Nonlinear Physics: From the Pendulum to Turbulence and Chaos*. Harwood Acad. Publ., Chur, 1988.
- [79] W. T. Coffey, D. S. F. Crothers, J. L. Dormann, Yu. P. Kalmykov, E. C. Kennedy, W. Wernsdorfer. Thermally activated Relaxation Time of a Single Domain ferromagnetic Particle subjected to a uniform Field at an oblique Angle to the easy Axis: Comparison with experimental Observations. *Phys. Rev. Lett.*, 80:5655–5658, 1998.

- [80] R. Hammerling, C. Uiberacker, J. Zabloudil, P. Weinberger, L. Szunyogh, J. Kirschner. Magnetic Anisotropy of thin Films of Co on Cu(111). *Phys. Rev. B*, 66:052402–1–4, 2002.
- [81] A. Hahlin, J. H. Dunn, O. Karis, P. Pouloupoulos, R. Nünthel, J. Lindner, D. Arvanitis. Ultrathin Co Films on flat and vicinal Cu(111) Surfaces: Per Atom Determination of orbital and Spin Moments. *J. Phys.: Cond. Matter.*, 15:S573–S586, 2003.
- [82] F. Schreiber, J. Pflaum, Z. Frait, T. Mühge, J. Pelzl. Gilbert Damping and g-Factor in $\text{Fe}_x\text{Co}_{1-x}$ Alloy Films. *Sol. Stat. Commun.*, 93:965–968, 1995.
- [83] T. Gerrits, J. Hohlfeld, O. Gielkens, K. J. Veenstra, K. Bal, T. Rasing, H. A. M. van den Berg. Magnetization Dynamics in NiFe thin Films induced by short in-plane magnetic Field Pulses. *J. Appl. Phys.*, 89:7648–7650, 2001.
- [84] W. E. Bailey, L. Cheng, D. J. Keavney, C.-C. Kao, E. Vescovo, D. A. Arena. Precessional Dynamics of elemental Moments in a ferromagnetic Alloy. *Phys. Rev. B*, 70:172403–1–4, 2004.
- [85] H. Suhl. *Relaxation Processes in Micromagnetics*. Oxford University Press Inc., New York, 2007.
- [86] C. Kittel. On the Theory of ferromagnetic Resonance Absorption. *Phys. Rev.*, 73:155–161, 1948.
- [87] M. Farle. Ferromagnetic Resonance of ultrathin metallic Layers. *Rep. Prog. Phys.*, 61:755–826, 1998.
- [88] S. M. Bhagat, P. Lubitz. Temperature Variation of ferromagnetic Relaxation in the 3d Transition Metals. *Phys. Rev. B*, 10:179–185, 1974.
- [89] B. Heinrich, D. J. Meredith, J. F. Cochran. Wave Number and Temperature dependent Landau-Lifshitz Damping in Nickel. *J. Appl. Phys.*, 50:7726–7728, 1979.
- [90] C. H. Back, D. Weller, J. Heidmann, D. Mauri, D. Guarisco, E. L. Garwin, H. C. Siegmann. Magnetization Reversal in ultrashort magnetic Pulses. *Phys. Rev. Lett.*, 81:3251–3254, 1998.
- [91] C. H. Back, R. Allenspach, W. Weber, S. S. P. Parkin, D. Weller, E. L. Garwin, H. C. Siegmann. Minimum Field Strength in precessional Magnetization Reversal. *Science*, 285:864–867, 1999.
- [92] M. Buess, T. Haug, M. R. Scheinfein, C. H. Back. Micromagnetic Dissipation, Dispersion, and Mode Conversion in thin Permalloy Platelets. *Phys. Rev. Lett.*, 94:127205–1–4, 2005.
- [93] J. Lindner, K. Lenz, E. Kosubek, K. Baberschke, D. Spoddig, R. Meckenstock, J. Pelzl, Z. Frait, D. L. Mills. Non-Gilbert-Type Damping of the magnetic Relaxation in ultrathin Ferromagnets: Importance of Magnon-Magnon Scattering. *Phys. Rev. B*, 68:060102–1–4, 2003.

- [94] E. Beaurepaire, J.-C. Merle, A. Daunois, J.-Y. Bigot. Ultrafast Spin Dynamics in ferromagnetic Nickel. *Phys. Rev. Lett.*, 76:4250–4253, 1996.
- [95] W. K. Hiebert, A. Stankiewicz, M. R. Freeman. Direct Observation of magnetic Relaxation in a small Permalloy Disk by time-resolved scanning Kerr Microscopy. *Phys. Rev. Lett.*, 79:1134–1137, 1997.
- [96] M. van Kampen, C. Jozsa, J. T. Kohlhepp, P. LeClair, L. Lagae, W. J. M. de Jonge, B. Koopmans. All-optical Probe of coherent Spin Waves. *Phys. Rev. Lett.*, 88:227201–1–4, 2002.
- [97] M. Bonfim, G. Ghiringhelli, F. Motaigne, S. Pizzini, N. B. Brookes, E. Petroff, J. Vogel, J. Camarero, A. Fontaine. Element-Selective Nanosecond Magnetization Dynamics in magnetic Heterostructures. *Phys. Rev. Lett.*, 86:3646–3649, 2001.
- [98] W. Bailey, P. Kabos, F. Mancoff, S. Russek. Control of Magnetization Dynamics in $\text{Ni}_{81}\text{Fe}_{19}$ thin Films through the Use of Rare-Earth Dopants. *IEEE Trans. Magn.*, 37:1749–1754, 2001.
- [99] J. O. Rantschler, R. D. McMichael, A. Castillo, A. J. Shapiro, W. F. Egelhoff, Jr., B. B. Maranville, D. Pulugurtha, A. P. Chen, L. M. Connors. Effect of $3d$, $4d$, and $5d$ transition Metal Doping on Damping in Permalloy thin Films. *J. Appl. Phys.*, 101:033901–1–5, 2007.
- [100] C. Scheck, L. Cheng, I. Barsukov, Z. Frait, W. E. Bailey. Low Relaxation Rate in epitaxial Vanadium-doped ultrathin Iron Films. *Phys. Rev. Lett.*, 98:117601–1–4, 2007.
- [101] J. A. C. Bland, B. Heinrich. *Ultrathin magnetic Structures III*. Springer, Berlin, 2005.
- [102] H. Suhl. Theory of the magnetic Damping Constant. *IEEE Trans. Magn.*, 34:1834–1838, 1998.
- [103] K. Lenz, H. Wende, W. Kuch, K. Baberschke, K. Nagy, A. Jánossy. Two-Magnon Scattering and viscous Gilbert Damping in ultrathin Ferromagnets. *Phys. Rev. B*, 73:144424–1–6, 2006.
- [104] V. Kamberský. On ferromagnetic Resonance Damping in Metals. *Czech. J. Phys. B*, 26:1366–1383, 1976.
- [105] J. Kuneš, V. Kamberský. First-Principles Investigation of the Damping of fast Magnetization Precession in ferromagnetic $3d$ Metals. *Phys. Rev. B*, 65:212411–1–3, 2002.
- [106] D. Steiauf, M. Fähnle. Damping of Spin Dynamics in Nanostructures: An *Ab initio* Study. *Phys. Rev. B*, 72:064450–1–13, 2005.
- [107] K. Gilmore, Y. U. Idzerda, M. D. Stiles. Identification of the dominant Precession-Damping Mechanism in Fe, Co, and Ni by First-Principles Calculations. *Phys. Rev. Lett.*, 99:027204–1–4, 2007.

- [108] C. Kittel. Excitation of Spin Waves in a Ferromagnet by a uniform rf Field. *Phys. Rev.*, 110:1295–1297, 1958.
- [109] R. F. Soohoo. General Exchange boundary Condition and Surface Anisotropy Energy of a Ferromagnet. *Phys. Rev.*, 131:594–601, 1963.
- [110] D. I. Sementsov. Spin-Wave Resonance in ferromagnetic Layer with Spins asymmetrically coupled on the Surface. *Fizika Metallov i Metallovedenie*, 38:247–253, 1974 (in Russian).
- [111] P. E. Kloeden, E. Platen, H. Schurz. *Numerical Solution of SDE through Computer Experiments*. Springer, Berlin, 1991.
- [112] A. Lyberatos, R. W. Chantrell. Thermal Fluctuations in a Pair of magnetostatically coupled Particles. *J. Appl. Phys.*, 73:6501–6503, 1993.
- [113] Y. Nakatani, Y. Uesaka, N. Hayashi, H. Fukushima. Computer Simulation of thermal Fluctuation of fine particle Magnetization based on Langevin Equation. *J. Magn. Mater.*, 168:347–351, 1997.
- [114] V. P. Antropov, S. V. Tretyakov, B. N. Hamon. Spin Dynamics in Magnets: Quantum Effects and numerical Simulations (invited). *J. Appl. Phys.*, 81:3961–3965, 1997.
- [115] J. Schnakenberg. *Algorithmen in der Quantentheorie und Statistischen Physik*. Zimmermann-Neufang, 1995.
- [116] A. Greiner, W. Strittmatter, J. Honerkamp. Numerical Integration of stochastic differential Equations. *J. Stat. Phys.*, 51:95–108, 1988.
- [117] W. Scholz, T. Schrefl, J. Fidler. Micromagnetic Simulation of thermally activated Switching in fine Particles. *J. Magn. Mater.*, 233:296–304, 2001.
- [118] M. Vomir, L. H. F. Andrade, L. Guidoni, E. Beaurepaire, J.-Y. Bigot. Real Space Trajectory of the Ultrafast Magnetization Dynamics in ferromagnetic Metals. *Phys. Rev. Lett.*, 94:237601–1–4, 2005.
- [119] J. C. Slonczewski. Current-Driven Excitation of magnetic Multilayers. *J. Magn. Mater.*, 159:L1–L7, 1996.
- [120] L. Berger. Emission of Spin Waves by a magnetic Multilayer traversed by a Current. *Phys. Rev. B*, 54:9353–9358, 1996.
- [121] C. Thirion, W. Wernsdorfer, D. Maily. Switching of Magnetization by nonlinear Resonance studied in single Nanoparticles. *Nat. Mater.*, 2:524–527, 2003.
- [122] Z. Z. Sun, X. R. Wang. Magnetization Reversal through Synchronization with a Microwave. *Phys. Rev. B*, 74:132401–1–4, 2006.
- [123] Z. Z. Sun, X. R. Wang. Theoretical Limit of the minimal Magnetization Switching Field and the Optimal Field Pulse for Stoner Particles. *Phys. Rev. Lett.*, 97:077205–1–4, 2006.

- [124] S. I. Denisov, T. V. Lyutyy, P. Hänggi, K. N. Trohidou. Dynamical and thermal Effects in Nanoparticle Systems driven by a rotating magnetic Field. *Phys. Rev. B*, 74:104406–1–8, 2006.
- [125] S. I. Denisov, T. V. Lyutyy, P. Hänggi. Magnetization of Nanoparticle Systems in a rotating magnetic Field. *Phys. Rev. Lett.*, 97:227202–1–4, 2006.
- [126] Z. Z. Sun, X. R. Wang. Fast Magnetization Switching of Stoner Particles: A non-linear Dynamics Picture. *Phys. Rev. B*, 71:174430–1–9, 2005.
- [127] Z. Z. Sun, X. R. Wang. Strategy to reduce minimal Magnetization Switching Field for Stoner Particles. *Phys. Rev. B*, 73:092416–1–4, 2006.
- [128] A. Sukhov, J. Berakdar. Temperature-Dependent Magnetization Dynamics of magnetic Nanoparticles. *J. Phys.: Condens. Matter*, 20:125226–1–9, 2008.
- [129] Numerical simulations of the magnetization dynamics in the presence of static and time-dependent fields can be viewed online. For this you need to log in with the user name "guest" on the remote computer "141.48.95.139" with the password "Thesis_Sukhov". All the simulations are saved in the folder "Thesis/Simulations". A description of the parameters chosen for the simulations can be found in "Readme.txt".
- [130] H. C. Siegmann, E. L. Garwin, C. Y. Prescott, J. Heidmann, D. Mauri, D. Weller, R. Allenspach, W. Weber. Magnetism with Picosecond Field Pulses. *J. Magn. Magn. Mater.*, 151:L8–L12, 1995.
- [131] C. H. Back, H. C. Siegmann. Ultrashort magnetic Pulses and the elementary Process of Magnetization Reversal. *J. Magn. Magn. Mater.*, 200:774–785, 1999.
- [132] M. Bauer, J. Fassbender, B. Hillebrands, R. L. Stamps. Switching Behavior of a Stoner Particle beyond the Relaxation Time Limit. *Phys. Rev. B*, 61:3410–3416, 2000.
- [133] D. J. Tannor. *Introduction to Quantum Mechanics: A Time-dependent Perspective*. University Science Books, New York, 2007.
- [134] A. Sukhov, J. Berakdar. Local Control of ultrafast Dynamics of magnetic Nanoparticles. *Phys. Rev. Lett.*, 102:057204–1–4, 2009.
- [135] D. C. Langreth, J. W. Wilkins. Theory of Spin Resonance in dilute magnetic Alloys. *Phys. Rev. B*, 6:3189–3227, 1972.
- [136] E. B. Myers, D. C. Ralph, J. A. Katine, R. N. Louie, R. A. Buhrman. Current-Induced Switching of Domains in magnetic Multilayer Devices. *Science*, 285:867–870, 1999.
- [137] M. Tsoi, A. G. M. Jansen, J. Bass, W.-C. Chiang, M. Seck, V. Tsoi, P. Wyder. Excitation of a magnetic Multilayer by an electric Current. *Phys. Rev. Lett.*, 80:4281–4284, 1998.

- [138] J. A. Katine, F. J. Albert, R. A. Buhrman, E. B. Myers, D. C. Ralph. Current-Driven Magnetization Reversal and Spin-Wave Excitations in Co/Cu/Co Pillars. *Phys. Rev. Lett.*, 84:3149–3152, 2000.
- [139] M. N. Baibich, J. M. Broto, A. Fert, F. Nguyen Van Dau, F. Petroff, P. Eitenne, G. Kreuzet, A. Friederich, J. Chazelas. Giant Magnetoresistance of (001)Fe/(001)Cr magnetic Superlattices. *Phys. Rev. Lett.*, 61:2472–2475, 1988.
- [140] G. Binasch, P. Grünberg, F. Saurenbach, W. Zinn. Enhanced Magnetoresistance in layered magnetic Structures with antiferromagnetic Interlayer Exchange. *Phys. Rev. B*, 39:4828–4830, 1989.
- [141] L. D. Landau, E. M. Lifshitz. *Quantum Mechanics: Nonrelativistic Theory*, volume 3. Oxford: Pergamon Press, 3rd edition, 1999.
- [142] M. D. Stiles, A. Zangwill. Anatomy of Spin-Transfer Torque. *Phys. Rev. B*, 66:014407–1–14, 2002.
- [143] D. C. Ralph, M. D. Stiles. Spin Transfer Torques. *J. Magn. Magn. Mater.*, 320:1190–1216, 2008.
- [144] G. Bertotti, C. Serpico, I. D. Mayergoyz, R. Bonin, M. d’Aquino. Current-Induced Magnetization Dynamics in Nanomagnets. *J. Magn. Magn. Mater.*, 316:285–290, 2007.
- [145] J. C. Slonczewski. Currents and Torques in metallic magnetic Multilayers. *J. Magn. Magn. Mater.*, 247:324–338, 2002.
- [146] Z. Li, S. Zhang. Domain-Wall Dynamics and Spin-Wave Excitations with Spin-Transfer Torques. *Phys. Rev. Lett.*, 92:207203–1–4, 2004.
- [147] V. K. Dugaev, V. R. Vieira, P. D. Sacramento, J. Barnaś, M. A. N. Araújo, J. Berakdar. Current-Induced Motion of a Domain Wall in a magnetic Nanowire. *Phys. Rev. B*, 74:054403–1–12, 2006.
- [148] B. Krüger, D. Pfannkuche, M. Bolte, G. Meier, U. Merkt. Current-Driven Domain-Wall Dynamics in curved ferromagnetic Nanowires. *Phys. Rev. B*, 75:054421–1–9, 2007.
- [149] P. P. Horley, V. R. Vieira, P. M. Gorley, V. K. Dugaev, J. Berakdar, J. Barnaś. Influence of a periodic magnetic Field and Spin-Polarized Current on the magnetic Dynamics of a monodomain Ferromagnet. *Phys. Rev. B*, 78:054417–1–15, 2008.
- [150] G. Meier, M. Bolte, R. Eiselt, B. Krüger, D.-H. Kim, P. Fischer. Direct Imaging of stochastic Domain-Wall Motion driven by Nanosecond Current Pulses. *Phys. Rev. Lett.*, 98:187202–1–4, 2007.
- [151] S. S. P. Parkin, M. Hayashi, L. Thomas. Magnetic Domain-Wall Racetrack Memory. *Science*, 320:190–194, 2008.
- [152] M. Hayashi, L. Thomas, R. Moriya, C. Rettner, S. S. P. Parkin. Current-Controlled magnetic Domain-Wall Nanowire Shift Register. *Science*, 320:209–211, 2008.

- [153] S. Krause, L. Berbil-Bautista, G. Herzog, M. Bode, R. Wiesendanger. Current-Induced Magnetization Switching with a Spin-Polarized Scanning Tunneling Microscope. *Science*, 317:1537–1540, 2007.

Eidesstattliche Erklärung

Hiermit erkläre ich, dass ich meine Dissertation selbständig und ohne fremde Hilfe verfasst und keine anderen als die von mir angegebenen Quellen und Hilfsmittel zur Erstellung meiner Dissertation verwendet habe. Den benutzten Werken wörtlich oder inhaltlich entnommene Stellen sind als solche gekennzeichnet.

Alexander Sukhov, _____

Halle an der Saale, den _____

Acknowledgements

This work would not have been performed in its present form without the help of many colleagues, coworkers and friends. Below I list those who have in some way contributed to the thesis with their comments, remarks, suggestions or discussions.

I express my thanks to **Prof. Dr. Jürgen Kirschner** for giving me the opportunity to carry out this work as a PhD student of the International Max Planck Research School for Science and Technology of Nanostructures (IMPRS).

I am deeply indebted to my supervisor **Prof. Dr. Jamal Berakdar** for the interesting topic of research, for many ideas and numerous discussions of the problems addressed in the thesis. I strongly appreciate his willingness to help and thank him for multiple advises and his patience and critical comments in writing publications.

My special thanks are due to all members of the theory group "Nonequilibrium Many-Body Systems" at the Martin Luther University Halle-Wittenberg. In particular, I am very thankful to **Dr. Chenglong Jia** for some discussions and to **Dr. Andrey Moskalenko** for his comments during the past seminars. **Dr. Yaroslav Pavlyukh** must be praised for helping in tracing the work and especially for the discussion to Section 7.2.1. I thank **Dr. Nicholas Sedlmayr** for a critical view of the thesis and wish to acknowledge **Berlinson Napitu** and **Johannes Hahn** and all other members for a friendly atmosphere in the group.

It is a pleasure for me to acknowledge **Prof. Dr. Patrick Bruno** for his unforgettable style of doing and listening talks during the seminars at the Max Planck Institute. Through those seminars I learned that not only seminar talks but also literature chats bring a lot of use, in particular for writing the thesis. Additionally, I want to thank **Dr. Leonid Sandratskii** for various useful recommendations and **Dr. Sergey Ostanin** for his wise advises.

I also would like to acknowledge a couple discussions with people from the Experimental Department I of the Max Planck Institute. These are: **Dr. Dirk Sander**, **Dr. Guillemin Rodary**, **Dr. Hirofumi Oka** and **Sebastian Wedekind**.

Numerous discussions with scientists of the mathematical department of the Martin Luther University on the numerical aspects of the presented stochastic method deserve to be mentioned. Here, I appreciate the invitation of **Prof. Dr. Wilfried Grecksch** to give a talk in his group and a couple discussions with **Dr. Lothar Boltze**.

I must thank my colleagues at the IMPRS for giving interesting talks during the IMPRS seminars and workshops. Special thanks go to the coordinator of the Research School **Dr. Monika Kaempfe** for her readiness to help in nonscientific questions.

The IMPRS gave the opportunity not only to practice scientific skills but also to organize scientific events. Thus, a workshop on "Advances in Science and Technology of Nanostructures" has been held in June 2008. For their enthusiasm and the willingness to assist in the organization I acknowledge **Martina Polok**, **Peter Bose**, **Michael Fechner** and **Ilja Gunkel**.

Last but not least I cordially thank my parents and sister for their support and love and on a personal level I am deeply indebted to my lovely wife **Dr. Ksenia Boldyreva** for her willingness to put up with my solitary behavior during the writing of the thesis.

Curriculum Vitae

Personal Information

Name: Alexander Sukhov
Date of birth: April 14, 1981
Place of birth: Ulyanovsk, Russia
Nationality: Russian
Sex: Male
Marital status: Married

Education

1987 - 1994: Primary School N7, Ulyanovsk, Russia
1994 - 1996: Secondary School N1, Ulyanovsk, Russia
1996 - 1998: Physical and Mathematical College-class of the Secondary School N40, Ulyanovsk, Russia
1997 - 1998: Distance Learning School, Moscow Institute of Physics and Technology
1998 - 2002: Study of Physics at the Ulyanovsk State University, Ulyanovsk, Russia
- Degree: Bachelor of Physics.
- Bachelor Thesis: "Ferromagnetic Resonance in thin Films magnetized parallel to their Surface".
Supervisor: Prof. Dr. D. I. Sementsov.
2002 - 2005: Study of Physics at the University of Duisburg-Essen (previously the Gerhard Mercator University), Duisburg, Germany
- Degree: Master of Physics.
- Master Thesis: "Computer Simulations for ferromagnetic Resonance of Nanoparticles".
Supervisors: Prof. Dr. K. D. Usadel, Prof. Dr. U. Nowak.
2006 - 2009: Study of Physics at the International Max Planck Research School for Science and Technology of Nanostructures, Max Planck Institute of Microstructure Physics, Halle an der Saale, Germany
- Expected Degree: Ph. D. (Dr. rer. nat.)
- Ph. D. Thesis: "Ultrafast Switching and Control of Nanoparticles' Magnetization".
Supervisor: Prof. Dr. J. Berakdar.

Alexander Sukhov, _____

Halle an der Saale, _____

List of Publications

Parts of this work are published as:

1. A. Sukhov and J. Berakdar. Temperature-Dependent Magnetization Dynamics of magnetic Nanoparticles, *Journal of Physics: Condensed Matter*, 20:125226-1-9, 2008.
arXiv:0802.1740.
2. A. Sukhov and J. Berakdar. Local Control of ultrafast Dynamics of magnetic Nanoparticles, *Physical Review Letters*, 102:057204-1-4, 2009.
arXiv:0812.0584.
3. A. Sukhov and J. Berakdar. Steering Magnetization Dynamics of Nanoparticles with ultrashort Pulses, *Physical Review B*, 79:134433-1-10, 2009.

Further publications:

1. A. Sukhov, K. D. Usadel, U. Nowak. Ferromagnetic Resonance in an Ensemble of Nanoparticles with randomly distributed Anisotropy Axes, *Journal of Magnetism and Magnetic Materials*, 320:31-35, 2008.

Conference Contributions and invited Talks

1. A. Sukhov. "Temperature-Dependent Magnetization Switching", International Max Planck Research School Workshop, Wörlitz, Germany, February 5 - 6, 2007, *Talk*.
2. A. Sukhov, J. Berakdar. "Temperature-Dependent Magnetization Switching", DPG-Spring Meeting, Regensburg, Germany, March 26 - 30, 2007, *Talk*.
3. A. Sukhov, J. Berakdar. "Temperature-Dependent Magnetization Reversal in magnetic Nanoparticles", International Conference on "Nanospintronic Design and Realization 2007", Dresden, Germany, May 21 - 25, 2007, *Poster*.
4. A. Sukhov. "Numerische Methoden zur Simulation der Landau-Lifshitz-Gilbert Gleichung", Oberseminar Stochastik (AG Prof. W. Grecksch), Halle an der Saale, Germany, November 15, 2007, *Invited Talk*.
5. A. Sukhov, J. Berakdar. "Temperature-Dependent fast Switching of magnetic Nanoparticles", DPG-Spring Meeting, Berlin, Germany, February 25 - 29, 2008, *Poster*.
6. A. Sukhov, J. Berakdar. "Stochastische Spindynamik", mathematisch-physikalisches Seminar, Halle an der Saale, Germany, April 14, 2008, *Invited Talk*.
7. A. Sukhov, J. Berakdar. "Switching in magnetic Nanoparticles using continuous and pulsed magnetic Fields", Workshop on "Advances In Science and Technology of Nanostructures", Halle an der Saale, Germany, June 3 - 4, 2008, *Poster*.
8. A. Sukhov, J. Berakdar. "Magnetization Dynamics of Nanoparticles in the Presence of Continuous Fields and short magnetic Pulses at finite Temperatures", International Max Planck Research School Workshop, Helfta, Germany, September 25 - 26, 2008, *Talk, Poster*.
9. A. Sukhov, J. Berakdar. "Local Control of ultrafast Dynamics in magnetic Nanoparticles" (*Talk*), "Magnetization Dynamics of Nanoparticles subject to continuous magnetic Fields or ultrashort magnetic Pulses" (*Poster*), DPG-Spring Meeting, Dresden, Germany, March 22 - 27, 2009.
10. A. Sukhov, J. Berakdar. "Local Control of ultrafast Dynamics in magnetic Nanoparticles", IEEE International Magnetism Conference "Intermag 2009", Sacramento, California, USA, May 4 - 8, 2009, *Poster*.